Depositional and structural relationships along the basement-Cambrian contact in the Hardangervidda area

Master of Science Thesis
in Geodynamics

Karoline Øvretveit

Department of Earth Science

University of Bergen

2016

Abstract

The Scandinavian sub-Cambrian peneplain is an important reference surface used in reconstructing the geological evolution from the Neoproterozoic to the present. A detailed study of the geomorphological and structural features of the peneplain, in addition to lithological and stratigraphic relations, is restricted for the Hardangervidda area. The current study area document a geological evolution including Neoproterozoic rifting from the breakup of Gondwana, followed by the Cambrian transgression, in addition to the events of Caledonian thrusting and post-Caledonian extension. On the basis of extensive fieldwork, thin-section analyses and Scanning Electron Microscope (SEM) analyses, in addition to contouring the sub-Cambrian peneplain, the geology of the Hardangervidda area has been examined. The lithological units represented in this area include unweathered and weathered Precambrian basement, basal conglomerate and meta-sediments, quartz schists, phyllites and gneisses of the Caledonian thrust sheet.

Microfabrics are mainly found in the weathered basement and the basal meta-sediments, and thin-section analyses of the phyllite unit display well-developed shear structures representing top-to-the-NW transport. Structural data of S-C structures, folds, and lineations recorded in the phyllite unit represent a prominent NW transport direction. Contour map and corresponding vertical profiles of the sub-Cambrian peneplain indicates irregularities with depressions up to 250 meters depth. Microstructures found in the weathered basement are proposed to have been formed during Caledonian and Devonian tectonic events. Poorly sorted basal conglomerate is suggested to have been deposited in a terrigenous environment by rivers or debris flow, possibly generated by Neoproterozoic faults. Local depressions of ca. 2 meter depths are likely to represent primary irregularities of the sub-Cambrian peneplain, whereas depressions up to ca. 250 meters are suggested to be representing later tectonic events and glaciations.

The metamorphic grade at Hardangervidda decreases to the east, and is proposed to represent the east-southeast tapering of Scandinavia. The structures indicating top-to-the-NW transport are likely to be related to the extensional collapse of the Caledonian wedge. In overall, the geological evolution of the study area includes Neoproterozoic rifting, followed by Caledonian thrusting, exhumation and post-orogenic extension, which thus might represent the Wilson Cycle.

Acknowledgement

First of all, I would like to thank Professor Haakon Fossen for giving me the opportunity to work with this interesting project, and for great supervision and introducing me to the field work. I am also very grateful to my co-supervisors Asbjørn Thon and Eivind Bastesen for scientific discussions and constructive comments and feedbacks to improve my work.

I had a lot of help during the fieldwork. Therefore, I would first of all like to thank my boyfriend Øyvind Nordvik for spending most of the field work with me. I have appreciated the discussions and great friendship. I would also like to thank Jorien Van der Wal from the University of Utrecht, Christoffer Røssevold Taule and my dad Karsten Øvretveit for being great field assistants and for providing new perspectives during the fieldwork.

I would like to thank Irina Dumitru for teaching and helping me with the sample preparation. I am also grateful to Egil Erichsen for teaching me how to use the Scanning Electron Microscope.

I would like to thank all my fellow geology students at the University of Bergen for five wonderful years with unforgettable memories from field trips and hours at the university, including cake Fridays and social events. Hallgeir Sirevaag is especially thanked for proof-reading some of my work.

Finally, I would like to thank my stepfather Øyvin Wold for showing interest in what I do, in addition to my boyfriend and my family for always supporting me, and for encouraging me to always do my best.

Bergen, 31 May 2016

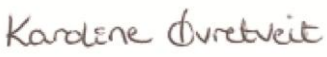

Karoline Øvretveit

Contents

1 Introduction

The Scandinavian sub-Cambrian peneplain is a palaeogeomorphic feature of remarkable extent and is an important reference surface used in reconstructing geological and geomorphic evolution from the Neoproterozoic to the present (e.g. Reusch, 1901; Rekstad, 1903; Goldschmidt, 1912b; Liestøl, 1960; Elvhage & Lindmar-Bergström, 1987; Nielsen & Schovsbo, 2011). The Hardangervidda area in central southern Norway is a key field area for studying the peneplain and the related lithologies, in order to address the depositional environments during the Cambrian transgression, tectonic events comprising Caledonian thrusting and post-orogenic extension, and Cenozoic vertical movement. Some geological investigations were conducted from the mid-1800's to the early 1900, and the focus during this period was to study lithological units and structural features. However, restricted detailed study of the contact zone between the Precambrian basement and the overlying Cambrosilurian meta-sediments has been published for the Hardangervidda area. The current study will present a systematic geological mapping of the exposed sub-Cambrian peneplain by means of detailed descriptions of the lithologies and the related structural significance. The state of weathering of the peneplain will be addressed in addition to the study of its structural influence. In addition, the strain gradient and sense of shear of the autochthonous units are studied in order to distinguish between the effect of thrusting and backsliding of the Caledonian wedge in the area.

1.1 Study area

In this study, the area between Ustaoset and Voss was examined (Fig. 1). Geologically, this area is characterized by Precambrian basement overlain by Cambro-Silurian meta-sedimentary rocks and remnants of the Caledonian thrust sheets. The sub-Cambrian peneplain, marked by the contact between the basement and the overlying meta-sediments, is well-exposed in the study area.

Fig. 1. Overview map of the study area, located in central southern Norway.

1.2 Research objectives

The lithological units on Hardangervidda were early investigated (e.g. Brøgger, 1893), and sequences for the autochthonous and allochthonous units were later suggested (Naterstad *et al.*, 1973; Andresen, 1978). The origin of the present known Caledonian thrust sheet brought into a heated debate between 1894 and early 1900s (Kjerulf, 1879; Törnebohm, 1888; Brøgger, 1893; Reusch *et al.*, 1902; Goldschmidt, 1912a). After concluding that the uppermost tectonic unit is part of an orogenic nappe, the transport direction of the nappe were discussed based on the foliations and folds observed in the autochthonous and allochthonous units. One characteristic feature of the phyllite on Hardangervidda, which constitute the bulk of the Caledonian décollement, is the well-developed S-C shear structure. Since the understanding of this type of kinematic indicator was not established before the late 1970's to 1980's (e.g. Berthé *et al.*, 1979; Knipe & White, 1979; Ponce de Leon & Choukroune, 1980; White *et al*,. 1980) , precise structural mapping of the Hardangervidda area, concerning the transport direction of the Caledonian thrust nappe, lacks in the pre-1990 literature.

A detailed study concerning the morphological, structural, stratigraphical, and lithological properties of the exposed sub-Cambrian peneplain is restricted for the Hardangervidda area. Altitude measurements and mapping of the peneplain have been conducted for parts of the study area (Rekstad, 1903; Goldschmidt, 1912b; Liestøl, 1960; Fossen & Hurich, 2005). A recent study of the sub-Cambrian peneplain of southern Norway has been conducted, which involves digital and systematic mapping of its morphological variance and structural, lithological and weathering characteristics (Jarsve *et al.*, 2014; Gabrielsen *et al.*, 2015). However, this study does not provide detailed descriptions of the basal sediments.

The main objective of this study is to present the characteristics of the sub-Cambrian peneplain in the central southern Norway, with special focus on detailed descriptions of the lithological units above and below the peneplain and the related Caledonian deformation and possible weathering of the basement.

The specific aims of the study are:

1. To characterize the morphology of the sub-Cambrian peneplain, and to describe the basal sediments resting on the basement.
2. To examine irregularities of the sub-Cambrian peneplain in the Hardangervidda area, and to determine whether there are primary Neoproterozoic depressions in the basement.
3. To describe variations in strain gradient and sense of shear at different locations and investigate how Neoproterozoic irregularities of the peneplain influence the strain distribution along the peneplain during the Caledonian thrusting.
4. To determine the presence of minerals and microfabrics in the different autochthonous units in order to determine the metamorphic conditions, and to relate the different microstructures to the different tectonic events.
5. To determine the state of weathering of the peneplain and describe it prior to deformation.

2 Geological setting

2.1 Precambrian

2.1.1 General setting

During the Precambrian, the Baltic Shield consisted of three terranes: Volgo-Uralia, Sarmatia and Fennoscandia. The Fennoscandian Shield, to which the Precambrian rocks in Norway belong, reflects several episodes of orogeny, volcanism and deformation from the Archean to the Neorpoterozoic. These numerous orogenic events have resulted in a complex geology of the basement in Norway.

A significant event during the Precambrian on global scale was the assembly of the supercontinent Rodinia 1.3-1.0 Ga ago, in which active continental margins generated formation of several major mountains ranges. The Baltic Shield, which was located near equator, comprised the eastern margin of the supercontinent (Meert & Torsvik, 2003; Torsvik & Cocks, 2005).

The breakup of Rodinia in the Neoproterozoic was characterized by the formation of several rift and sag basins in the western part of Baltica (Kumpulainen & Nystuen, 1985), which led to the opening of the Iapetus Ocean. At the same time, Baltica underwent rotation of more than 120^0 towards lower latitudes (Cocks & Torsvik, 2005).

2.1.2 Formation of the Precambrian basement in southern Norway

The basement of southern Norway mainly evolved from two orogenic cycles. The Gothian orogeny (1.75-1.50 Ga) resulted in a progressive accretion of plutonic rocks and deformation along the western margin of Baltica (Gaál & Gorbatschev, 1987). A significant portion of the Precambrian basement of Fennoscandia was formed during this orogenic cycle.

At the end of the Mesoproterozoic, the Fennoscandian margin was extensively reworked during the Sveconorwegian orogeny (1.25-0.9 Ga) (Gaál & Gorbatschev, 1987). It is believed that the orogeny primarily evolved from a collision with another major continent, possibly Amazonia (Bingen *et al.*, 2008). In addition, the orogeny was characterized by several minor stages of collisions between Gothic micro-continents and post-Sveconorwegian volcanic terranes (e.g. the Telemarkia Supracrustals, c. 1.5-1.1 Ga). In addition to collisions

and subsequent intense deformation, the convergence also generated granite bodies which constituted new terranes (Bingen *et al.*, 2008). These terranes were finally assembled involving lateral displacement that promoted shear zones characterized by strong plastic deformation. In southern Norway and Sweden the shear zones dissect the basement into several terranes (Fig. 2). Also note that central southern Norway is characterized by the N-S trending Mandal-Ustaoset fault, which splits the basement into two units (Sigmond, 1985).

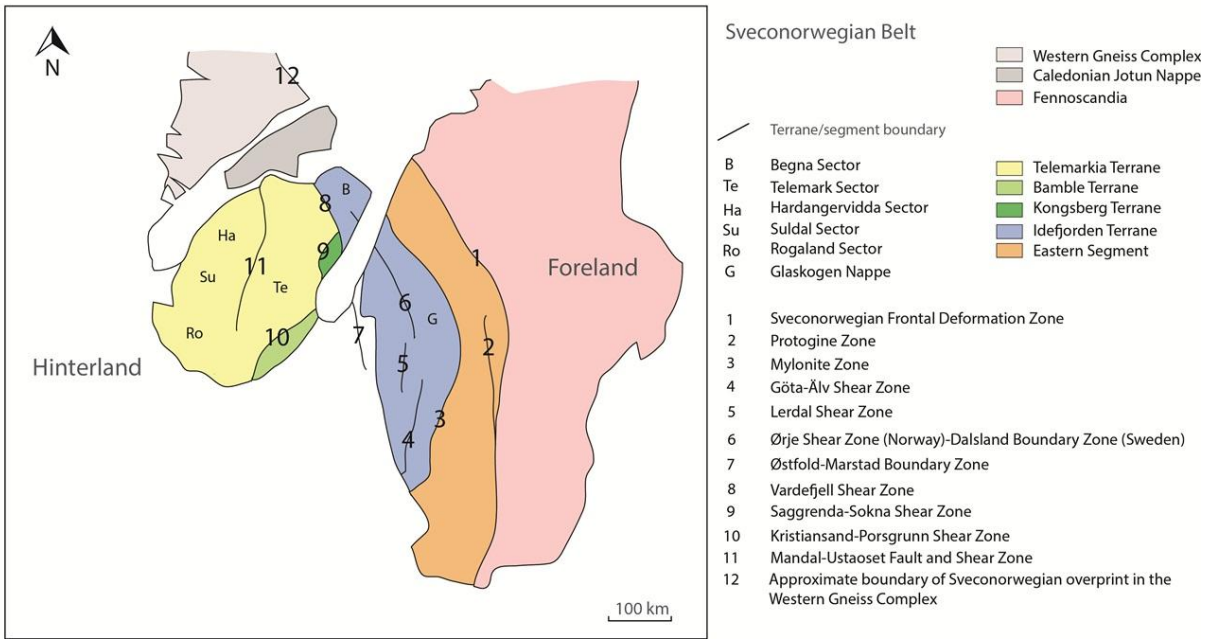

Fig. 2. Subdivision of the basement in Fennoscandia. The mosaic of crustal domains is separated by Sveconorwegian shear zones (Modified after Bingen *et al.*, 2008).

2.1.3 Subaerial exposure and weathering of the basement

The Sveconorwegian orogeny entered the last tectonic phase at the end of the Neoproterozoic, when the orogen got uplifted and underwent gravitational collapse (Gabrielsen *et al.*, 2015). It is believed that Baltica was situated at lower palaeolatitudes at that time (Torsvik & Rehnström, 2001). This increased the temperature and precipitation and thus erosion and weathering, resulting in a low altitude and relief surface of remarkable extent, known as the sub-Cambrian peneplain (Nielsen & Schovsbo, 2011). During the Precambrian, the weathering was quite different from that of today, as there was no plant life on land to give a high humic acid. This resulted also in direct rainfall and a great runoff (Ollier & Clayton, 1984; Egli *et al.*, 2008; Stanley, 2009). In the late Neoproterozoic ice caps covered continents in parts of the world, and probably the physical weathering would have been intense (Ollier & Clayton, 1984).

2.2 Transgression in Early Palaeozoic

2.2.1 General setting

The dawn of the Palaeozoic was mainly characterized by persistent massive rifting as a last chapter of the breakup of Rodinia. Hence the Iapetus Ocean was at its widest during the Ordovician. At the same time, a global Cambrian transgression took place which proved to be of great importance for the geological evolution of the Baltic terrane, including South Norway (Cocks & Torsvik, 2005). At first, it was suggested by Harland (1964) that the transgression was generated by the melting of a large ice sheets in Gondwana in the Neoproterozoic. Subsequently, a hypothesis was introduced that the sea level rise could reflect a mass supply generated by the global scale rifting during the breakup of Rodinia (Matthews & Cowie, 1979).

2.2.2 Deposition of Cambrian-Ordovician marine sediments

The rising early Cambrian sea-level caused flooding of the sub-Cambrian peneplain in southern Norway, where packages of marine sediments were deposited. Two depositional phases are suggested by Nielsen & Schovsbo (2011) which are mainly distinguished by the level of clastic supply. The initial stage of the sea-level rise was characterized by minor cycles of normal regressions, as the system prograded as a result of a high sediment influx. Thin units of conglomerates and quartz arenites were draped on the basement in a shallow water environment (Fig. 3). The mineralogic compositions of pebbles in the basal conglomerates found in the central southern Norway (e.g. Goldschmidt, 1912a) suggest that they represent erosional products of the Precambrian basement.

During mid-Cambrian to early Ordovician, the periphery of Baltica became extensively flooded which greatly reduced the clastic supply (Nielsen & Schovsbo, 2011). Green-grey shales where deposited in a marginal shelf, and as the system retrograded, black alum shale were deposited in an outer shelf environment. In addition, the initial phase of the major sea-level rise was associated with deposition of cool-water limestone, reflecting the absence of clastic supply. The alum shale in southern Norway is believed to have evolved in an anoxic environment due to evolution of an outer passive margin of Baltica which indicated the initial stage of the later Caledonian orogeny (Gee, 1987). Index fossils, including trilobites, graptolites, and brachiopods, have been found in shales at Hardangervidda, and represent deposits from this time period (Dahll, 1861; Brøgger, 1893; Goldschmidt, 1912a;

Goldschmidt, 1925; Størmer, 1925; Størmer, 1941; Henningsmoen, 1952; Andresen, 1974; Andresen, 1978; Bruton *et al.*, 1984; Riis *et al.*, 2011). A final isolation of the Baltic shield was attained in the transition between Cambrian and Ordovician time. Together with requisite factors like proper climate conditions and water depths, precipitation of carbonate was able to occur in the South Norway during Ordovician time (Cocks & Torsvik, 2005).

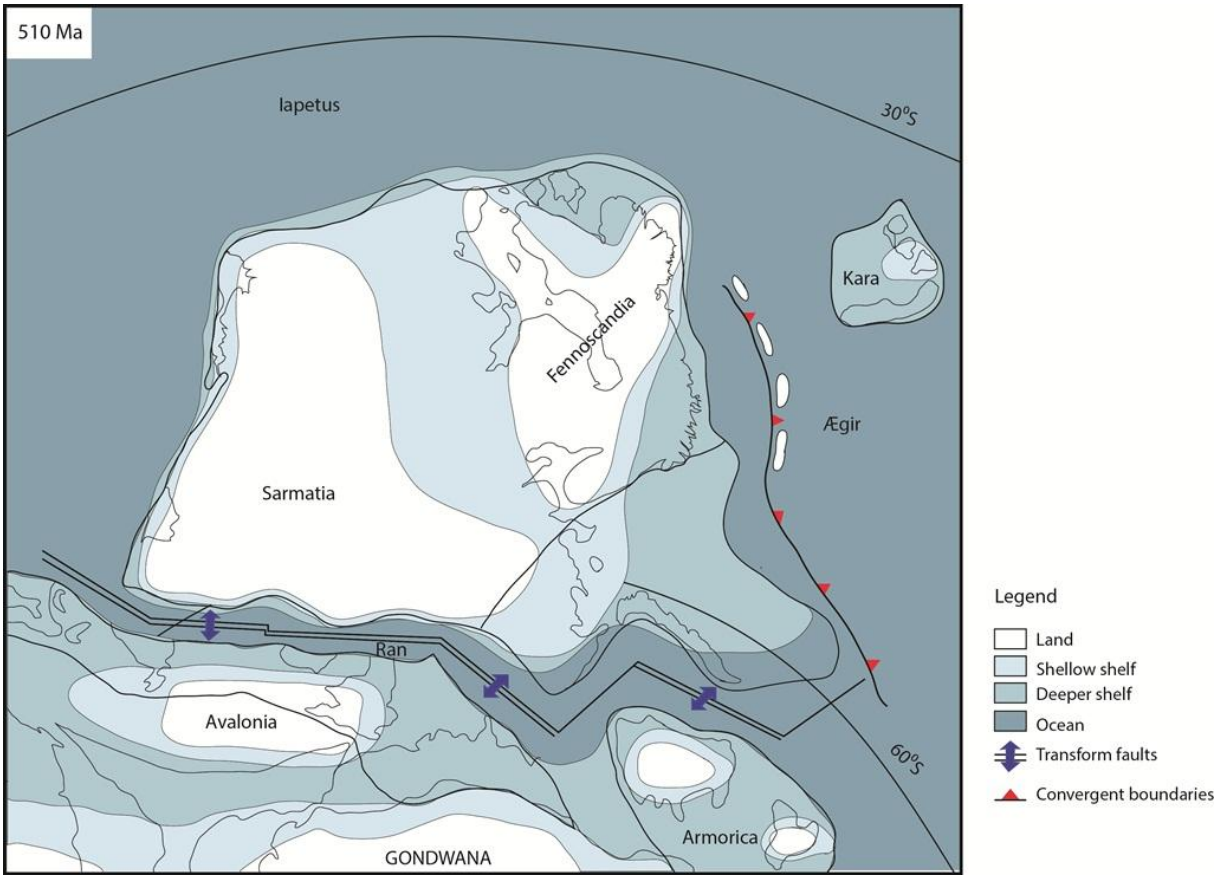

Fig. 3. Shallow-water facies environment characterized the southern Norway in early Cambrian time. Modified after Cocks & Torsvik, 2005.

2.3 The Caledonian orogeny

2.3.1 General setting

The continental rifting from the breakup of Gondwana, led to the opening of the Iapetus Ocean which separated Baltica and Laurentia during the Cambrian (Cocks & Torsvik, 2005). A change from divergent to convergent plate motion occurred in latest Cambrian with development of island arcs in the Iapetus Ocean. The persistent subduction of the Baltic margin initially caused several continent-arc collisions, before the final closure of the Iapetus Ocean took place in the early Silurian, when Laurentia collided with Baltica (Stephens, 1988).

This resulted in the formation of the Caledonian orogenic belt which involved western Scandinavia and East Greenland (Gee *et al.*, 2008).

2.3.2 The Scandinavian Caledonides

The Scandinavian Caledonides were assembled during the collision between Baltica and Laurentia. Subduction of the Baltoscandian margin beneath Laurentia has mainly been proved by high pressure eclogites and locally coesite and microdiamonds found in the Precambrian basement of the western range of the Baltic shield (Dobrzhinetskaya *et al.*, 1995; Gee *et al.*, 2008). Based on thermobarometric values of these parageneses, it is estimated that the subduction slab exceeded a depth of 100 km (Fossen, 2000). Additional studies of increasing heterogenous shearing and deformation towards western Norway strengthened the theory of west-vergent subduction of the Baltic shield (Dietler *et al.*, 1985).

The Scandinavian Caledonides is dominated by thrust tectonics, where numerous allochthonous units are stacked on top of the weaker autochthonous sequence that acted as a décollement. The eastward translation of the nappes is estimated to be up to several hundreds of kilometers (Roberts & Gee, 1985). The tectonostratigraphy of the allochthon in South Norway comprises three complexes (Fig. 4) that mainly originate from the Baltic margin and the Iapetus Ocean. The Lower Allochthonous is dominated by Early Palaeozoic sediments, including quartzites, shales, limestone and, most likely, some slices of Precambrian crystalline rocks (Roberts & Gee, 1985). The overlying Middle Allochthonous is mainly composed of Precambrian basement which was derived from the western Baltoscandian margin and translated eastwards. In parts of the orogenic wedge, the Precambrian crystallines appear as thicker zones where intense Sveconorwegian deformation structures are preserved. The Upper Allochthon is composed of volcanic rocks, partly metamorphosed, which probably originated from island arcs and ophiolites evolved in the Iapetus Ocean during the Cambrian and Ordovician (Roberts & Gee, 1985; Gee *et al.*, 2008).

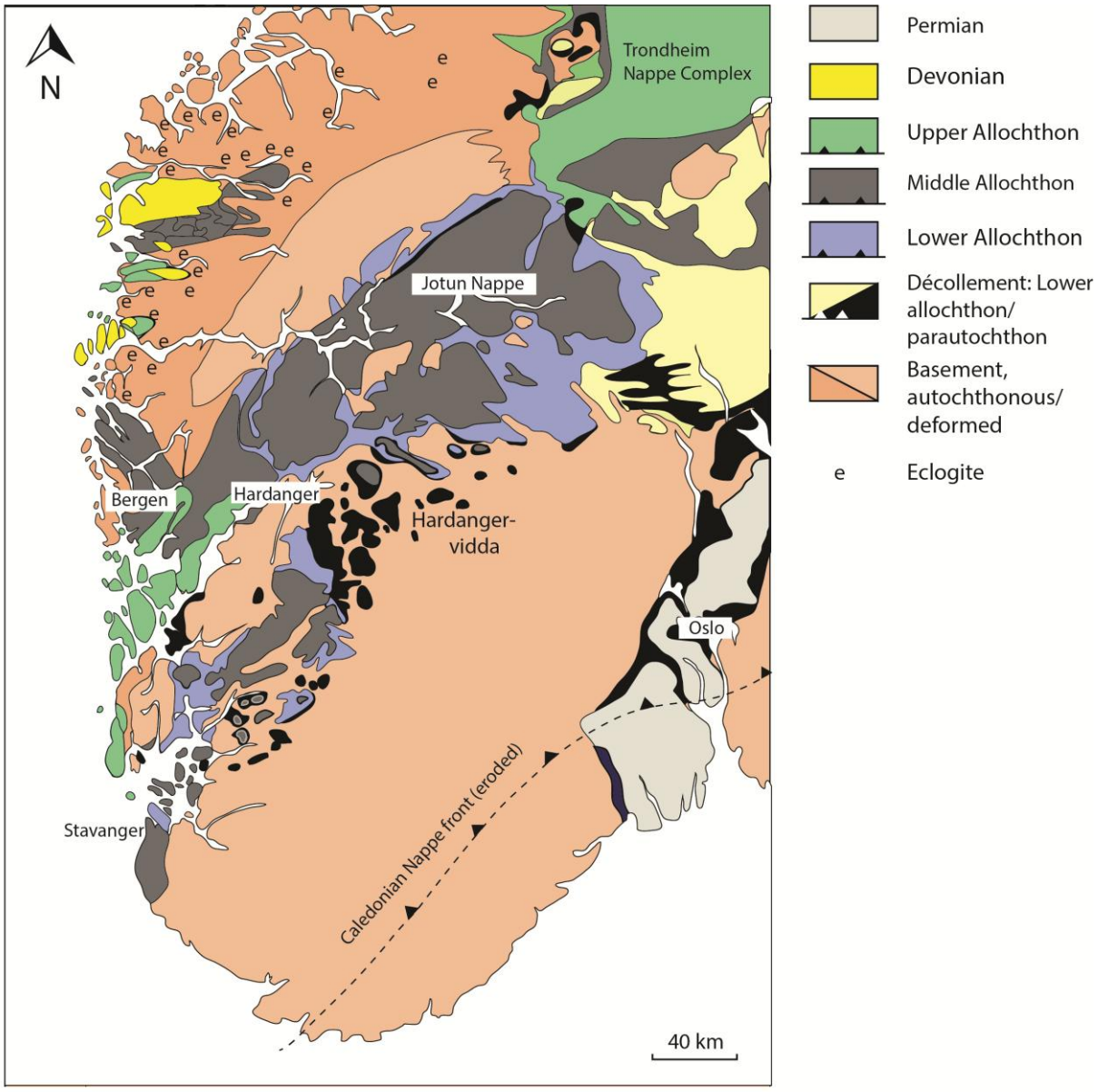

Fig. 4. The distribution of the three allochthonous units in South Norway (Modified after Fossen *et al.*, 2013, pp.221).

2.4 Post-Caledonian collapse

In the Early Devonian, the Scandinavian Caledonides started to collapse, and was followed by extensional tectonics. A possible factor regarding extension of the orogenic wedge may be related to the decreased stress rate expressed from the subduction slab, in which the stress could not maintain equilibrium with the gravitational stress, and thereby not sustain the critical taper (Fossen, 1992). The post-orogenic collapse is interpreted to have occurred during three main extension stages (Fossen, 1992; Fossen, 2000; Fossen, 2010).

2.4.1 Mode I: Backsliding of the orogenic wedge

The first stage of the extension tectonic entailed back movements of the Caledonian nappes toward the hinterland (Fig. 5a) along the basal décollement with an angle of approximately 5^0, in which the translation is strain estimated to be somewhere between 20-36 km (Fossen & Holst, 1995). A study of kinematic indicators in the weak décollement zone, such as S-C fabrics, shear bands, cleavages, asymmetric folds and boudins, displayed a top-to-the-WNW shear (Fossen, 1992). These shear structures overprint the top-to-the-ESE thrust structures, which hence clearly proved a reversal of shear sense along the décollement zone and hence a transition from a compressional to tensional tectonic regime (Fossen, 1992; Fossen & Rykkelid, 1992; Fossen & Holst, 1995).

Thermochronological studies of mylonites have been conducted from the Caledonian orogeny in southwestern Norway. $^{40}Ar/^{39}Ar$ dating applied to mylonites showing contractional fabrics give an age range of 415-408 Ma, whereas dating of muscovite concentrates collected from phyllite with top-to-the-foreland fabric defines an age between 402 and 395 Ma. Hence, a rapid change from a contractional to extensional regime must have taken place between 408-402 Ma (Fossen & Dunlap, 1998).

2.4.2 Mode II: Crustal collapse

Subsequent to the first stage of the extension, the orogenic wedge was preceded by development of hinterland-dipping shear zones (Fossen, 2000). It is suggested that the shear zones were developed due to exhumation of the detachment in the hinterland, which consequently lowered the dip of the detachment zone (Fossen, 2000). Hence it was harder for backsliding to occur and the result was crustal collapse and formation of larger ductile shear zones. The vertical detachment of the shear zones is expected to exceed about 2 km, in which some of them cut the Caledonian nappe stratigraphy and penetrate the Precambrian basement (Fossen, 1992; Fossen, 2010).

2.4.3 Mode III: Brittle faulting

The formation of ductile shear zones was followed by brittle faulting and evolution of fault systems (Fig. 5b). As the continental crust was uplifted, the temperature decreased and intersected the brittle-ductile transition, causing evolution of brittle fault systems that emerged under the same stress field as the ductile shear zones. A slip analysis of the Bergen Arc fault system (Fossen, 1998) indicated an NW-SE extension direction dominated by cohesive fault

rocks, which is believed to represent the brittle faulting event. In addition, U-Pb dating of the associated fault rocks (Pedersen *et al.*, 1999) indicates that much of the fault activity initiated in the lower Devonian.

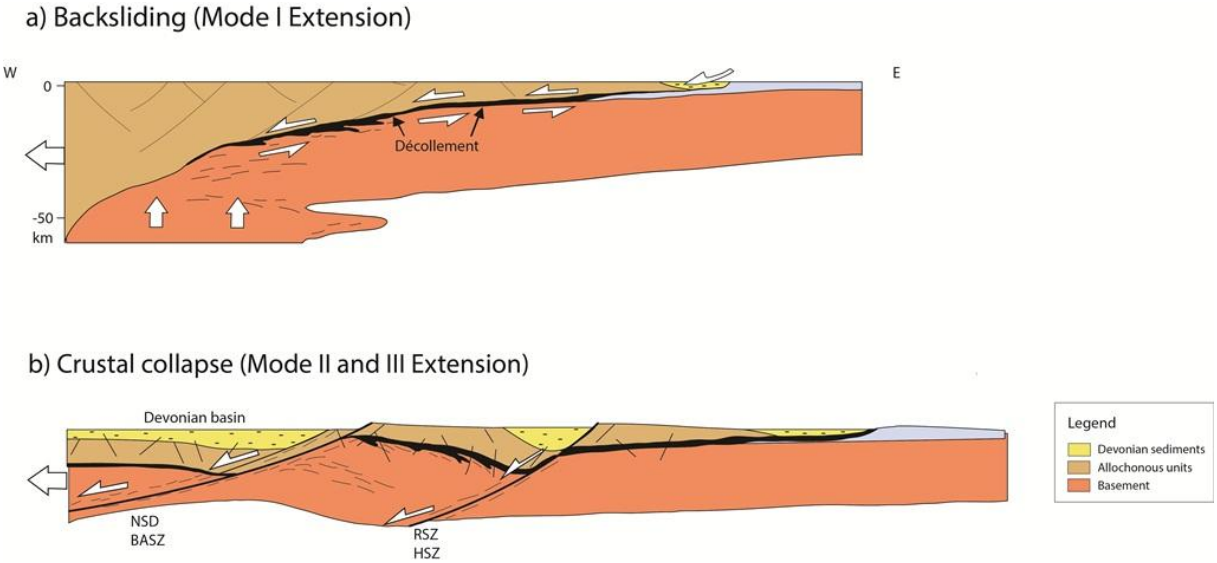

Fig. 5. Three stages of extension involving (a) backsliding of the orogenic wedge and (b) crustal collapse characterized by NW- dipping shear zones and further brittle faulting. **HSZ**: Hardangerfjord Shear Zone; **RSZ**: Røldal Shear Zone; **NSD**: Nordfjord-Sogn Detachment; **BASZ**: Bergen Arc Shear Zone. Modified after Fossen, 2000.

2.5 Previous geological surveys in the Hardangervidda area

2.5.1 The tectonic units and the deformation history of the area

The geological mapping of the different lithological units in the central southern Norway started already in the middle of the 18th century. The introductory topic that raised interest among the geologists was the tectonic setting resulted in metamorphism of the meta-sediments and overlying gneissic rocks. In 1879, Kjerulf published his work of geologic mapping in southern Norway carried out over a period back to 1849. Among other topics he introduced the idea of a contact metamorphism located between the present basement and the overlying Cambro-Silurian meta-sediments and Caledonian nappes of southern Norway, and he assumed the basement to be a younger granitic intrusion that caused the metamorphism (Kjerulf, 1879, pp.143-146). In a yearbook of the Norwegian Geological Survey from 1893, Brøgger presented a suggestion of a geological stratigraphy on Hardangervidda based on his observations and mapping in 1877 (Brøgger, 1893). In addition, his early knowledge of the geology in this area enabled him to discuss the statement of Kjerulf. If the basement

originated from a granite intrusion, the unit located directly above the basement should have been intensively deformed compared to the uppermost unit located at greater distance from the zone of metamorphism. Since phyllites form during lower degree metamorphism relative to gneiss, it was thereby difficult for Brøgger to accept this statement. Instead he came up with an explanation that the source of deformation must have derived from above, conceivably from a great younger laccolith. Beside the contact metamorphism applied by the laccolith, Brøgger believed that the mass itself applied vertical stress to the underlying units high enough to cause intensive deformation (Brøgger, 1893).

Subsequently, in 1888 the Swedish geologist Alfred Elis Törnebohm introduced a new theory that entailed a completely different understanding of origin and development of the units in the central southern Norway. Contrary to previous hypotheses, he suggested that the crystalline schists and gneisses in the uppermost unit could have been laterally transported over a distance of approximately 100 km (Törnebohm, 1888). This statement captured the curiosity of several geologists, and in 1902 H. Reusch, J. Rekstad and K. O. Bjørlykke conducted geological mapping of the southern part of Hardangervidda with the aim of obtaining more information about the stratigraphy and to conduct further surveys to evaluate the theories of Brøgger and Törnebohm. Their observations indicated that the upper unit of shale and gneiss seemed to be analogous to the crystalline basement, and thus they endorsed Törnebohms theory (Reusch *et al.*, 1902). Further geochemical analysis of the gneiss and granite at Finse, Hardangervidda was conducted by Goldschmidt in 1912. The result proved a significant correlation between these rock units, and thus enhanced the theory of a translated upper unit (Goldschmidt, 1912a).

In 1916, Goldschmidt commenced a study of the so called "Høifjeldskvarts", first named by Kjerulf, which included the upper tectonic unit on Hardangervidda. The purpose was to gain a better understanding of the formation of the orogeny in South Norway. Based on observations, he drew parallels between the "Høifjeldskvarts" and flysch sediments in the Alps and in context believed that these rocks had been formed during the orogeny (Goldschmidt, 1916). This statement was not further investigated, but would prove to be supportive of the theory of a tectonic nappe pile in recent years. Beside of studying the "Høifjeldskvarts" Goldschmidt investigated the basal sediments at different localities on Hardangervidda. For instance, observations of basal sediments at Ustaoset (Goldschmidt, 1925) became associated with similar sediments at Finse (Goldschmidt, 1912a). Goldschmidt

reported that the sediments at Ustaoset are less affected by metamorphism than at Finse, and therefore assumed an increasing metamorphic grade towards northwest.

In the middle of the 1900s, tectonic structures found in units on Hardangervidda brought the question of transport direction of the nappe units into the new debate. A study by Kvale during the period 1945-1947 refers to observation of northwest-bending foliation on Hardangervidda (Kvale, 1948; Kvale & Dons, 1960). Limited knowledge of the tectonic evolution of the Caledonian orogeny at that time made it difficult to correlate the development of this direction of foliation to a specific event, and additionally set it in context with opposite movement directions observed in adjacent areas. Nevertheless, Kvale assumed that the foliation bending to the northwest indicated a west-northwest movement of the uppermost units, linked to a late Caledonian tectonic phase. Further mapping of folds in the quartz schist as part of the lowermost nappe unit on Hardangervidda (Naterstad *et al.*, 1973) indicated a top-to-the-northwest movement, and was believed to represent a later stage of the Caledonian orogeny. Beside this observation, Naterstad et al. (1973) reinforced the theory of a lateral transport of the crystalline rocks, primarily based on observation of a tectonic contact between the autochthonous unit and the lowermost nappe rocks, in addition to irregular occurrence of the autochthonous rocks.

In contrast to the theory of a northwest movements of the allochthon, Banham et al. (1979) introduced the hypothesis of a possible Jotunheim suture, meaning that the Jotun complex is located in its original position. The foundation of this hypothesis was based on the NW-vergence of folds, in which was assumed to evolve from underthrusting in the hinterland, and observed ophiolite rocks. Subsequent studies of structures in Jotunheimen (Milnes & Koestler, 1985) indicating a movement to the northwest was interpreted to be a result of back thrusting during a late phase of Caledonian contraction. Later studies of the basal thrust zone revealed that the décollement had a dip toward northwest at the end of a later phase of Caledonian thrusting (Hossack & Cooper, 1986). A tectonic model presented by Andresen & Jamtveit (1990), suggested the extensional deformation to be explained by collapse of the orogenic wedge. This was countered by Fossen (1992) suggesting that a forland-thinning of the orogenic wedge would have resulted in continued thrusting rather the back movement, and thus would not explain the structures indicating movement to the northwest as suggested from the kinematic indicators observed by Andresen & Jamtveit (1990).

2.5.2 The sub-Cambrian peneplain

The sub-Cambrian peneplain has been among the subjects of a numerous geological surveys from 1800`s and early 1900`s (e.g. Brøgger, 1893; Reusch, 1901; Reusch *et al*., 1902; Rekstad, 1903; Goldschmidt, 1912b; Ahlmann, 1919; Goldschmidt, 1925). A study of the difference in altitude of the peneplain in the Hardangervidda area, performed by Rekstad in 1901 and 1902, indicates an average elevation of 1374 m a.s.l. and a maximum difference in altitude of 281 meters (Rekstad, 1903). Especially he noted that the peneplain at Hardangervidda was almost horizontal compared to the areas to the east and west, characterized by a more uneven and fractured basement surface.

A more detailed mapping of the sub-Cambrian peneplain was introduced by Goldschmidt in 1912, when he contoured the contact between the upper surface of the Precambrian basement and the overlying meta-sediments (Goldschmidt, 1912b). The distinct and revealed irregularities of the peneplain were then suggested to have developed in a time gap from Eocambrian to Present. A more precise suggestion that the irregularities were advanced by Caledonian folding and probably later Tertiary faulting was eventually suggested by Strøm (1948). Contour map of the Hardangervidda area and Haukelifjell was later constructed by Liestøl (1960), which also displayed local irregularities of the peneplain and the results were suggested to be related to Caledonian deformation (Strand, 1960). The morphological variations of the peneplain in southern Norway has also lately been contoured (Fossen & Hurich, 2005) and additionally performed more precicely by digital mapping (Jarsve *et al.*, 2014).

A more complex study of the sub-Cambrian peneplain, considering its morphological significance, structure, weathering characteristics and stratigraphic and lithologic properties, has been implemented in the area ranging from Hardangervidda to the west of Sweden (Gabrielsen *et al.*, 2015). Among the results are that the peneplain is suggested to have been only mildly tectonized as (nearly) primary basal sediments and weathering profiles of the Precambrian basement are locally preserved, and the fracturing of the peneplain was assumed to be related to Tertiary exhumation of the southern Scandes.

2.6 Geological framework of NW Hardangervidda

The geology of the present study area can be tectonostratigraphically divided into three main units (Fig. 6) including the Precambrian basement, the autochthonous Cambro-Silurian rocks and remnants of the Caledonian nappe pile.

2.6.1 Lithologies

The Precambrian basement of Hardangervidda is situated west of the Mandal-Ustaoset fault zone (Fig. 6) and is mainly composed of granites and gneisses (Fig. 6, number 22). Plutons of granitic composition cover most of the study area, in which the texture varies locally from being medium-to coarse-grained to porphyritic dominated by phenocrysts of feldspar. Based on radiometric dating, the granites are believed to have been emplaced 1100-900 Ma ago, probably associated with an intrusive phase during the Sveconorwegian orogeny. In addition to the prevalence of plutons, granitic and granodioritic gneisses are situated at Hardangervidda. The texture varies from augen to a more even-grained gneiss, and xenoliths of older migmatites and gneisses are locally found (Sigmond, 1998). U-Pb dating of zircons from magmatic gneisses from southeastern Hardangervidda has been conducted and refers to an initial event of plutonic crystallization c. 1670 Ma ago, followed by deformation 1470 Ma ago which probably can be associated with the Sveconorwegian orogeny (Sigmond *et al.*, 2000). For the present study site the granites appear mainly with a porphyritic character and are found at Finse and Hardangerjøkulen, Sandå and Hallingskeid in the northwest. The gneisses are found mainly as augen gneiss at Ustaoset in east of the study site and as migmatittic gneiss to the west on Osafjellet (Sigmond, 1998).

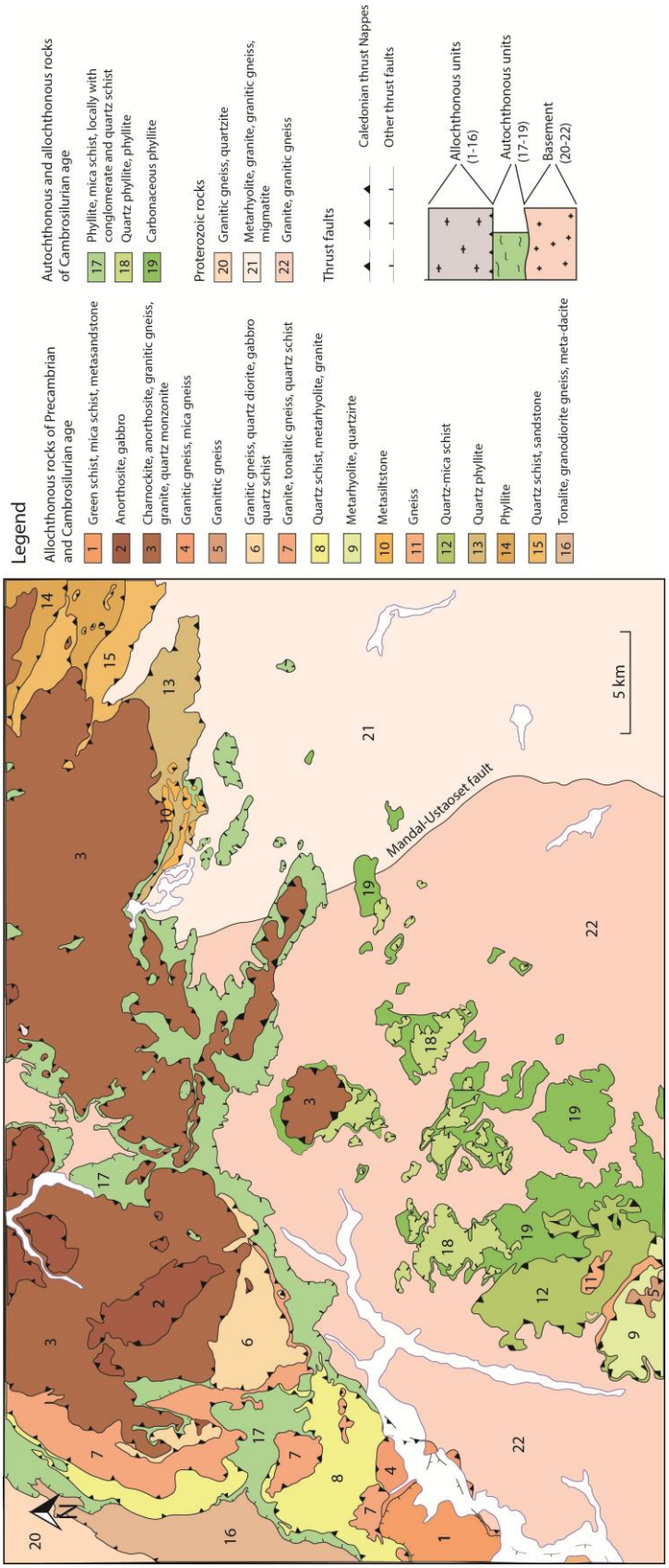

Fig. 6. Simplified map of the Hardangervidda area, roughly dividing the Precambrian basement into west and east segments by the Mandal-Ustaoset fault zone in addition to illustrate the exposure of the Cambrosilurian meta-sediments and remnants of the Caledonian nappes. Modified after Sigmond, 1998.

The autochthonous succession of Cambrosilurian age rest on the sub-Cambrian Peneplain exposed as a horizontal erosional surface at several locations in NW Hardangervidda. A proposal to an autochthonous succession on Hardangervidda, presented by Brøgger in 1893, roughly divides the meta-sediments into five units; the alum shale, quartzite, calcareous and marble unit, phyllite, and various crystalline schists, currently known as the Caledonian thrust nappes (Brøgger, 1893). Almost hundred years later, a lithostratigraphy of the autochthonous sediments was introduced, named the Hardangervidda Group (Andresen, 1974; Andresen, 1978). This subdivision was based on sedimentary facies and their corresponding ages determined by discoveries of index fossils (Fig. 7).

The faunas in the sequence of the Hardangervidda group are based on correlation with sequences elsewhere on the Baltic platform, for instance with the classical Cambro-Silurian stratigraphy in the Oslo Region in eastern Norway. Compared to the sequence thickness ranging from 400-687 m on Hardangervidda, the stratigraphy in Oslo constitutes a thickness estimated to range from 1335-2120 m (Bjørlykke, 1974; Andresen, 1978; Bjørlykke, 1983; Worsley *et al.*, 1983; Bruton *et al.*, 1984). These significant thickness variations might be explained by the tectonic disturbance during the Caledonian folding and thrusting. Since Hardangervidda is located closer the hinterland compared to the Oslo Region, it is likely that the sediments have been more intensively affected and reworked. Therefore, the sequence at Hardangervidda is thinner and occurs rarely as a coherent stratigraphy, but rather represent segments of it. The prominent lithologies are phyllite and mica schists of greenschist facies (Fig. 6, number 17), locally mingled with calcite and deformed quartz lenses. Additionally, basal conglomerates of the Låven Formation are found in some locations of the study area (Askvik, 2008).

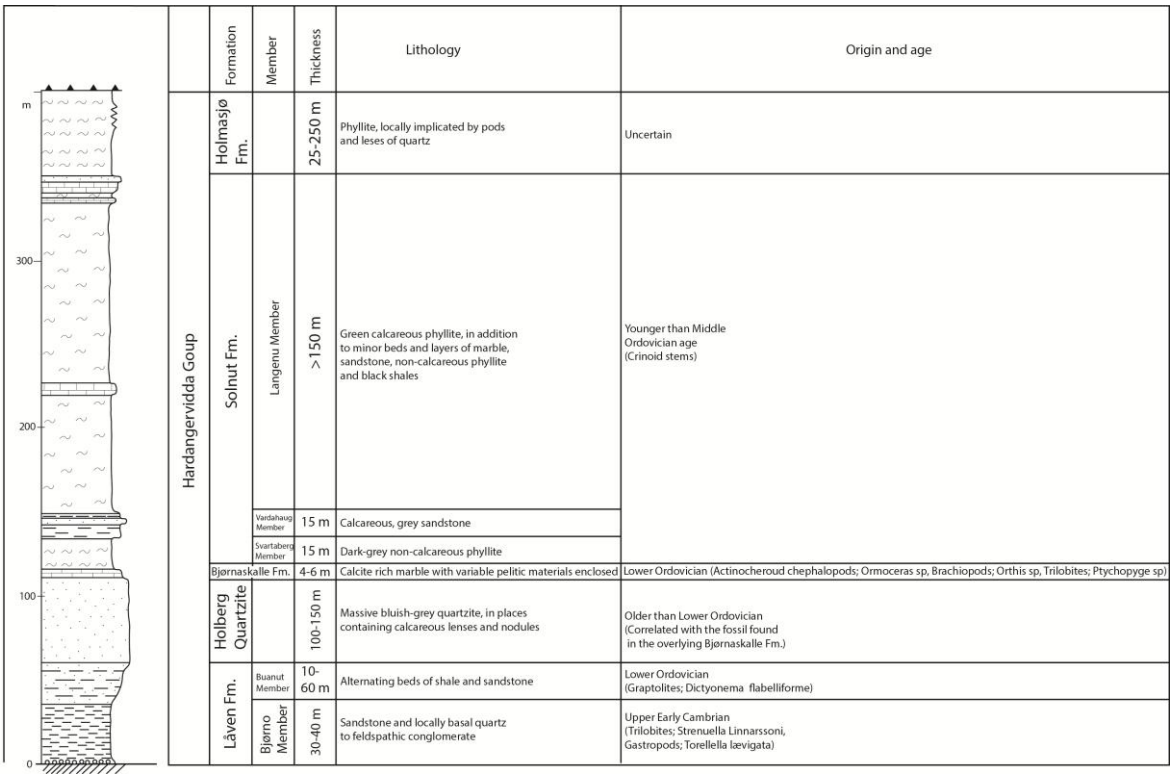

Fig. 7. Lithostratigraphy of the Cambro-Silurian meta-sediments on Hardangervidda. Data from Dahll, 1861; Goldschmidt, 1912a, Goldschmidt, 1925, Størmer, 1925, Andresen, 1974; Andresen, 1978, Bruton *et al.*, 1984.

The allochthonous rocks preserved in the NW Hardangervidda represents the Hardangervidda-Ryfylke nappe complex (HRNC), assigned to the Caledonian Middle Allochthon. Most of the HRNC are sheets of gneisses and schists which probably originated from the granites of the Precambrian basement (Naterstad *et al.*, 1973). The tectonic succession of HRNC comprises in a total of five allochthonous units, based on tectonic boundaries of Precambrian and Silurian ages (Table 1). Beside the tectonic boundaries, the rock mass of the Hardangervidda-Ryfylke nappe complex indicates Proterozoic metamorphism with high P-T conditions of granulite-amphibolite facies during several tectonic events (Naterstad *et al.*, 1973).

Table 1: Tectonostratigraphy of the allochthonous units on Hardangervidda. Data from Naterstad *et al*., 1973.

Tectonic unit	Lithology	Origin and age
Revsegg Formation	Mica gneiss rich in quartz and plagioclase pods, and hornblende-biotite gneiss	Uncertain
Kvitenut Complex	Mylonitic gneiss with granitic to dioritic composition, intruded by diorites and granites	Precambrian
Dyrskard Group	Orthogneiss, amphibolites alternated with bands of quartzite, quartzite mingled with bands of quartz-rich schists	The lithologies are correlated to the Precambrian basement, Eocambrian sediments and Ordovician rocks
Nupsfonn Complex	Paragneiss and orthogneiss of granitic to granodioritic composition	Believed to originally belonged the Kvitenut Complex and the Dyrskard Group
Holmasjø Formation	Quartz schist and phyllite, locally implicated by lenses of quartz	Assumed to be of an autochthonous origin outside Hardangervidda area and later thrusted into its present location during Caledonian events Eocambrian to Ordovician

The units of the HRNC are assumed to be correlated with the Jotun Nappe, which is subdivided into the lower unit of gneiss of Proterozoic origin, and an upper unit composed of anorthosite, gabbro and gneiss (Sigmond, 1998). In the NW Hardangervidda area the allochthonous rocks representing the upper unit are composed of charnockite, amphibolite, and gneisses with granitic and monzonitic origin (Fig. 6, Number 3).

2.6.2 Tectonics

In the study site at Hardangervidda the Precambrian basement is influenced by the greater Mandal-Ustaoset shear zone of Sveconorwegian age. Even though nearly all of the deformation took place along the east side of the fault zone, some plastic deformation of the granites affected the western hanging wall (Sigmond, 1998). The major and most significant tectonic imprints in the study site are presented in the autochthonous and allochthonous units. Structural mapping of the weaker phyllites and mica schists in the central southern Norway indicates an E-W to ENE-WSW oriented cleavage dipping towards S or SSE. In addition, the trends of fold hinges refer to a relative top-to-the-N or NNW movement (Sigmond, 1998). The complexity of tectonic structures in the allochthonous thrust nappes reflecting

deformation of Precambrian and Silurian age. The most prominent southeast-dipping cleavage and foliation in the study site indicating a northwest movement, and is suggested to reflect the early Devonian backsliding of the Caledonian nappes (Naterstad *et al.*, 1973; Sigmond, 1998). Kinematic studies of the Bergsdalen Nappes southwest of the study site refers to two Caledonian deformation events, in which thrust structures indicating movement toward east is overprinted by extensional structures indicating a WNW-directed movement (Fossen, 1993).

3 Methods

3.1 Fieldwork and sampling

The present study is based on fieldwork carried out during July-September 2015. The field work focus on 7 main localities, ranging from Ustaoset in the east to Voss in the west (Fig. 9). A total of 30 samples were collected for thin-section micro textural and micro tectonic analyses. Structural data were recorded at most of the locations.

3.1.1 Mapping of the stratigraphy and the exposed contact

In order to reconstruct the development history of the sub-Cambrian peneplain, the occurrence of lithologies resting on the peneplain, presented by simple logs, and its local morphologic variations were examined in the study area. A contour map and corresponding essential selected profiles crossing the study area were prepared for the peneplain by means of the geological map Odda 1:250 000 (Sigmond, 1998) for examine its morphological variations. Based on field work the boundary between the basement and phyllite is assumed to correspond to the sub-Cambrian peneplain. The contour map was prepared based on 751 points along the boundary which in turn were divided into 13 contour intervals with altitude steps of 100 meters.

3.1.2 Sampling strategy

The geological bedrock maps Odda 1:250 000 by Sigmond (1998) and Hardangerjøkulen 1:50 000 by Askvik (2008) were consulted during the development of a sampling strategy. Samples from every lithological unit were collected for mineralogical description and investigation for evidence of deformation at the microscale. Essentially, oriented samples of phyllite in the Caledonian décollement zone were collected to search for kinematic indicators at microscale. An overview of sampling localities are shown in figure 9 and a summarized table of the samples, including lithology, locality and UTM coordinates is given in appendix A.

State of weathering of the basement

As part of the fieldwork, comparison of unweathered granite and the corresponding weathered granite was performed in order to determine the state of weathering during early Palaeozoic.

A total of seven samples of the basement were collected in the study area, three of them representing unweathered granite (KOE-8, KOE-18, KOE-19) and four constituting weathered granite (KOE-6, KOE-10, KOE-17, KOE-20) collected at the surface of the sub-Cambrian peneplain.

Textural descriptions and mineral composition in nearly unweathered and weathered granites is presented for the different locations in the study area in order to determine the state of weathering and to further compare potential local variations. Mesoscale textural analyses focused on variations in crystal grain size, degree of fracturing and color differences, whereas thin-section analyses mainly examines the variation in mineral content for the fresh and weathered granites in addition to study the grain boundaries and contact, evidence of sericitization of plagioclases and alteration of K-feldspars (Ollier & Clayton, 1984), and bleaching and oxidation of biotites (Irfan & Dearman, 1978). Some of the samples contain a fine-grained material to which the optical microscope did not provide sufficient details in determining type of mineral present. By means of the Scanning Electron Microscope (SEM), the chemical composition of the applicable material was calculated. These data are summarized in appendix D. Eventually the state of weathering was determined based on the petrographic classification system of weathered granites provided by Irfan and Dearman (1978), and following named after the updated classification system of weathered rocks by Wyllie *et al.* (2004, pp.386).

Furthermore, comparison of recorded microfabrics in the unweathered and weathered granites was done to determine whether the state of weathering and thus weakening of the granite may have led to a greater ability to accumulate strain during the Caledonian orogeny.

Lithological variations and shear strain in the décollement zone

Sampling of Cambrosilurian meta-sediments was conducted in order to examine the local variations of the lithologies and strain gradient in the study area. The phyllites, which constitute the bulk of the décollement zone, were sampled at almost every location focusing on variation in mineralogical composition and kinematic indicators at the macro- and micro-scale. In order to determine the transport direction of the Caledonian nappes, oriented samples of the phyllite and gneiss were collected.

3.1.3 Field measurements and structural mapping

Structural mapping and field measurements were mainly focusing on the weak phyllites of the décollement zone comprising numerous shear strain indicators. Measurements of fold axial planes, fold axis and limbs were conducted for asymmetric folds. C-, and S-planes in shear zones were measured, and accompanying sketches with orientation were documented. The S-C crenulation axes, which represent the intersection between the C- and S- surface (Fig. 8), was used in order to determine the sense of shear as the orientation of the axes are perpendicular to the shear direction. By comparing with the orientation of the foliation (S-surface), the transport direction can exactly be determined. The angle (θ) of which the shear band intersects the foliation (S-surface) was used in order to determine the degree of shearing, as lower angles represent a higher strain gradient (Barker, 1990). Additional structural features like lineation and foliation were also measured. Eventually, all the structural measurements and field observations were compared and combined to reveal the movement direction of the nappe pile during the Caledonian events. Additional structural mapping of the basement and the Caledonian nappes were completed by measuring orientation of fractures and folds. Analysis and presentation of all the structural data were made by means of Stereonet v9.0 by Allmendinger (Allmendinger *et al.*, 2013; Cardozo & Allmendinger, 2013). The main locations of measured structural data are framed in sections in figure 9, and a summarized table of the measurements, which is sorted by the locations (data set) and UTM coordinates, is given in appendix B. Note that the boldface data are calculated in Stereonet v9.0 based on the field measurements.

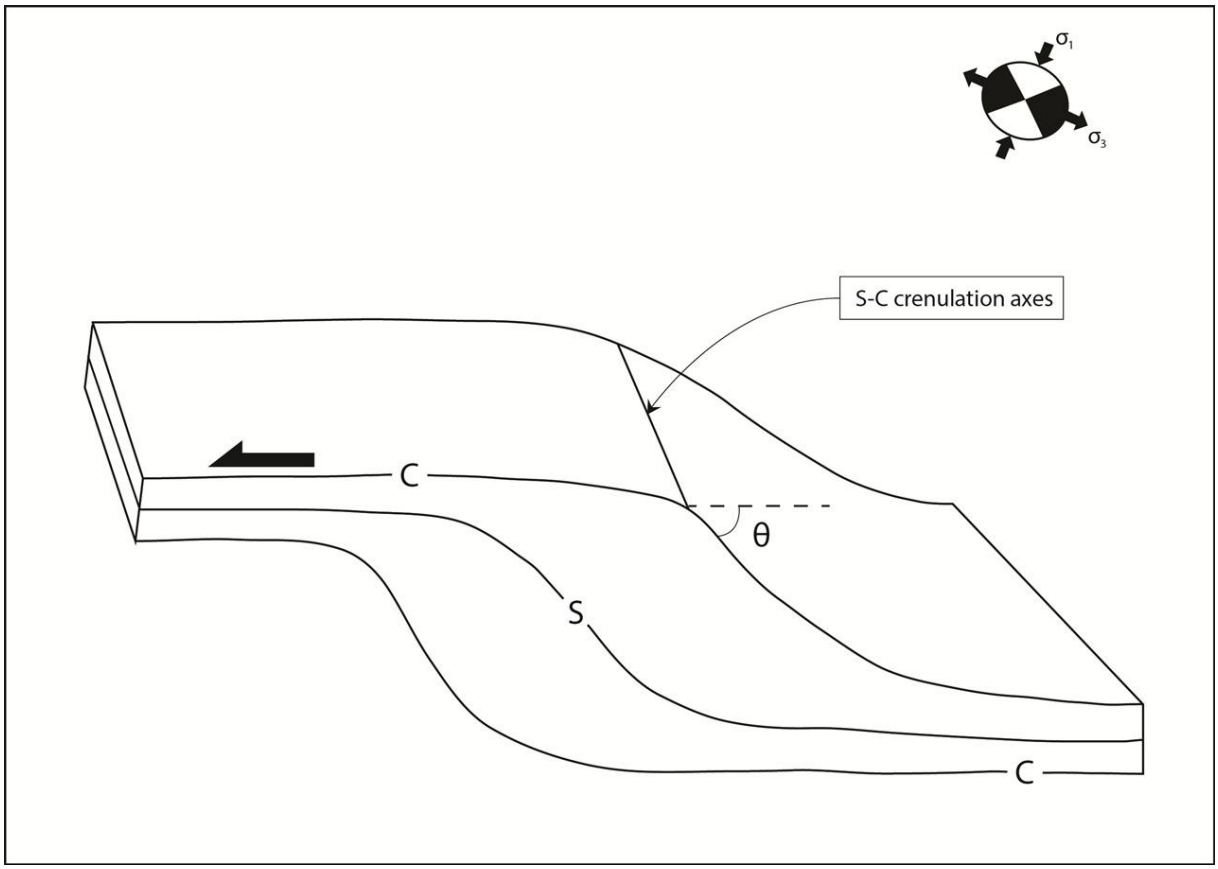

Fig. 8. The orientation of the S-C crenulation axes forms perpendicular to the shear direction and is used as a kinematic indicator in the phyllite.

3.2 Sample preparation and micro-scale analyses

3.2.1 Sample preparation

Petrographic thin-sections were prepared in collaboration with research technician at the University of Bergen (UiB). The oriented samples of phyllites and gneiss were cut normal to the foliation and parallel to the stretching lineation in order to obtain the best section showing kinematic indicators. Two grinding discs, one coarse grained consisting of diamond and one finer grained consisting of silica, were used for polishing the samples. Glass slides were glued to the samples, followed by cutting the samples to a thickness of approximately 2 mm for further polishing. The Astera Grinding Robot instrument was used to grind the samples to a thickness of 1500 mesh, and eventually the Struers DP-U2 polishing instrument was used to grind the sample down to a thickness of 35 µm, and the final polishing down to 30 µm was done with the aid of a polishing slab.

3.2.2 Thin-section analyses

Thin-section analyses was implemented in order to examine the texture, deformation structures and mineral composition for the lithological units. Estimated volume percentages of the mineral assemblage of the samples are given in appendix C. Different characteristic features from the lithological units were emphasized in order to address the aims of the study. For instance, the textural variations for unweathered and weathered basement was examined for comparison and determination of state of weathering, whereas shear structures were studied in the phyllite in order to determine strain gradient and movement of the Caledonian nappe pile. Furthermore, the thin-section analyses was correlated with the field observations to compile a geological evolution of the study area.

3.2.3 Scanning Electron Microscope (SEM) analyses

By means of the Scanning Electron Microscope (SEM) available at the University of Bergen (UiB), thin-sections of weathered basement were examined in order to determine chemical composition of the finer grained material, in which the optical microscope did not provide sufficient details, and to confirm the complete mineralogy of the sample. Backscattered images and calculated chemical compositions are attached in appendix D.

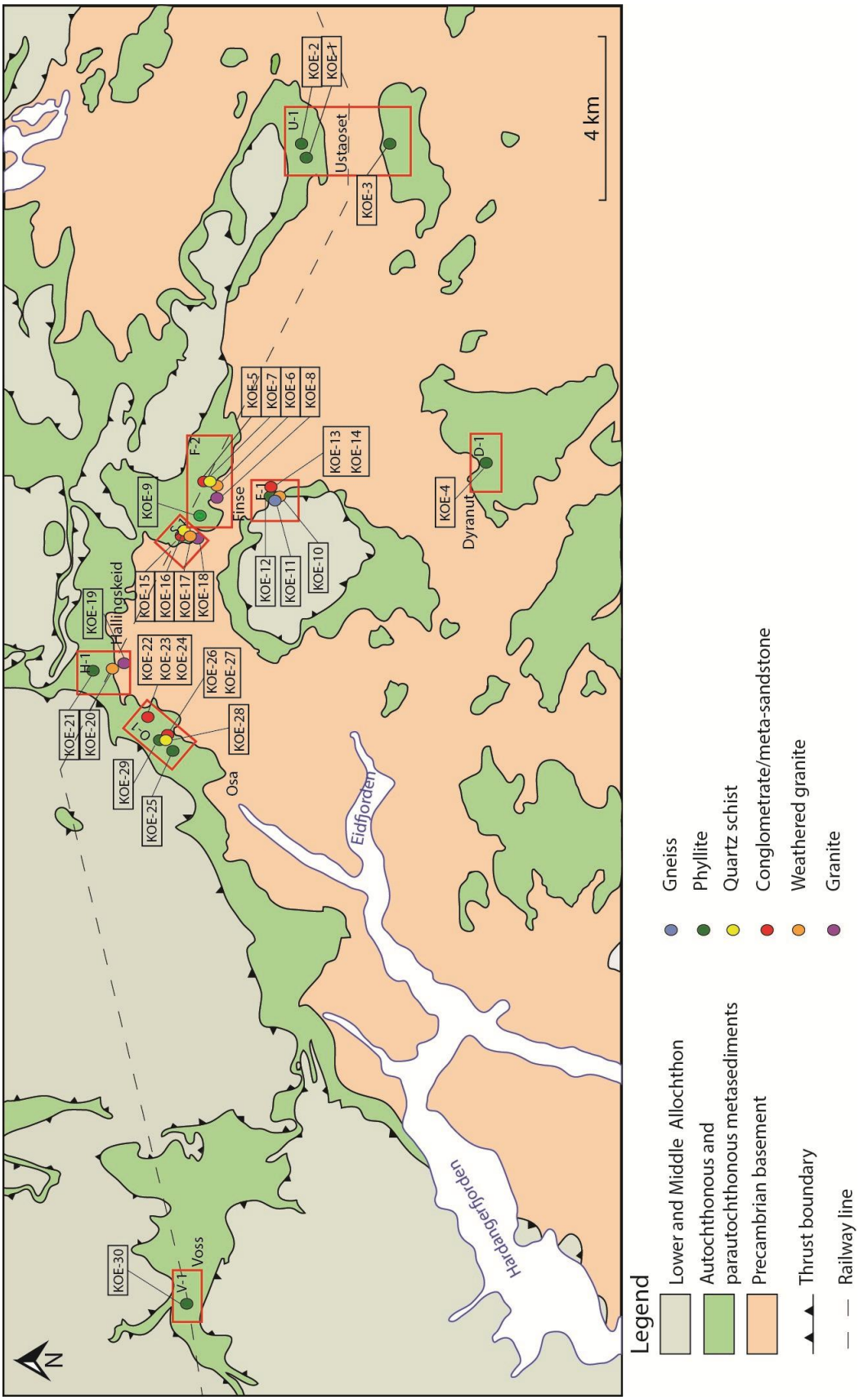

Fig. 9. Overview of the sample locations and sites for structural measurements.

3.3 Limitation of data

3.3.1 Fieldwork and sampling

The field work for the present study was limited to the season of minimum snow cover from mid-July to early September. Because of the abnormal low temperatures in the high mountains during the spring of 2015, some of the main locations were covered by snow until late September, which made it difficult or impossible to examine some of the areas selected for this project. This was specifically the case for the Osafjell area and key localities in the area west of Finse and Hardangerjøkulen. At Hardangerjøkulen, for instance, two blocks containing poorly sorted conglomerate was found close to the contact to the basement (Fig. 19), but the contact was buried under the snow. The trail to Kyrkjedøri at Finse was influenced by unstable snow covers that was dangerous to cross when being alone in the field, thus restricted field mapping.

3.3.2 Thin-section analyses

Considering the determination of the volume percentages of mineral assemblage in the samples, this was done by estimates from thin-section. A suggested point counting in regular grids with same distance between the points would have given more precise values. However, considering the main objectives with the study and the time limits, this was decided to not focus on.

4 Results

The following subchapters will introduce the stratigraphies with lithological descriptions at macro- and micro-scale for the main localities. Deformation structures and microfabrics in the different units are subsequently presented. Finally, the sub-Cambrian peneplain is described from its morphology, and the stratigraphic and lithological properties.

4.1 Lithology and stratigraphy

In overall, the lithologies found at Hardangervidda include Precambrian granites and gneisses, basal conglomerates and meta-sediments, quartz schist, phyllite and, at some locations, gneiss of the Caledonian thrust sheet. At some locations, the Precambrian basement is characterized by a weathered zone located at the transition to the overlying Cambro-Silurian meta-sediments. For this reason, the basement is subdivided in two units which are presented as 1a and 1b and represent the unweathered and weathered granite. Basal conglomerates and meta-sandstones are found in some of the locations, and these are generally overlain by quartz schist.

4.1.1 Finse

In general two stratigraphies are prepared for Finse; one from Jomfrunuten located in the area north of the railway station on Finse (lithostratratigraphy A, Fig. 10), and one NE of the Hardangerjøkulen (lithostratigraphy B, Fig. 10). The main difference is the characteristics of the basal sediment, in which gravel are found on the irregular surface of the basement at Jomfrunuten, whereas meta-sandstone rest at the basement in the Blåisen area, NE of Hardangerjøkulen.

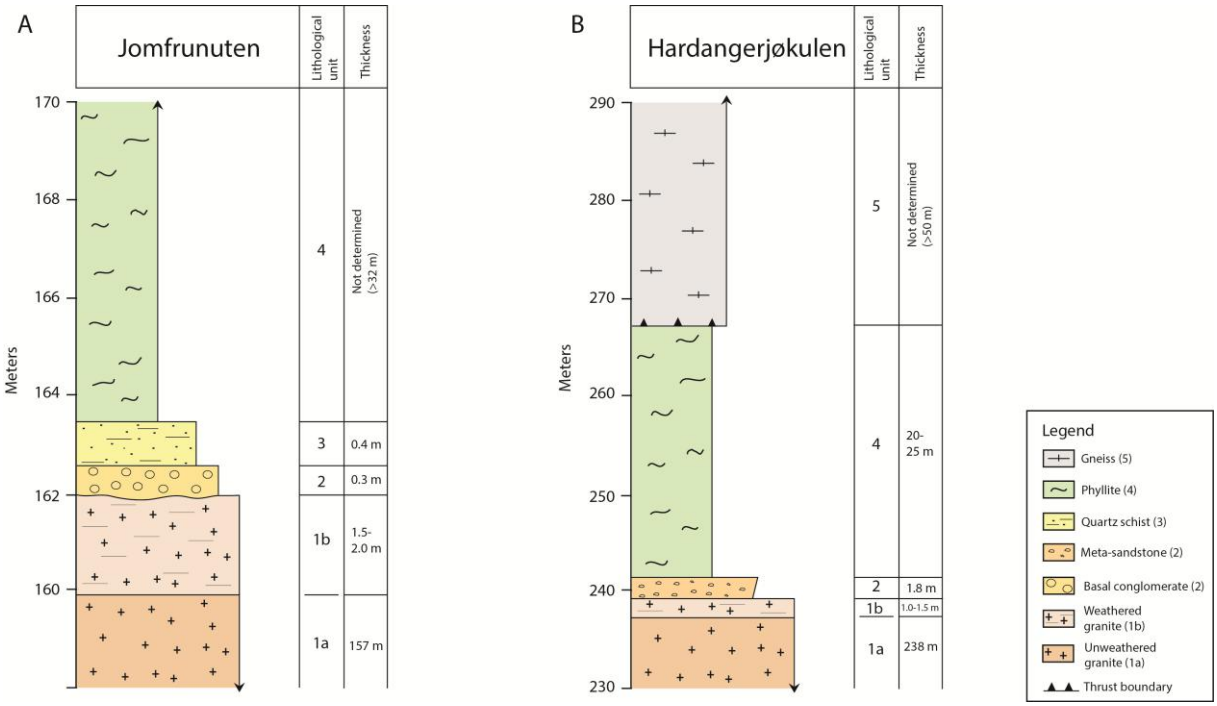

Fig. 10. Simplified lithostratigraphies from Jomfrunuten (A) and from Hardangerjøkulen (B) at Finse.

Unit 1: Unweathered and weathered granite

The unweathered granite at Finse (unit 1a) is inequigranular, composed of phenocrysts of pink or milky white alkali feldspar and elements of moss green epidote (<12 mm), enclosed by minor crystals of quartz and biotite (smaller than 1.1 mm) (Fig. 11a). The phenocrystals normally appear with a subhedral shape, however perfect euhedral crystals of alkali feldspar are sometimes visible (Fig. 11b).

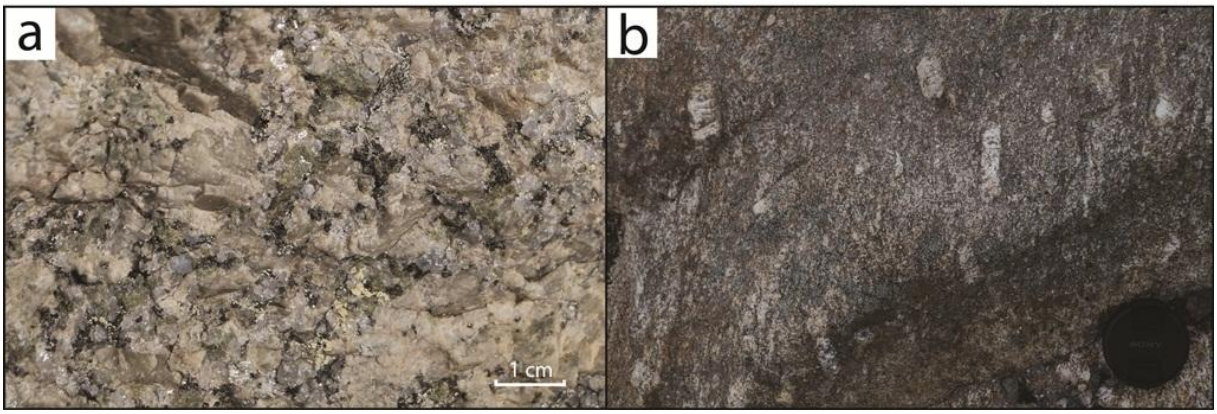

Fig. 11. Characteristics of the unweathered granite at Finse. **a)** The granite has an inequigranular texture composed of pink alkali feldspar and green epidote enclosed by minor crystals of quartz and biotite. **b)** Euhedral crystals of alkali feldspars exposed in the granite on the footpath to Blåisen, Hardangerjøkulen.

The uppermost 1.5-2.0 meters of the basement are unconsolidated and bleached, which is defined as the weathered zone of the basement (unit 1b). At Jomfrunuten the weathered zone mainly appears as gravel in which phenocrysts of alkali feldspar and quartz remain almost unaltered in the fine-grained weathering product composed of white mica and iron-oxides (Fig. 12a). Cross-sections of the weathered granite at Jomfrunuten display thin subhorizontal fractures (~2 mm) sited between less altered zones (~1 cm). The fractures are filled with a fine-grained material composed of mica and iron-oxides, characterized by the rusty brown colour (Fig. 12b).

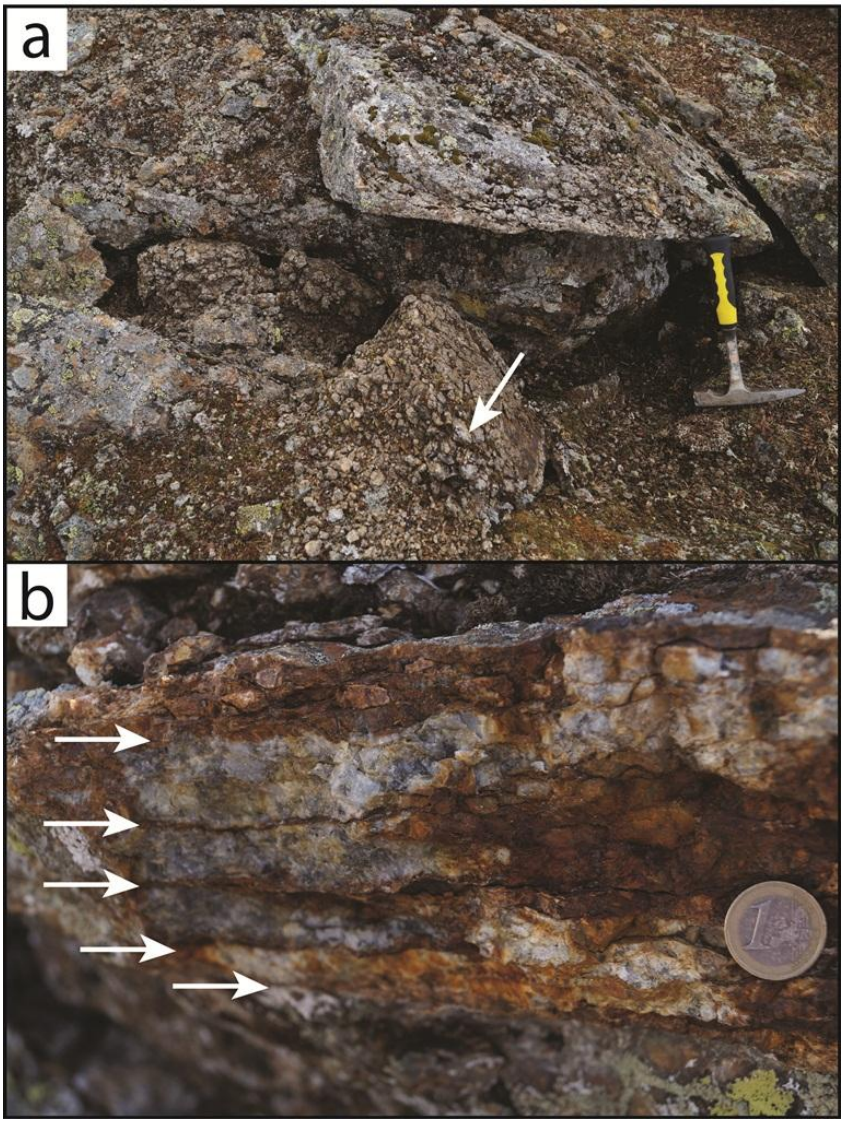

Fig. 12. The appearance of weathered basement located near the transition to the overlying Cambrosilurian meta-sediments. **a)** Intensely weathered basement with residual alkali feldspars and quartz in a fine-grained mass of weathering products, found in the area north of the railway station on Finse. **b)** Subhorizontal fractures (marked with arrows) filled with weathering product, at Jomfrunuten on Finse.

Great textural differences for the unweathered and weathered granites at Finse are indicated by the absence of phenocrystals (Fig. 13a-c), the reduction in crystal size from <4.2 mm to <1.3 mm, and the poorly defined grain boundaries in the weathered granites (Fig. 13b-c). Fractures filled with ferrous material are characteristic for the weathered granite at Jomfrunuten (Fig. 13b) indicating selective chemical weathering along weakness zones.

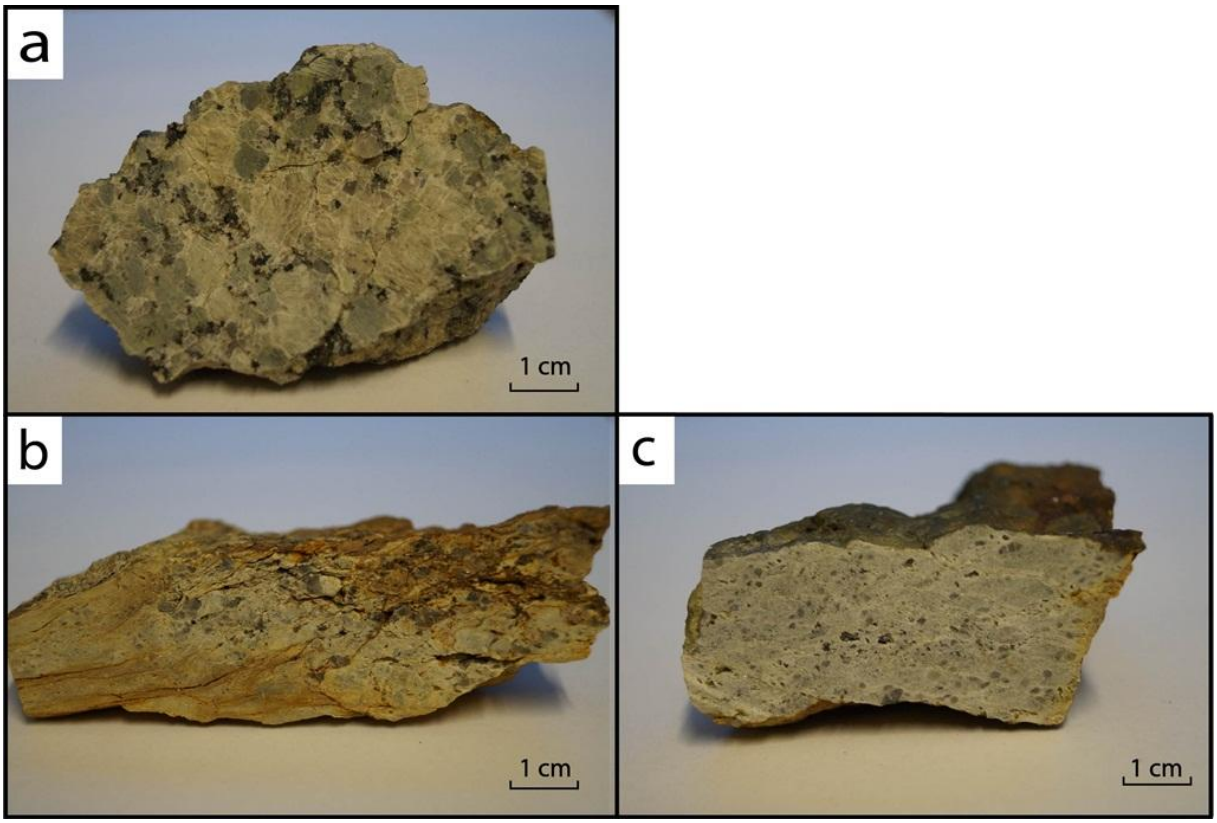

Fig. 13. a) Unweathered holocrystalline granite with well-defined grain boundaries. Sample KOE-8, Finse. **b)** Weathered granite composed of smaller crystals with poorly defined grain boundaries. The cross-section display irregular fractures filled with iron-rich materials. Sample KOE-6, Jomfrunuten. **c)** Weathered granite composed of smaller crystals with poorly defined grain boundaries. Sample KOE-10, Hardangerjøkulen.

Calculated volume percentages and distribution of minerals in the unweathered and weathered granites on Finse are summarized in figure 14. Contrary to the unweathered granite, the proportion of quartz, muscovite and iron-oxides are considerably higher in the weathered granites, whereas the amount of epidote and biotite are less or zero. The amount of microcline and plagioclase in sample KOE-6 is greater and almost equal relative to the unweathered granite, whereas the amount of feldspar is significantly lower in sample KOE-10. The presence of accessory minerals like apatite, titanite and staurolite found in the unweathered granite are lower or lacks in the weathered granites.

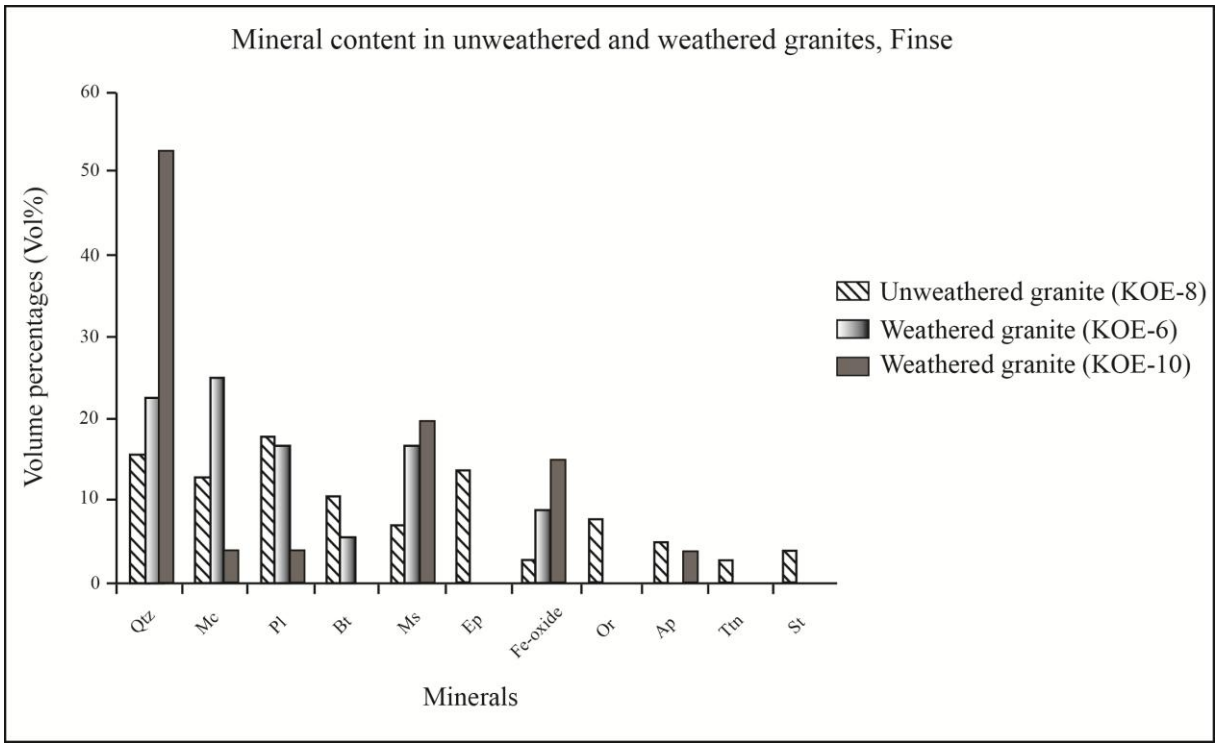

Fig. 14. Estimated volume percentages (Vol%) of the mineral content and distribution in the weathered and unweathered granites at Finse. **Qtz**: Quartz; **Mc**: Microcline; **Pl**: Plagioclase; **Bt**: Biotite; **Ms**: Muscovite; **Ep**: Epidote; **Or**: Orthoclase; **Ap**: Apatite; **Ttn**: Titanite; **St**: Staurolite.

Thin-section analyses indicates clear and well-defined grain boundaries in the unweathered granite (Fig. 15a) compared to the weathered granites characterized by fractured and altered grain boundaries (Fig. 15b, c, e, i). The weathered granite at Jomfrunuten (KOE-6) is penetrated by ~3.4 mm thick fractured zones composed of iron-oxides and sheet silicates (Fig. 15b). These characteristic altered zones lacks in the weathered granite at Hardangerjøkulen (KOE-10), where the granite is only cut by single fractures (Fig. 15c). In the unweathered granite inclusions of finer-grained micas are normally concentrated at or near the core of the plagioclase crystals (Fig. 15d). Compared with the weathered granites, the mica inclusions occur with a greater crystal size and are normally scattered throughout the plagioclases to efface the original crystal habit (Fig. 15e-f). A common feature in the unweathered and weathered granites is the acicular iron-oxides in the biotite crystals that is oriented nearly parallel to the (001) cleavages. In addition, there is a remarkable difference in the intensity of pleochroism of the biotites in the granites, like for instance the difference between the dark olive green-colored biotite in the unweathered granite (Fig. 15g) and the bleached and pale brown-colored biotite in the weathered granite (Fig. 15h).

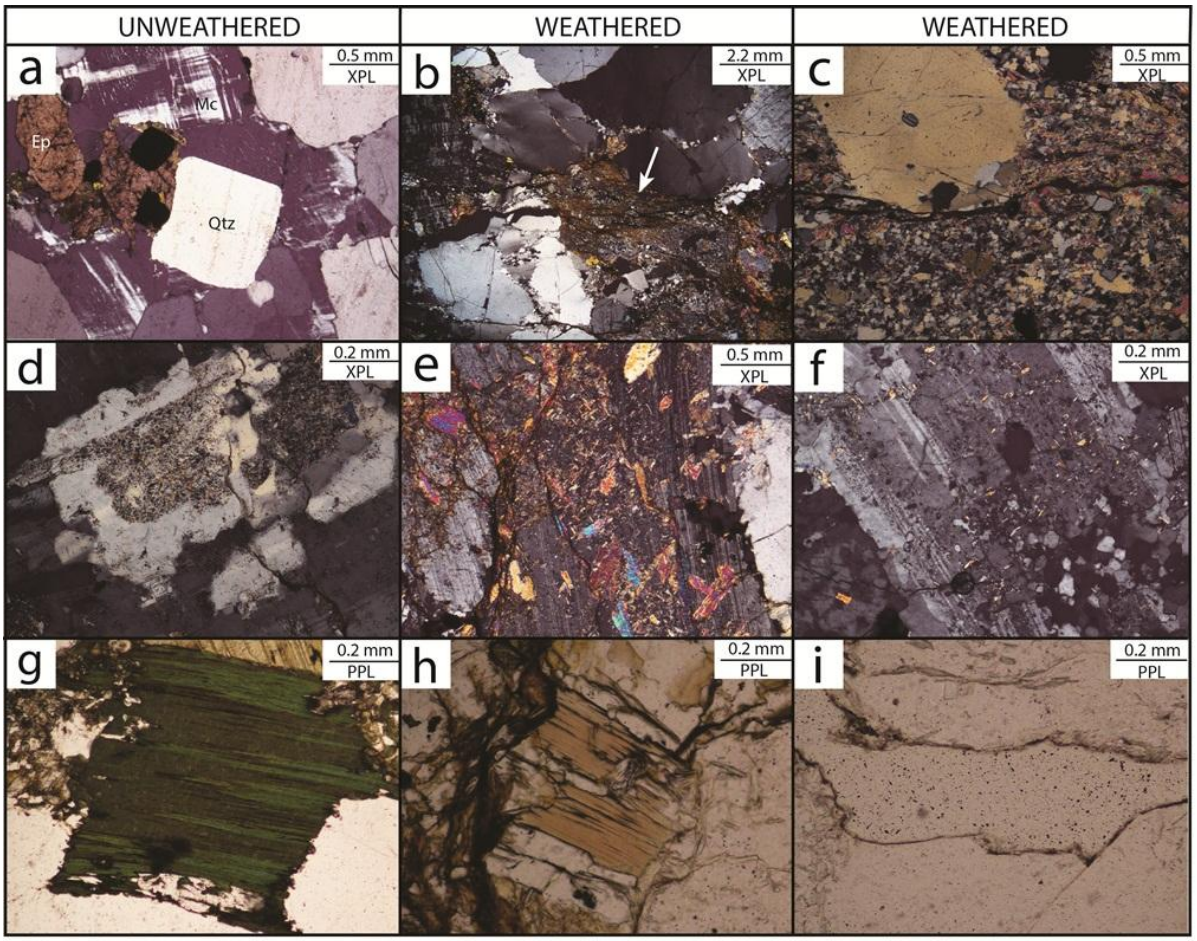

Fig. 15. Grain contacts, inclusions in feldspars and properties of biotite in unweathered granites at Finse (a, d, g) (sample KOE-8), and weathered granites at Jomfrunuten (b, e, h, sample KOE-6) and northeast of Hardangerjøkulen (c, f, i, sample KOE-10). **a)** Sharp grain boundaries between quartz, epidote, microcline and iron-oxides. **b)** Fractured grain boundaries filled with brown colored iron-oxides, subgrains of quartz and feldspar, and micas. **c)** Single fractures presist throughout the sample. **d)** Inclusions of fine-grained micas concentrated in the core of the plagioclase crystal. **e-f)** Larger crystals of white mica scatter the plagioclases. **g)** Dark olive green colored biotite with content of iron-oxides and zircon with pleochroic haloes. **h)** Bleached biotite crystal containing iron-oxides oriented parallel to the cleavage. **i)** Fractured grain boundaries filled by iron-oxides.

SEM-analyses of the fine-grained material that comprising the inclusions in the feldspars and in the altered zones in the granites, reveals well-developed acicular crystals of white mica (Fig. 16a, b). Spot analyses in BSE (Back-scattered Electron Detector) indicates the material to be magnesium-rich, specifically phengite ($K(AlMg)_2(OH)_2(SiAl)_4O_{10}$) (e.g. Mason, 1978; Nesse, 2009). The main differences between the weathered and unweathered granite is the higher weight percentage of magnesium presented in the weathered granite is the higher weight percentage of magnesium presented in the weathered granite, in addition to the well-developed crystals which seem to have a preferred orientation.

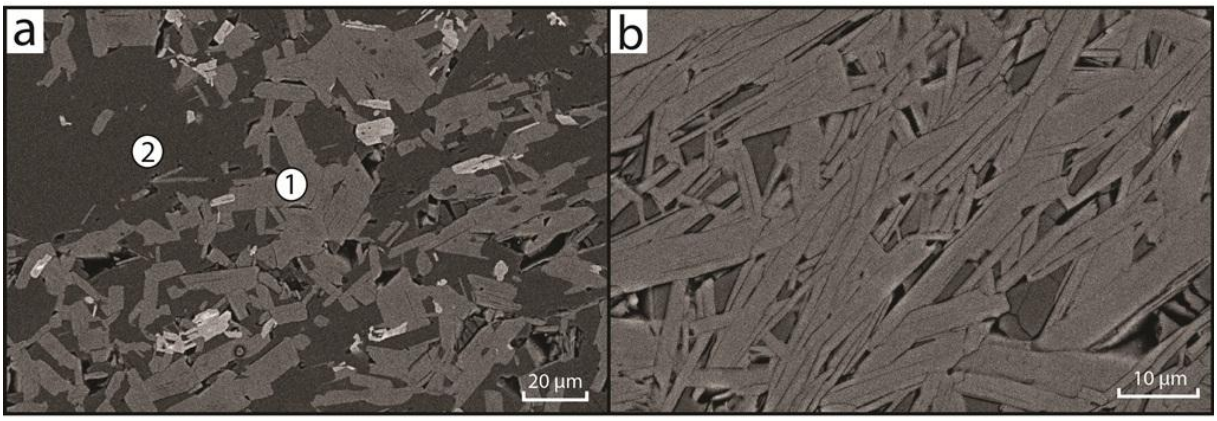

Fig. 16. Backscatter images of the finer-grained material in feldspars in the unweathered granite (sample KOE-8) and altered zones in the weathered granite (sample KOE-6) at Finse. **a)** Randomly oriented phengite crystals (1) sited in the feldspar crystal (2). **b)** Acicular crystals of phengite displayed with a preferred orientation located in the altered zone in the weathered granite.

Unit 2: Basal conglomerate and meta-sandstone

The conglomerate at Jomfrunuten has a thickness of about 30 cm, and is stratigraphically located in a depression in the basement (unit 2 in lithostratigraphy A, Fig. 10) and is overlain by quartz schist. The conglomerate is matrix supported and moderately sorted. The sub-rounded to rounded gravels and pebbles of the conglomerate are mainly composed of quartz with a size ranging from 0.2 mm to 1.0 mm (Fig. 17b). Thin-section analyses reveals a calcite-cemented matrix, with minor amounts of chlorite, iron-oxides, muscovite and apatite (sample KOE-5). Field observations indicates a few internal layers (<1.5 cm) composed of moderately sorted and medium-grained sand.

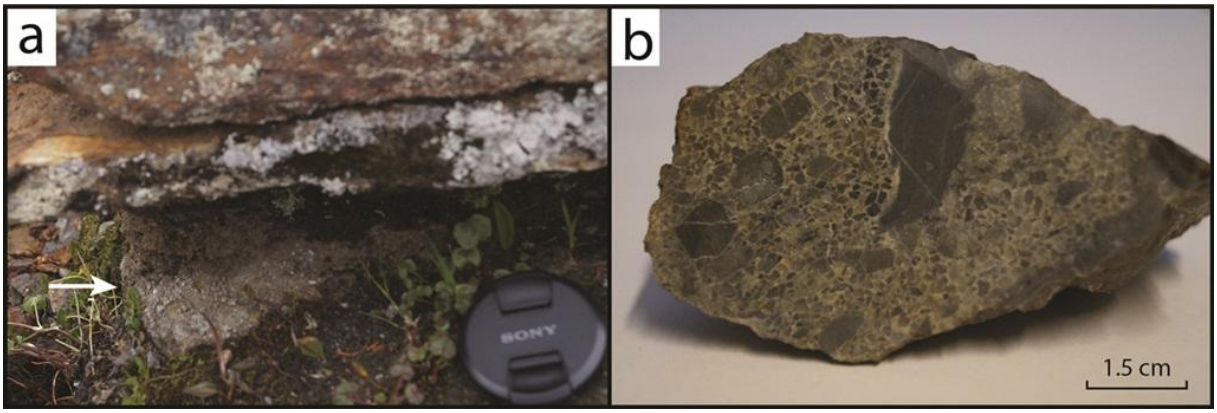

Fig. 17. Basal conglomerate at Jomfrunuten, Finse. **a)** Conglomerate stratigraphically situated between the basement and overlying arkose. **b)** Sampled conglomerate characterized as oligomictic, moderately sorted and matrix supported. Sample KOE-13.

Two distinctive types of meta-sandstones occur in the area northwest of Blåisen (unit 2 in lithostratigraphy B, Fig. 10), which constitute a total thickness of ~1.8 meter. A greyish-black colored medium-grained and well-sorted meta-sandstone rest directly above the basement (Fig. 18a). Thin-section analyses indicate an enrichment of calcite, quartz and biotite (sample KOE-13). About 2-3 meters to the southwest there is a gradual transition into a well sorted and very coarse grained meta-sandstone (0.2 mm to 1.5 mm) scattered with larger crystals of alkali feldspar (Fig. 18b). Thin-section analyses display larger anhedral crystals of quartz and biotite surrounded by fine-grained mica (sample KOE-14).

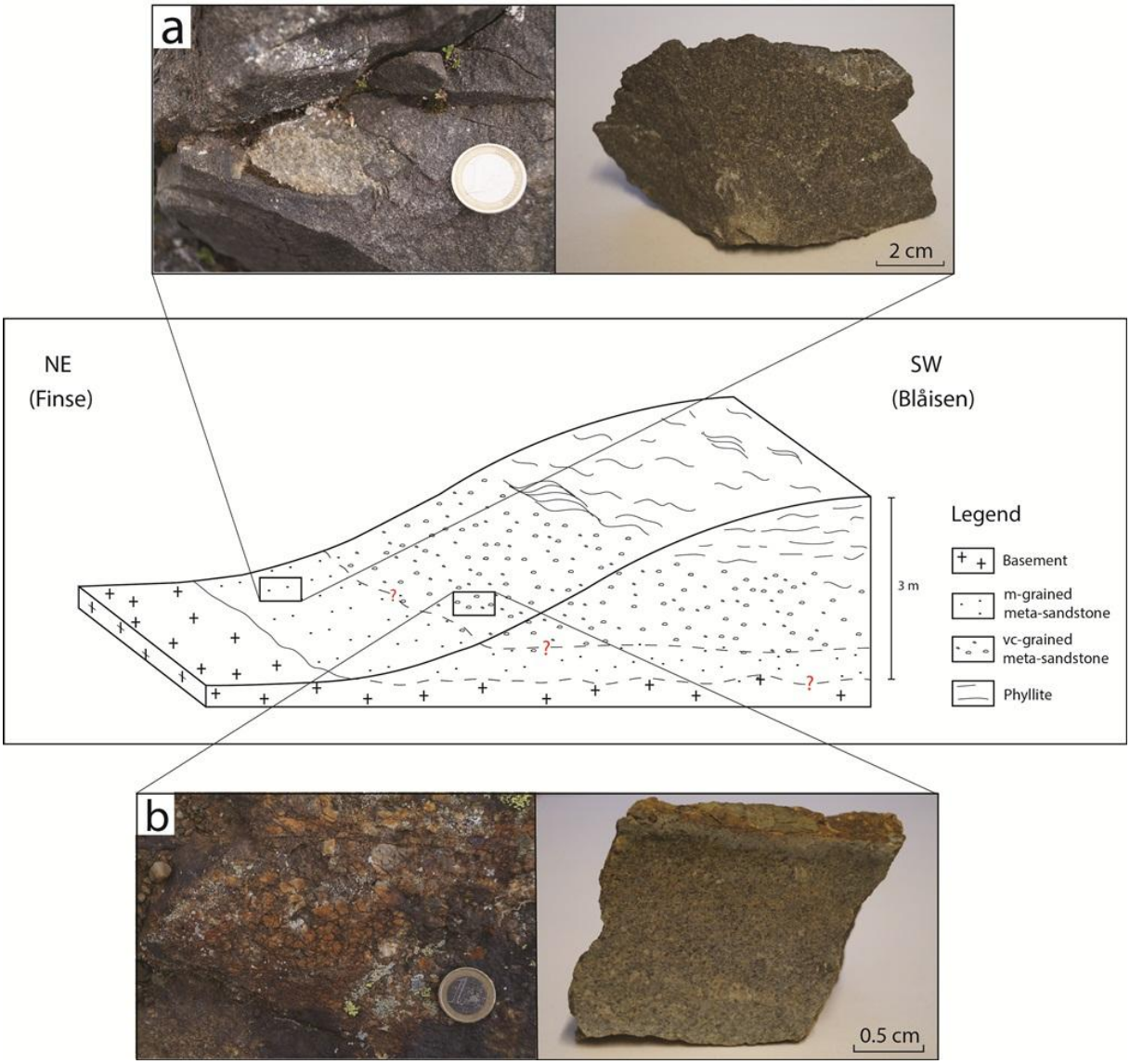

Fig. 18. Overview of the occurrence of meta-sandstones in the area northwest of Blåisen which rest on the basement. **a)** Greyish black sandstone that is randomly scattered with clasts enriched with quartz and feldspar. Sample KOE-13 is illustrated to the right. **b)** Coarse sandstone implicated with crystals of alkali feldspar. Sample KOE-14 is illustrated to the right.

Two blocks of conglomerate rest on the basement a few tens of meters east of the sampling location near Blåisen. The conglomerate is composed of pebbles (<10 cm) composed of granite surrounded by a matrix of phyllite. Subhedral crystals of alkali feldspar are also found in the conglomerate (Fig. 19). One of the blocks includes both segments of the basement and conglomerate that is separated by a sharp boundary which seems to represent the stratigraphic transition between the lithological units. Since the transition between the basement and the phyllite at this location was covered by snow, further detailed studies of a conceivable present conglomerate were not possible. Samples were not collected from the blocks with respect to the uncertainty of their origin and distance to the source.

Fig. 19. Block displaying the transition between Precambrian basement rock (left side of the dashed line) and poorly sorted conglomerate, found NE of Hardangerjøkulen. See text for further descriptions of the conglomerate.

Unit 3: Quartz schist

The quartz schist at Jomfrunuten on Finse constitutes a thickness of approximately 40 cm. It has a rusty orange color and is slightly foliated. The quartz schist is well-sorted and fine-grained, and thin-section analyses indicates a main composition of quartz and micas with minor amounts of feldspar and iron-oxides. A great and suggested top-surface of the quartz

schist is exposed at this location, in which well-preserved symmetrical north-trending ripple marks are found (Fig. 20).

Fig. 20. Extant north-trending wave ripple marks in the quartz schist at Jomfrunuten on Finse.

Unit 4: Phyllite

The phyllite at Finse is charactericed by the greyish black color and well-developed foliation which occurs in straight planes and have a metallic luster. Segregated quartz lenses occur locally in the phyllite, with a lower amount at Hardangerjøkulen compared to in the phyllite in the areas at Jomfrunuten and Store Finsenuten. This is also indicated from petrographic analyses as the phyllite at Hardangerjøkulen (KOE-12) has a lower content of quartz (24 %) compared to the phyllite at Store Finsenuten (KOE-9) (38%).

Unit 5: Gneiss

The remnants of the Caledonian nappe found at Hardangerjøkulen, mainly comprises a bright grey colored and fine-grained gneiss (Fig. 21a). Thin-section analyses indicates alternating layers composed of quartz and feldspar, and additional amounts of mica, including biotite and muscovite, and some crystals of calcite are found. Acicular iron-oxides appear as accessory phases in the sample. Gneissic banding constitutes the mylonitic texture, in which the distance between the foliation domains are in millimeter to centimeter scale. Intrusions composed of

crystalline and felsic material occur locally with a thickness about 43 cm (Fig. 21b). Additionally, undulating veins of feldspar and quartz (~0.5 cm) occurs.

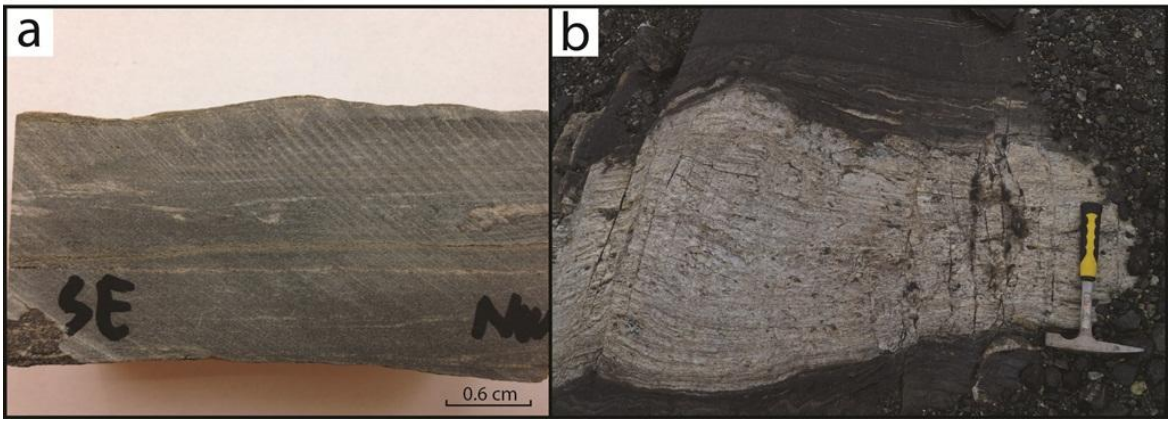

Fig. 21. Mylonitic gneiss at Hardangerjøkulen. **a)** Fine-grained and bright colored gneiss with foliation domains with millimeter scale distances. Undulating and deformed small scale veins of quartz and feldspar are displayed in the cross-section. Sample KOE-11. **b)** Bright colored crystalline intrusion that is locally found in the nappe pile. Note the thin, undulating veins of feldspar sited above the intrusion.

4.1.2 Sandå

The litostratigraphy presented at Sandå is almost similar to the stratigraphy at Jomfrunuten on Finse, with exception of the thickness of the different lithologies and some characteristic features which are following described. Basal conglomerate rest on a weathered zone of the basement, and furthermore the conglomerate is overlain by quartz schist (Fig. 22).

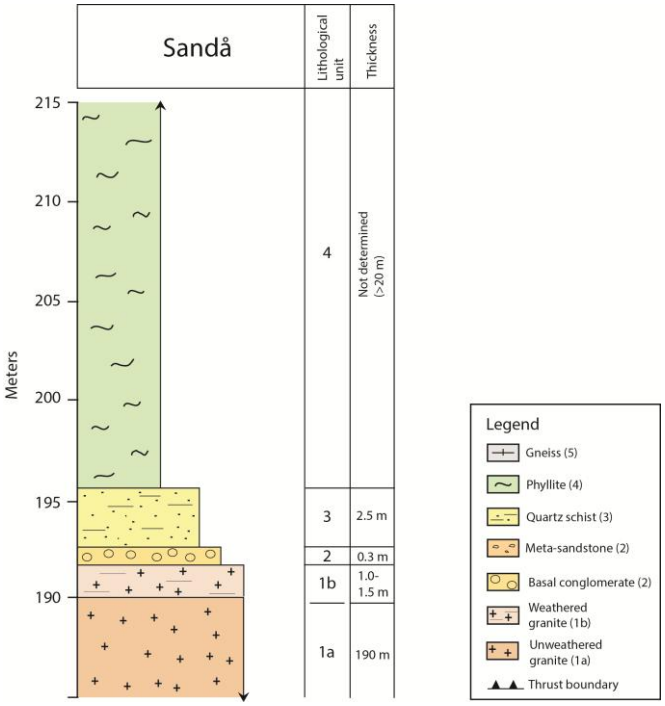

Fig. 22. Simplified lithostratigraphy from Sandå.

Unit 1: Unweathered and weathered granite

The unweathered granite on Sandå (unit 1a) is holocrystalline and has a phaneritic texture, in which larger crystals of quartz and pink colored alkali feldspar (~6 mm) are enclosed by minor crystals of quartz and biotite (~1 mm) (Fig. 24a). The uppermost zone of the basement appears as weathered and unconsolidated (unit 1b), indicated by remnants of quartz and alkali feldspar surrounded by a fine-grained ferrous and micaceous-rich material (Fig. 23).

Fig. 23. Intensively weathered basement at Sandå with remnant crystals of alkali feldspar and quartz.

The main textural variations for the unweathered and weathered granites at Sandå are the smaller grain size (<6 mm to <3 mm) and poorly defined grain boundaries in the weathered granite (Fig. 24a-b). A distinct outer weathering rim with a thickness of 1-1.5 cm consisting of iron precipitations, quartz and alkali feldspar is distinctive for the weathered sample (Fig. 24b). Several fractures that commonly follow the grain boundaries of the alkali feldspars are also presented in the weathered granite.

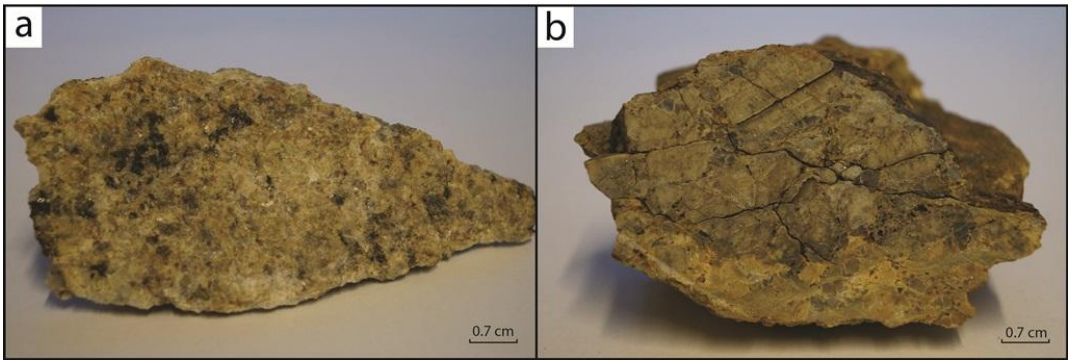

Fig. 24. a) Unweathered holocrystalline granite with defined grain boundaries. Sample KOE-18. **b)** Stained weathered granite with a characteristic outer weathering rim and internal fractures that follows the grain boundaries, especially the alkali feldspars. Sample KOE-17.

The mineral distribution in the unweathered and weathered granites clearly indicates a significantly higher content of muscovite, in addition to iron-oxides and microcline in the weathered granite (Fig. 25). Especially notice the significant difference in volume percentage of muscovite constituting 16 % for the unweathered and the weathered granite. The presence of plagioclase, epidote and biotite are slightly lower or lacks in the weathered granite.

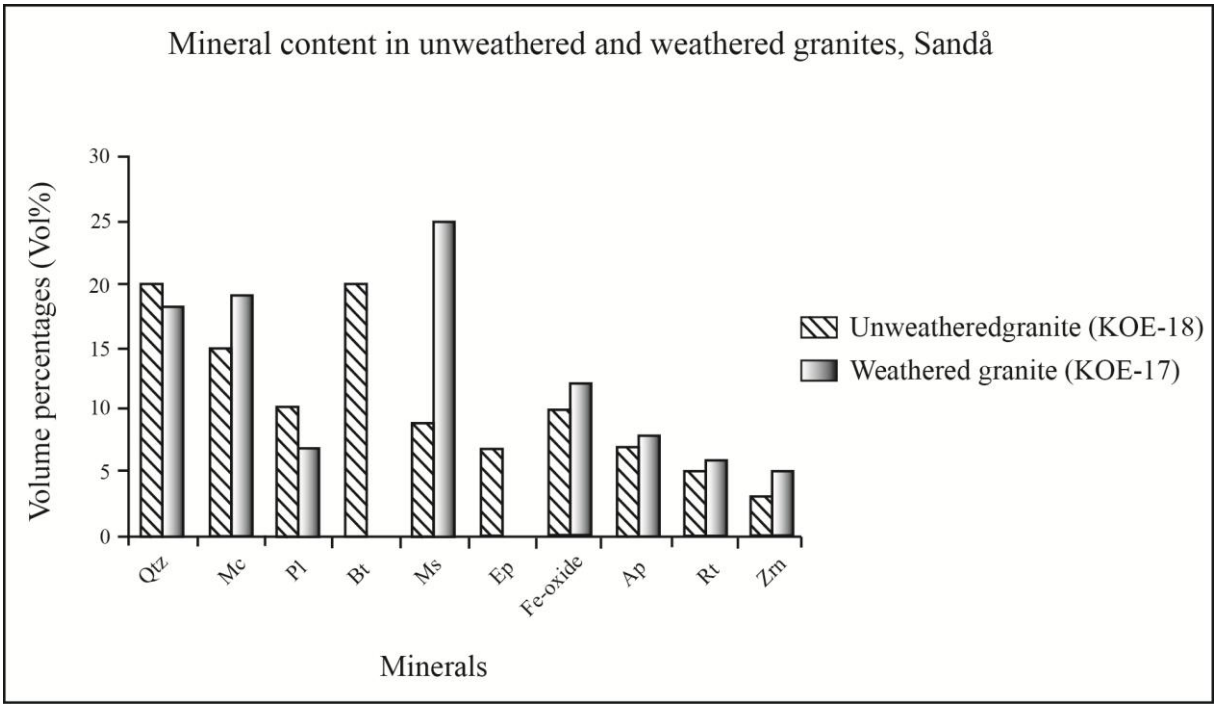

Fig. 25. Estimated volume percentages (Vol%) of the mineral content and distribution in the weathered and unweathered granites at Sandå. **Qtz**: Quartz; **Mc**: Microcline; **Pl**: Plagioclase; **Bt**: Biotite; **Ms**: Muscovite; **Ep**: Epidote; **Or**: Orthoclase; **Ap**: Apatite; **Rt:** Rutile; **Zrn**: Zircon.

The grain boundaries appear as defined and irregular in the unweathered granite (Fig. 26a), whereas in the weathered granite the grains are separated by single fractures and altered zones composed of mica, iron-oxides and subgrains of quartz (Fig. 26b). Albite-rich lamellae are found in the microclines in the unweathered and weathered granites (Fig. 26c-d). Additional fractures filled with iron-oxide and mica truncates the feldspar in the weathered granite (Fig. 26d). Most of the plagioclases in the weathered granites are highly sericitized (Fig. 26f). The biotites are characterized by a strong pleochroism in the unweathered granite (Fig. 26e), whereas biotite lacks in the weathered granite (Fig. 25).

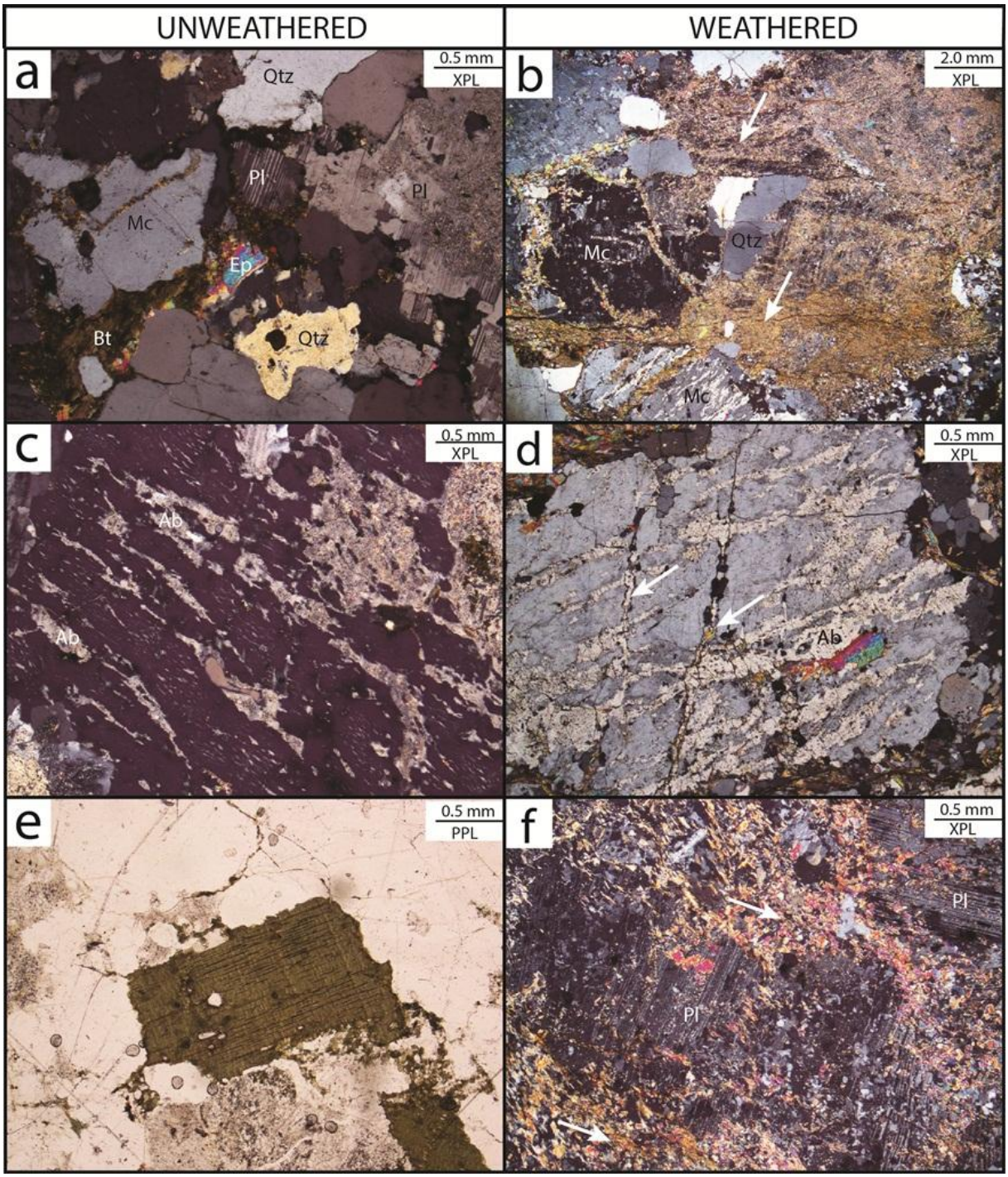

Fig. 26. Grain contacts, inclusions in feldspars and features of biotite in unweathered (a, c, e, sample KOE-18) and weathered granites at Sandå (b, d, f, sample KOE-17). **a)** Defined and irregular grain boundaries between quartz, microcline, plagioclase, epidote, biotite and iron-oxide in the unweathered granite. **b)** Interaction of larger grains of quartz, surrounded by weathering products. **c)** Altered albite-rich lamellae in microcline. **d)** Altered albite-rich lamellae and intersected fractures filled with mica and iron-oxide in the microcline crystal. **e)** Olive green biotite surrounded by quartz and clouded feldspars. **f)** Highly sericitized plagioclase crystal. The habit of the crystal is no longer visible.

Spot analyses in BSE indicates the fine-grained material in feldspar and the altered zones in the unweathered and weathered granites to be phengite, in which the amount of magnesium, iron and barium in the phengite crystals is larger in the weathered granite (Appendix D).

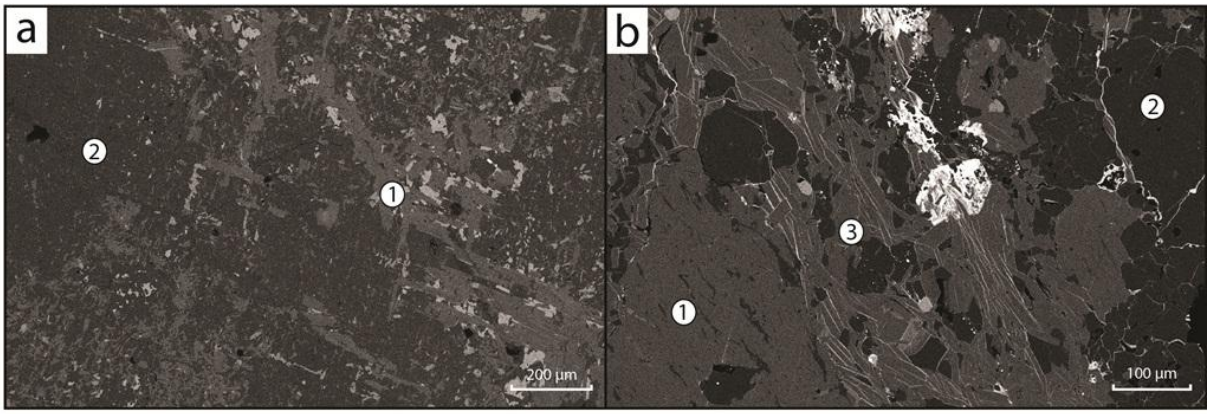

Fig. 27. Backscattered images of the finer-grained material in feldspar found in the unweathered granite (sample KOE-18), and in the altered zones in the weathered granite (sample KOE-17) at Sandå. **a)** Phengite is displayed as the bright grey material (1) between darker grey and albite-rich plagioclase (2). **b)** Altered Mg-rich phyllosilicate (phengite) are displayed as the bright material in the altered zone, located among the K-feldspar (1, 2).

Unit 2: Basal conglomerate

The conglomerate is resting directly on the unweathered to slightly weathered basement (Fig. 28a), and constitutes a total thickness of 30 cm. The grain size ranges from very coarse sand to gravel (0.2-2.0 cm) and the clast are mainly rounded consisting of quartz and alkali feldspars (Fig. 28b). In overall the conglomerate is composed of alternating zones of well-sorted medium sand, and zones consisting of poorly-sorted sand (0.5-2.0 cm) scattered by crystals of alkali feldspar. Thin-section analyses reveals a fine-grained carbonate-rich matrix.

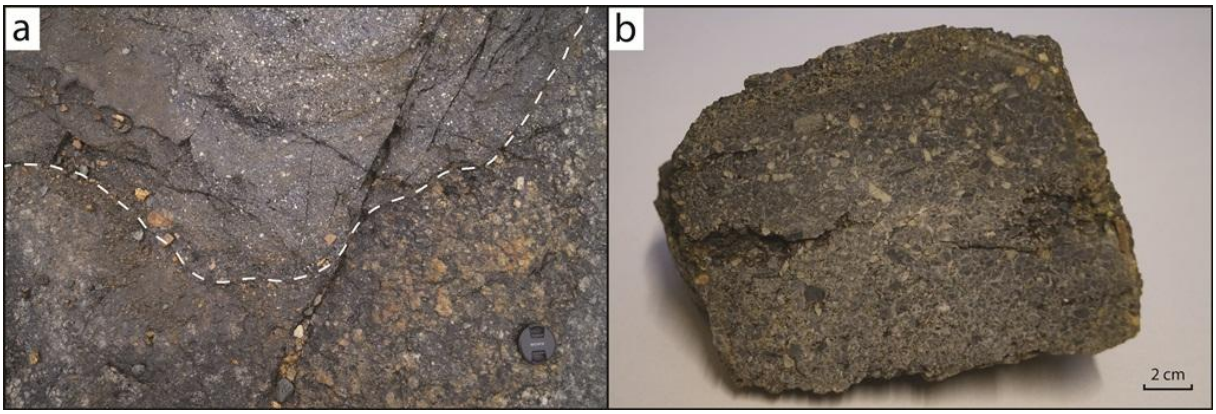

Fig. 28. Basal conglomerate at Sandå. **a)** The conglomerate, located above the dashed line, rest on the basement and the sub-Cambrian peneplain. **b)** Cross-section of the conglomerate. Sample KOE-15. See text for further description.

Unit 3: Quartz schist

The quartz schist at Sandå is found above the basal conglomerate (Fig. 29a) and appears with an overall thickness of 2.5 meters. The stratigraphic transition between the quartz schist and the overlying phyllite seem to be gradual, as quartz schist is mixed with the lowermost section of the phyllite unit.

The quartz schist is characterized by a rusty brown color, and well-developed foliation occurs in wavy to straight planes (fig. 29b). Thin quartz veins (0.6 cm thick) are locally found in the quartz schist, in which some of them appear as parasitic folds (Fig. 29c). Thin-section analyses (sample KOE-16) indicates a main composition of quartz and muscovite, in addition to some iron oxides.

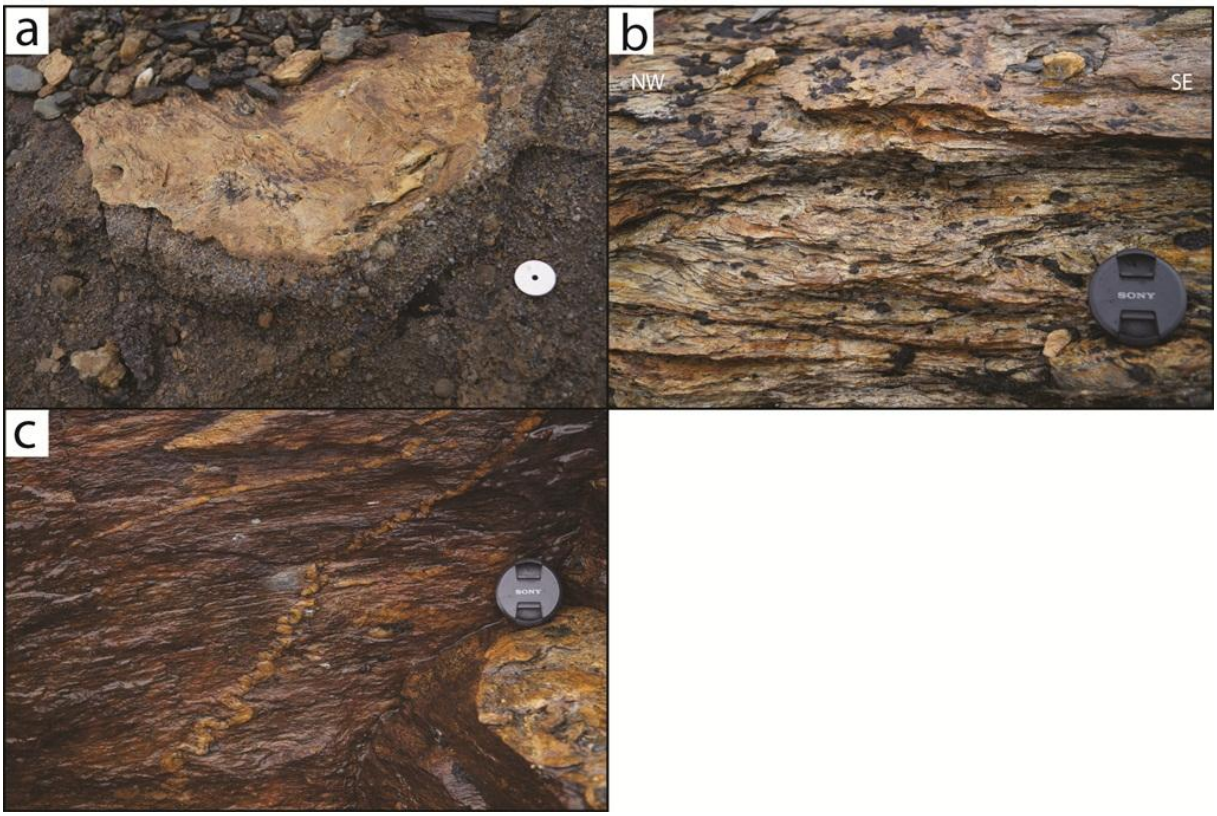

Fig. 29. Characteristics of the quartz schist at Sandå. **a)** The quartz schist is located directly on the basal conglomerate indicated by the sharp transition. **b)** The quartz schist occurs with an orange surface color and is characterized by the planar to slightly wavy foliation. **c)** Ptygmatically folded quartz veins in the quartz schist.

Unit 4: Phyllite

The phyllite at Sandå has a dark grey color and the wavy foliation planes have a metallic luster. Compared to the other main locations, the phyllite at Sandå show limited or lacks quartz veins. Most of the outcrops were covered by lichen.

4.1.3 Hallingskeid

From the railway station at Hallingskeid and further to the NW along the Rallarvegen, the different lithologies of the stratigraphy are presented (Fig. 30). The Precambrian basement is mainly composed of granite, however zones of gneiss are also found. A weathered upper zone of the basement is located in the transition to the overlying phyllite.

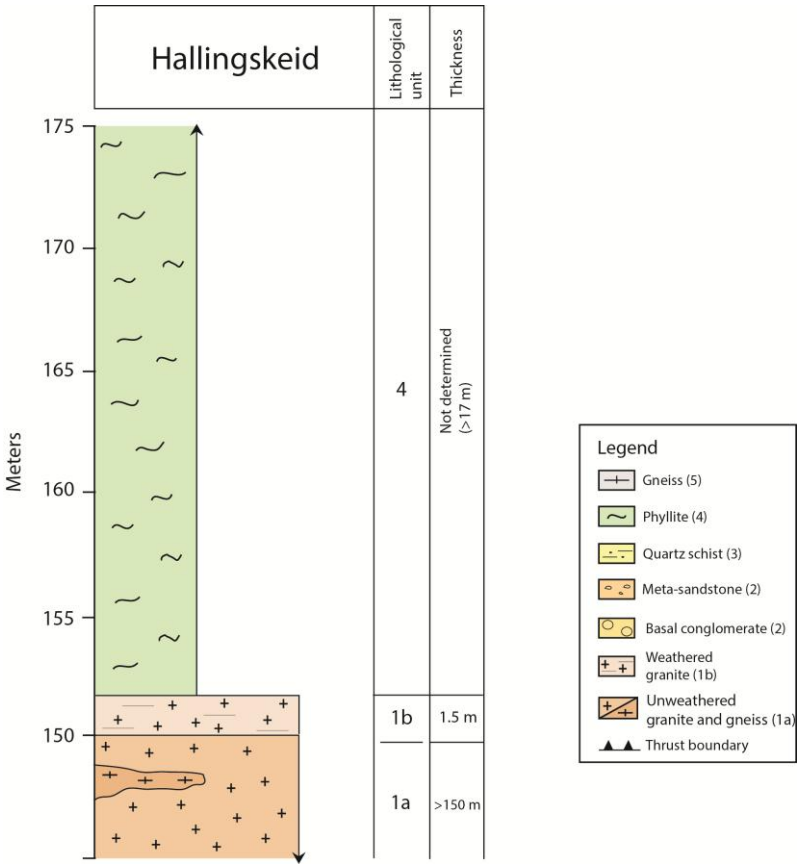

Fig. 30. Simplified lithostratigraphy at Hallingskeid.

Unit 1: Unweathered and weathered granite

The granite at Hallingskeid (unit 1a) is composed equigranular of quartz, alkali feldspar and biotite with an average crystal grain size of 1.5 mm. A minor zone of augen gneiss are found along Rallarvegen, which is characterized by oval phenocrysts of alkali feldspar and quartz enclosed in a greyish black colored and fine-grained mass that is slightly foliated (Fig. 31a). The gneiss is intruded by fine-grained dikes of granite which are truncated by thin calcite-filled fractures (3 mm-1 cm). The uppermost 1.5 meters of the basement represent a weathering zone (unit 1b) which appears as massive and has a smooth and brown colored surface (Fig. 31b).

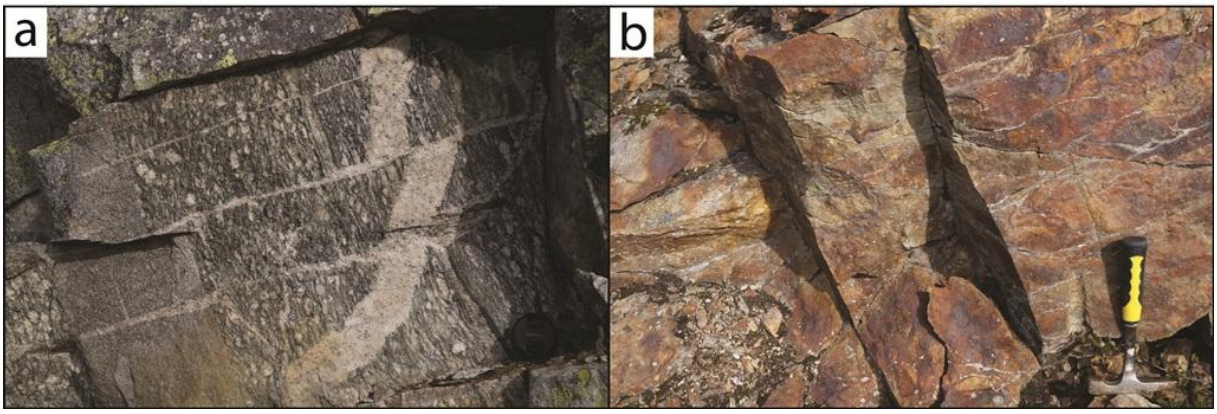

Fig. 31. a) Gneiss occur among the granite of the Precambrian basement at Hallingskeid. Intrusions of granitic dikes are truncated and displaced by fractures filled by calcite. Camera lens for scale. **b)** Bleached and weathered basement.

Textural variations between the unweathered and weathered granite (Fig. 32a-b) are mainly determined by the diffuse grain-boundaries, randomly fractures and the lack of the dark biotites in the weathered granite. In addition, the weathered sample is characterized by a ~2.5 cm wide weathering rim (Fig. 32b), similar to what is observed for the weathered granite at Sandå.

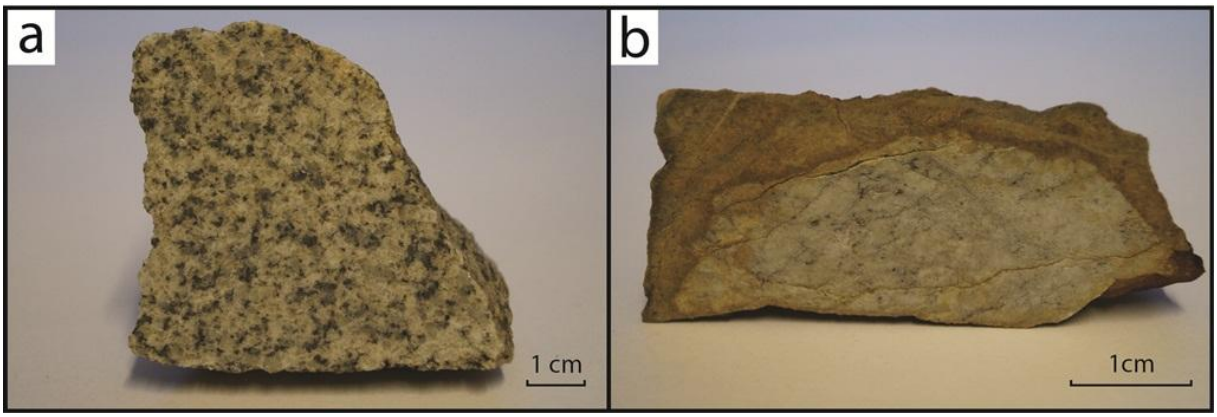

Fig. 32. a) Unweathered equigranular granite with defined grain boundaries. Sample KOE-19. **b)** Weathered granite with an iron-stained outer weathering rim and internal fractures. Sample KOE-20.

Mineral distribution in the unweathered and weathered granites clearly indicates a higher concentration of muscovite, iron-oxides and stable minerals as microcline in the weathered granite, in addition to a lower content of epidote, biotite and plagioclase (Fig. 33).

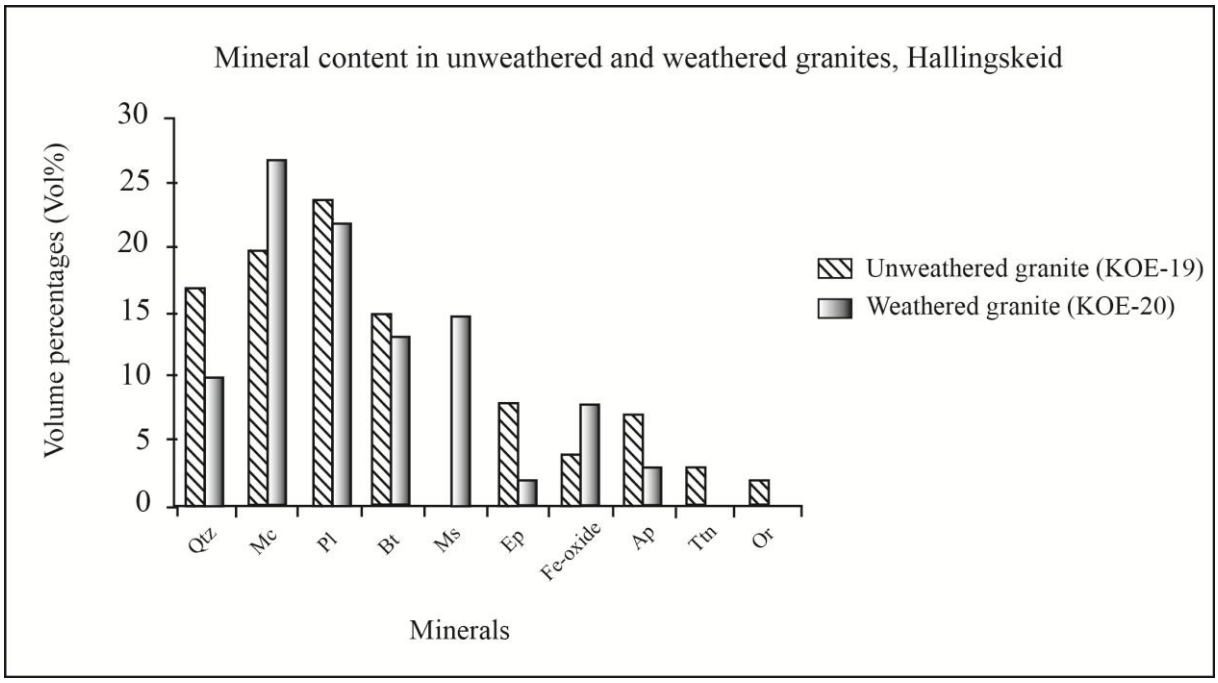

Fig. 33. Estimated volume percentages (Vol%) of the mineral content and distribution in the weathered and unweathered granites at Hallingskeid. **Qtz**: Quartz; **Mc**: Microcline; **Pl**: Plagioclase; **Bt**: Biotite; **Ms**: Muscovite; **Ep**: Epidote; **Ap**: Apatite; **Ttn:** Titanite; **Or**: Orthoclase.

Optical microscope analyses indicates well-defined grain boundaries in the unweathered granite (Fig. 34a) compared to the weathered granite of which the grains are internally fractured and surrounded by altered products like muscovite and iron-oxides (Fig. 34b). Restricted differences in the content of inclusions in the plagioclases are observed for the two granites (Fig. 34c-d). In fact, the plagioclases in the weathered granite have a lower content of inclusions and are displayed as subhedral crystals compared to the unweathered granite. Biotite appears with a strong pleochroism in both the unweathered and weathered granites (Fig. 34e-f). However, measurement of the c-axis of the biotites in the two granites indicates a slightly difference in grain size, from 0.2 to 0.6 mm.

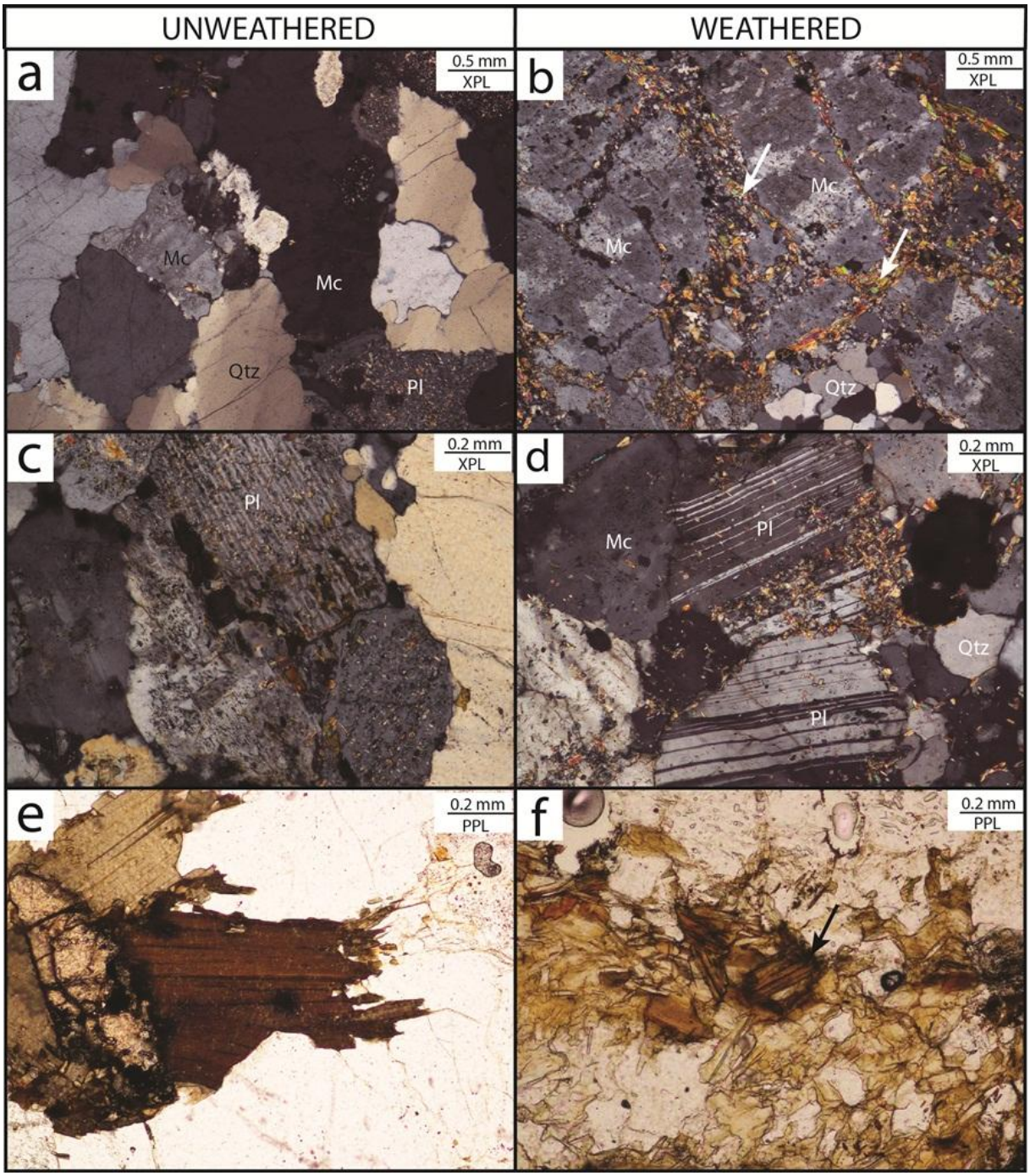

Fig. 34. Thin-section photographs of unweathered (a, c, e, sample KOE-19) and weathered (b, d, f, sample KOE-20) granites at Hallingskeid. **a)** Well defined grain boundaries between quartz, microcline and plagioclase. **b)** Inclusions of white mica in plagioclase. **c-d)** Plagioclase crystals showing sub to euhedral shape, characteristic polysynthetic twinning and inclusions of white mica. **e)** Dark brown colored biotite appears with strong pleochroism and contains spots of zircons surrounded by pleochroic haloes. **f)** Small grained and brown colored biotite crystals occur as aggregates in the weathered granite.

Chemical analyses of the finer grained material located in the feldspar crystal in the weathered granite (Fig. 35) indicates clay minerals with content of magnesium, iron, barium and titanium (Appendix D). By comparing the weight percentages of these elements with the ones at Sandå and Finse, the amounts of the metals are somewhat lower at Hallingskeid.

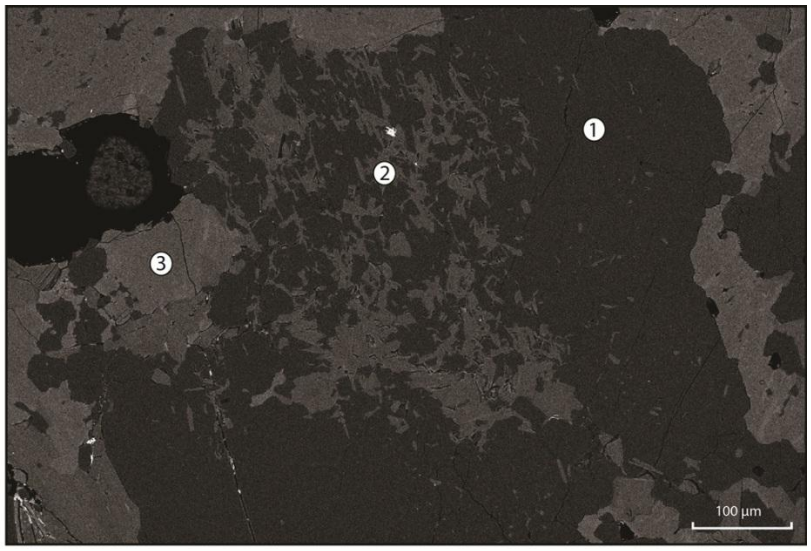

Fig. 35. Backscatter image of altered K-feldspar in the weathered granite at Hallingsked (sample KOE-20). Phyllosilicates (2) are seen as the bright material enclosed in the dark colored K-feldspar (1, 3).

Unit 4: Phyllite

The phyllite at Hallingskeid is well-foliated that occurs with wavy planes. It has a greyish black color and a large content of quartz veins (Fig. 36a) compared to the phyllites at the other main locations. Some of the quartz lenses are calcareous, as indicated by the yellowish-brown colored spots. Petrographic studies indicate that besides the content of quartz and muscovite, minerals like garnet and chlorite appear in the phyllite (Fig. 36b).

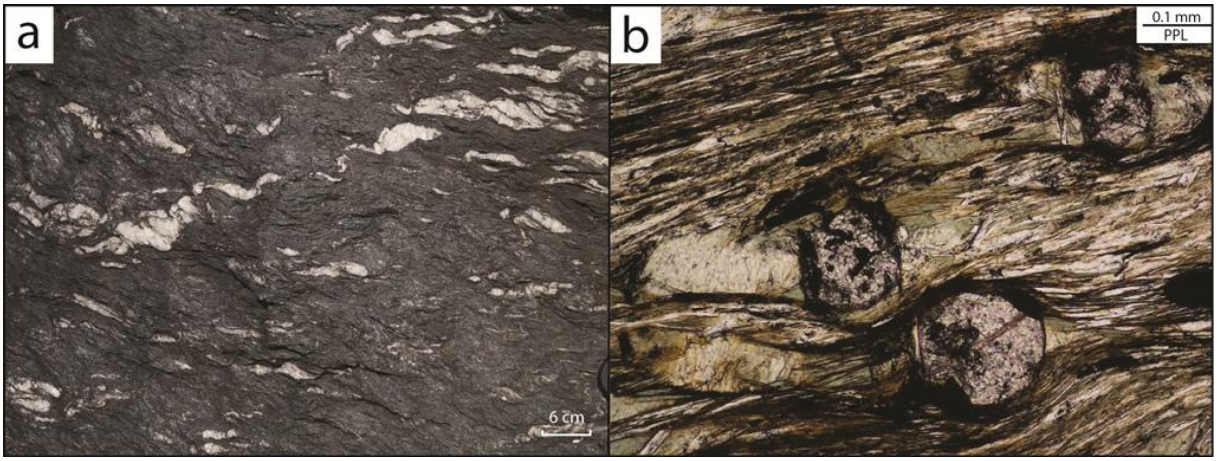

Fig. 36. a) Greyish black colored phyllite with a high content of segregated quartz veins. **b)** Garnet and chlorite surrounded by white mica and quartz. Sample KOE-21.

4.1.4 Osa

Two stratigraphies are presented for the location at Osa (Fig. 37); one from Buadalsbrotet (A), and the other from the area close to Hegrenuten (B). The main difference is the presence of quartz schist on Hegrenuten (unit 3), and the slightly different character of the phyllite which is following described.

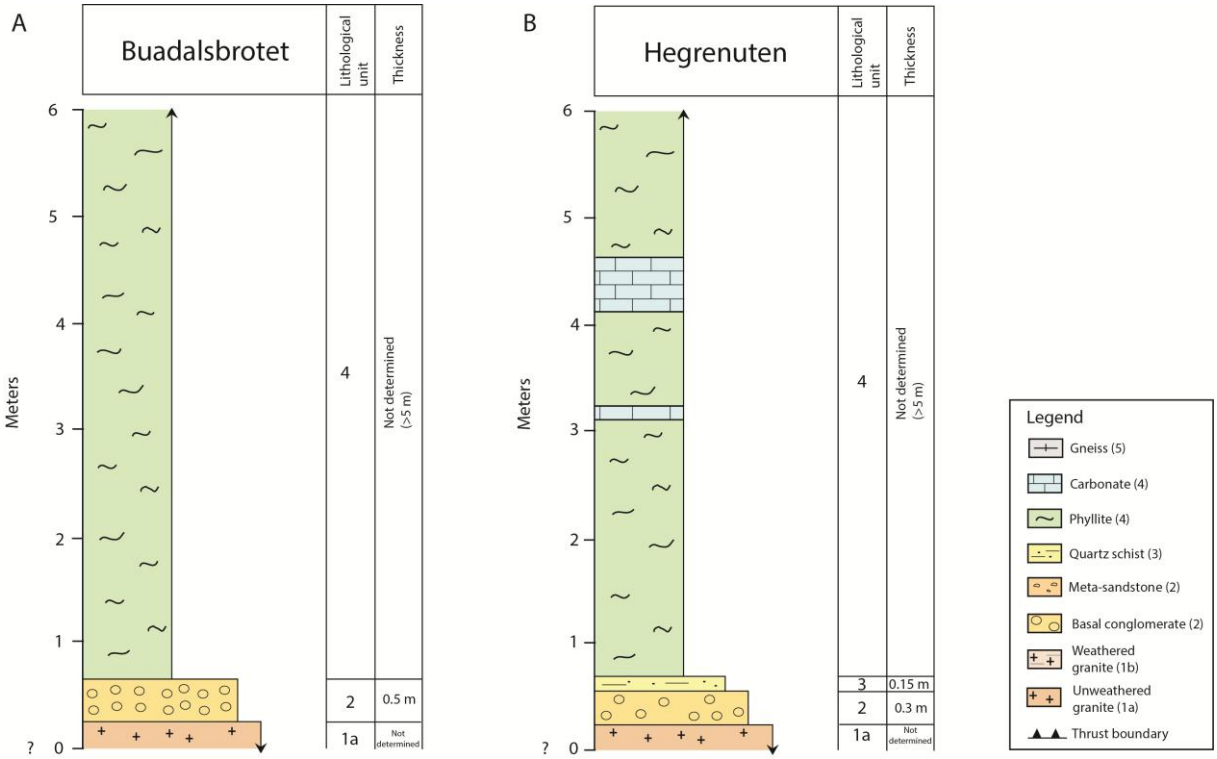

Fig. 37. Simplified lithostratigraphies from Buadalsbrotet (A) and Hegrenuten (B) at Osa.

Unit 2: Basal conglomerate

At Buadalsbrotet (unit 2 in lithostratigraphy A, Fig. 37) the conglomerate is poorly sorted and occurs as polymict composed of gneiss (Fig. 38a), granite and quartzite. The size of the clasts is polymodal, varying from 6.6 cm to as much as 51 cm (measured of longest axis). The mean size frequency is, however, in a range between 23 cm to 34 cm. The largest clasts show a subangular shape, and the degree of roundness increases in proportion to the decreasing grain size. The conglomerate is matrix supported that mainly is composed of phyllite (Fig. 38b) and constitutes 25 % of the conglomerate. An elongated zone with a thickness of about 18 cm crops out in the conglomerate (Fig. 38). In this zone, the matrix appears as coarse-grained,

and further micro-scale studies indicate a composition of well-rounded quartz grains (<3 mm) surrounded by opaque material, calcite and smaller grains of quartz (Fig. 38c).

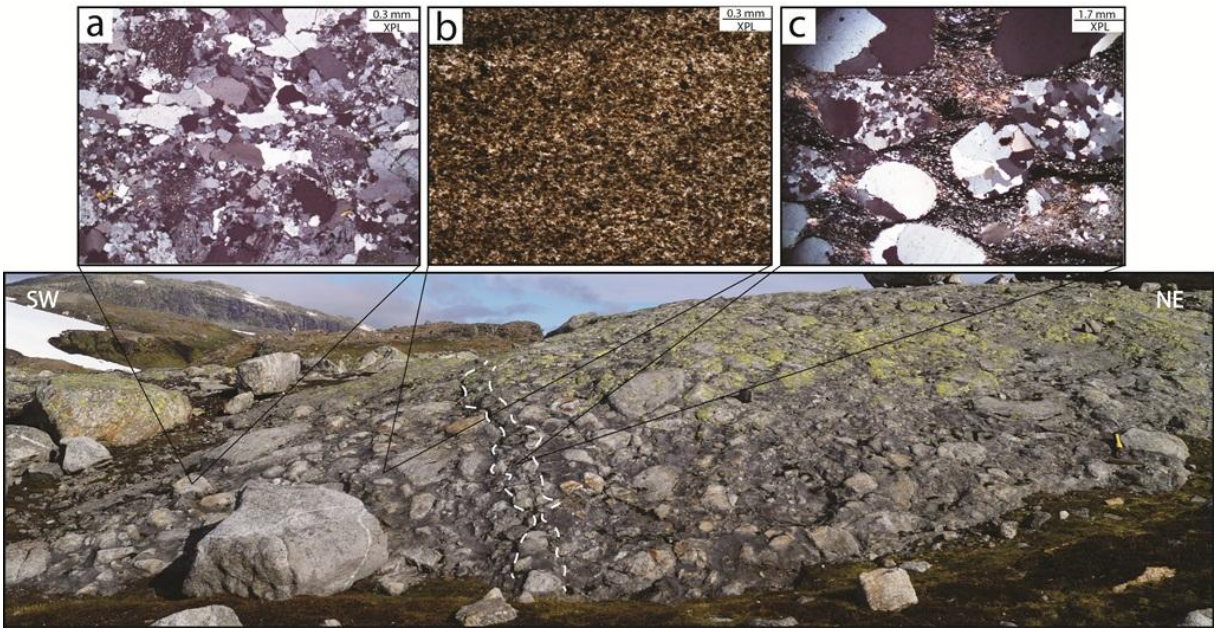

Fig. 38. Overview of the conglomerate at Buadalsbrotet (hammer for scale) with corresponding thin-section images presenting the texture and the different components in the conglomerate. **a)** Thin-section analyses from one of the clasts indicates a gneissic compostion including quartz,biotite, feldspar, calcite, chlorite and muscovite. Sample KOE-23. **b)** Fine-grained matrix mainly composed of biotite and quartz. Sample KOE-22. **c)** Coarse-grained matrix sampled from the elongated zone of the conglomerate. Larger grains of quartz are surrounded by fine-grained calcite, subgrains of quartz and organic material. Sample KOE-24.

Further towards southeast in the study area, just north of Hegrenuten, a conglomerate occurs (unit 2 in lithostratigraphy B, Fig. 37) with almost equal features to the ones at Buadalsbrotet. The conglomerate is matrix supported and consists of sub-rounded to rounded clasts with a granitic and quartz-rich composition (Fig. 39a). However, the sizes of the clasts are in general smaller, ranging from 4.0 cm to 19.3 cm, and the matrix constitutes a slightly higher portion (35%) compared to the conglomerate at Buadalsbrotet. Micro-scale analyses indicates that the matrix consists of fine-grained (meta-) sandstone composed of quartz, mica and feldspar, that is scattered by larger grains of quartz (<0.53 mm) (Fig. 39b).

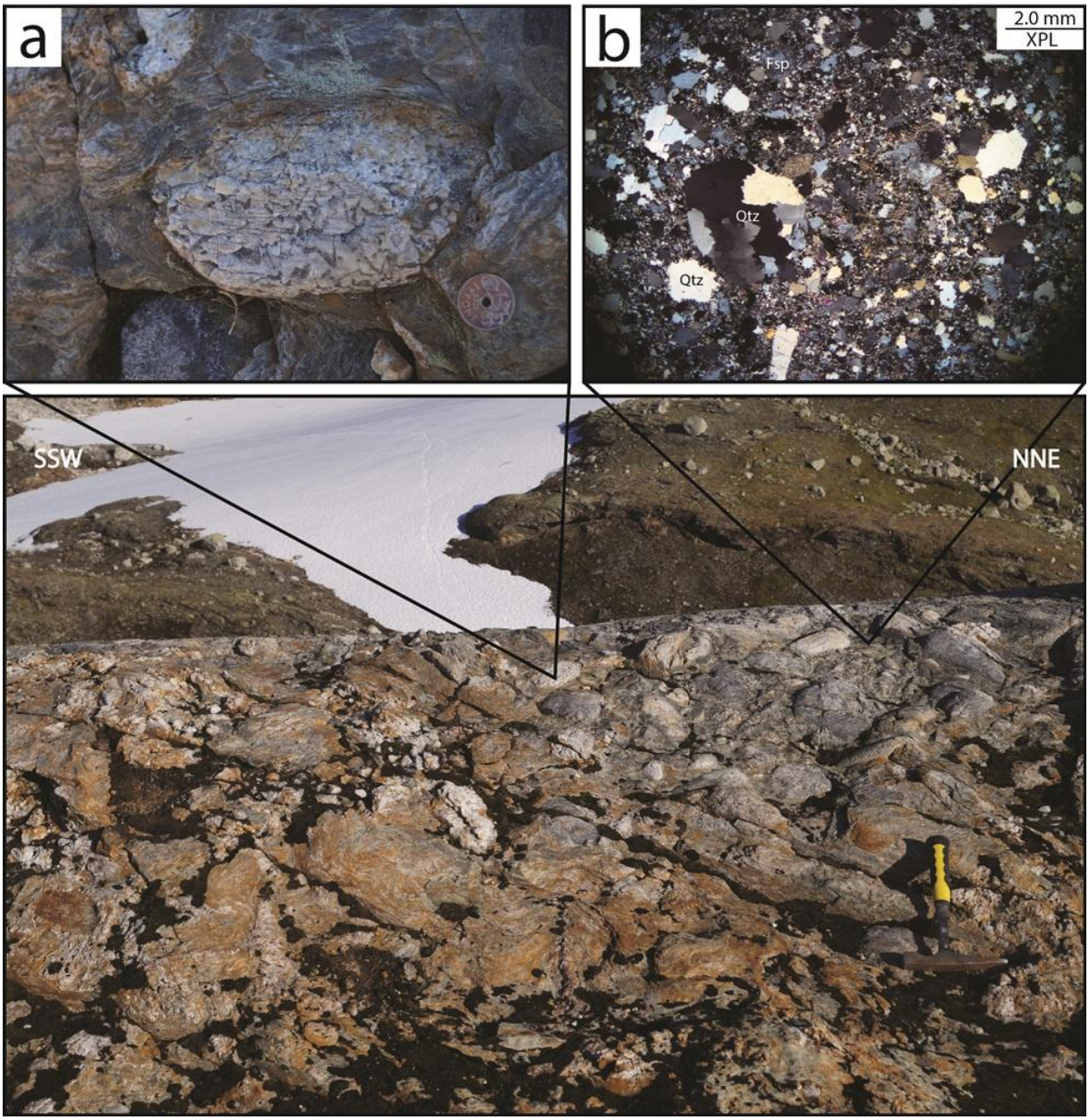

Fig. 39. Overview of the conglomerate located north of Hegrenuten. **a)** Clast composed of quartz and feldspar in the conglomerate. **b)** Coarse-grained matrix composed of larger grains of quartz mixed with finer crystals of quartz, mica and feldspar. Sample KOE-26.

Unit 3: Quartz schist

Quartz schist appears with a thickness of 15 cm and is sited on the conglomerate at Hegrenuten (unit 3 in stratigraphy B, Fig. 37). It is characterized by a yellow-orange color and slightly foliated. Thin-section analyses reveals a content of quartz, muscovite and iron-oxides, and additionally subhedral crystals of zircon (<0.05 mm) are accumulated mainly in layers of muscovite (Fig. 40) and constitute a volume percentage of 15 % of the sample.

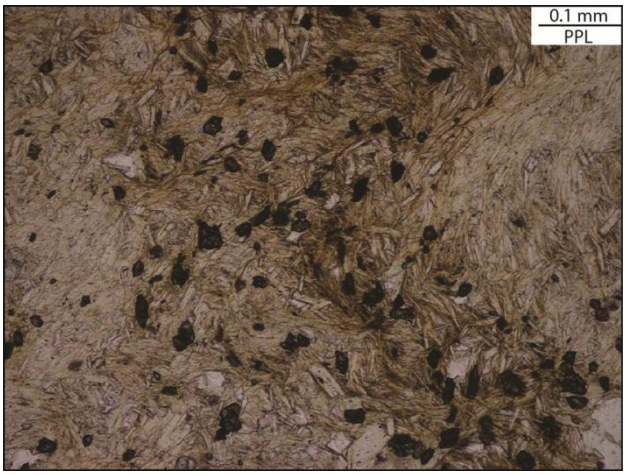

Fig. 40. Subhedral zircon crystals concentrated in the interlayers of muscovite in the quartz schist at Hegrenuten. Sample KOE-28.

Unit 4: Phyllite

The phyllite at Osa is well-foliated which occurs in straight to slightly wavy planes. It has a metallic luster and a brown colored weathering surface that is generally covered by lichen. Petrographic analyses of the phyllite indicates a complete mineralogical composition of quartz, muscovite, biotite, iron-oxides, and sheared opaque material. In the area close to Hegrenuten, the phyllite is interlayered by northeast-dipping beds enriched in carbonate (Fig. 41), in which the thickness ranges from 3 cm and up to 42 cm.

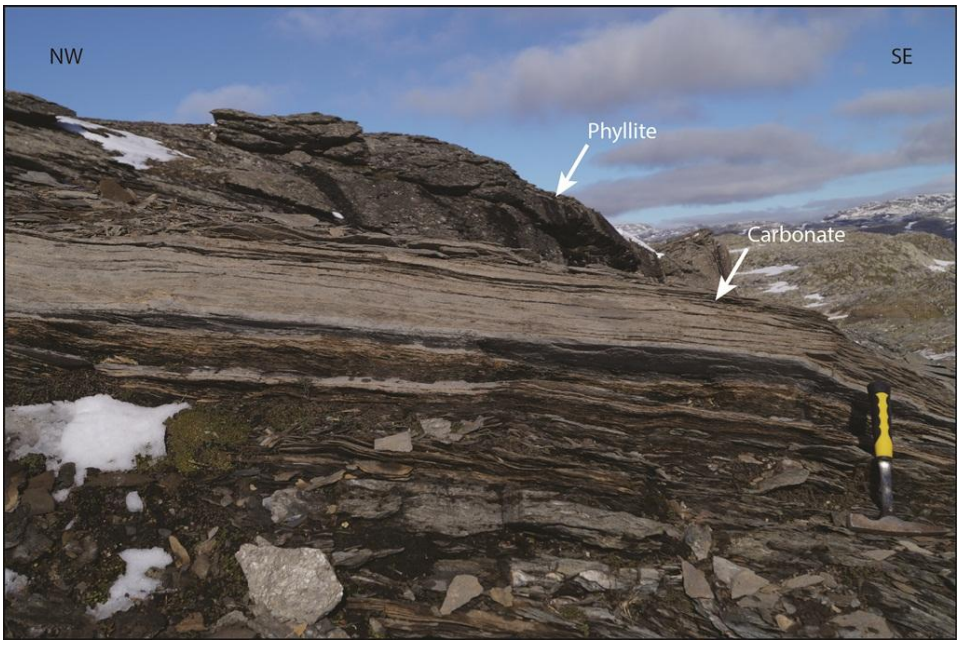

Fig. 41. Carbonate-rich layers occur in the phyllite at Osa.

4.1.5 Voss

The locality at Voss only representing the phyllite unit of the stratigraphy (Fig. 42) and is following described.

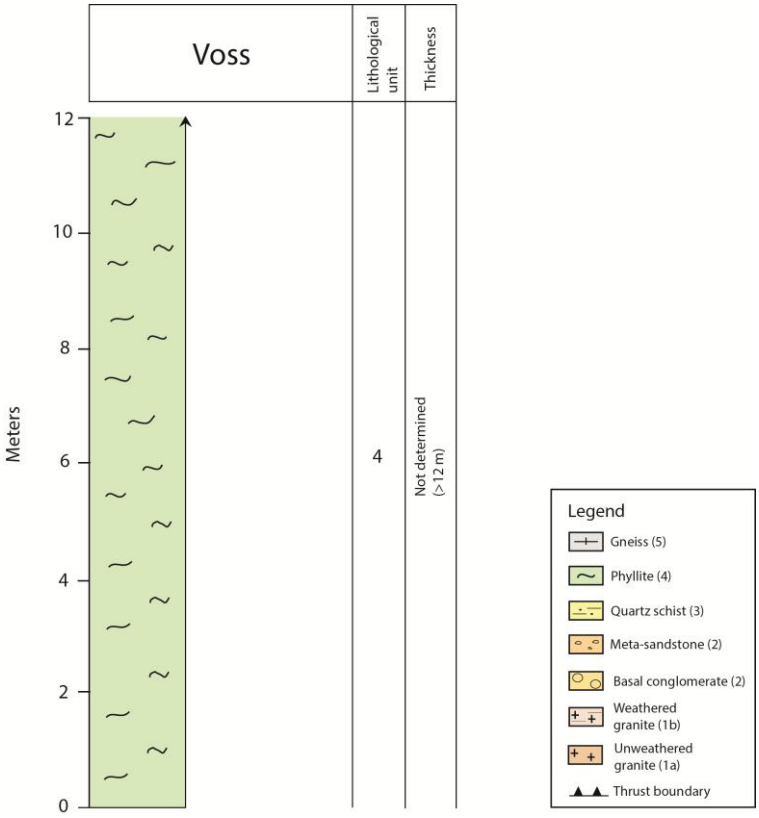

Fig. 42. Simplified lithostratigraphy at Voss.

Unit 4: Phyllite

The phyllite has a bright to darker grey color, and relatively large minerals of mica have grown at the foliation surface which gives a metallic luster. It has a high content of quartz veins, estimated to be approximately 15 % estimated from the outcrops. Some of the quartz veins have a brown colored and calcareous outer rim. Thin-section analyses indicates a main composition of quartz, muscovite, bitoite, calcite and iron-oxides.

4.1.6 Dyranut

Similar to the location at Voss, the phyllite is the only unit representing parts of the lithostratigraphy at Dyranut (Fig. 43).

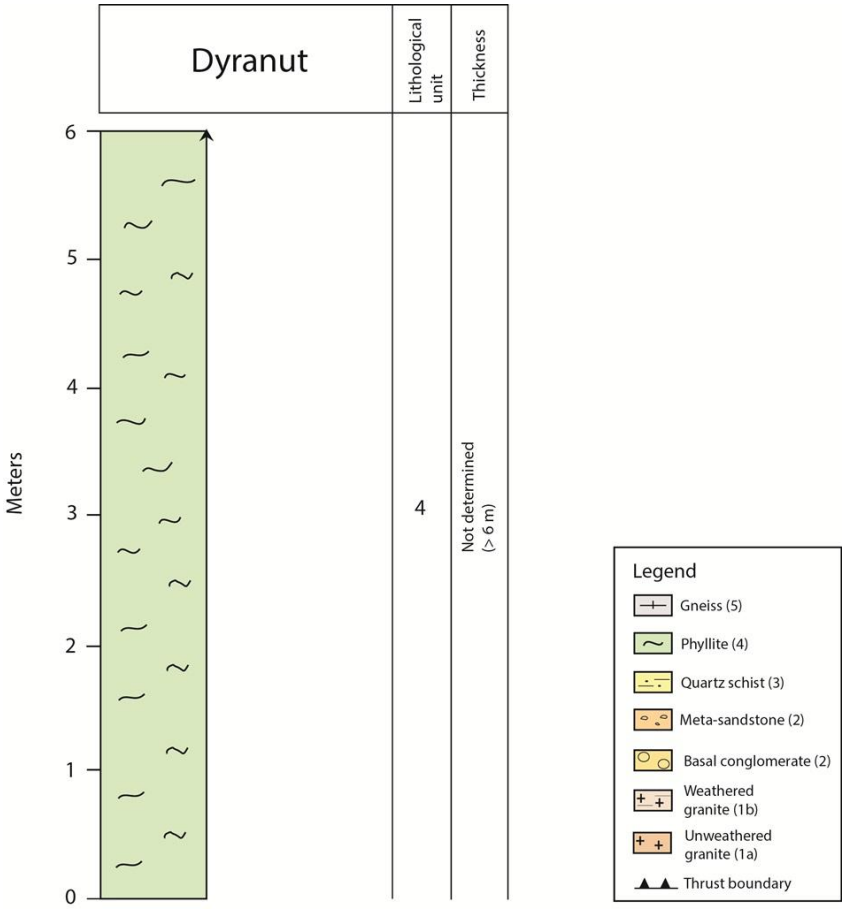

Fig. 43. Simplified lithostratigraphy at Dyranut.

Unit 4: Phyllite

The phyllite at Dyranut has a bright grey color. It is characterized by the well-developed foliation which occurs in straight planes and has a shiny metallic luster. The phyllite contains folded quartz veins, and thin-section analyses indicates a main content of quartz and muscovite, with some portions of chlorite and calcite.

4.1.7 Ustaoset

Two lithostratigraphies are presented for the locality at Ustaoset; one at Usteberget (Lithostratigraphy A, Fig. 41) and one at Rukenhovda (Lithostratigraphy B, Fig. 41), where the main difference is the presence of meta-sandstone resting on the basement at Usteberget, and the different mineralogical composition of the phyllite at Rukenhovda.

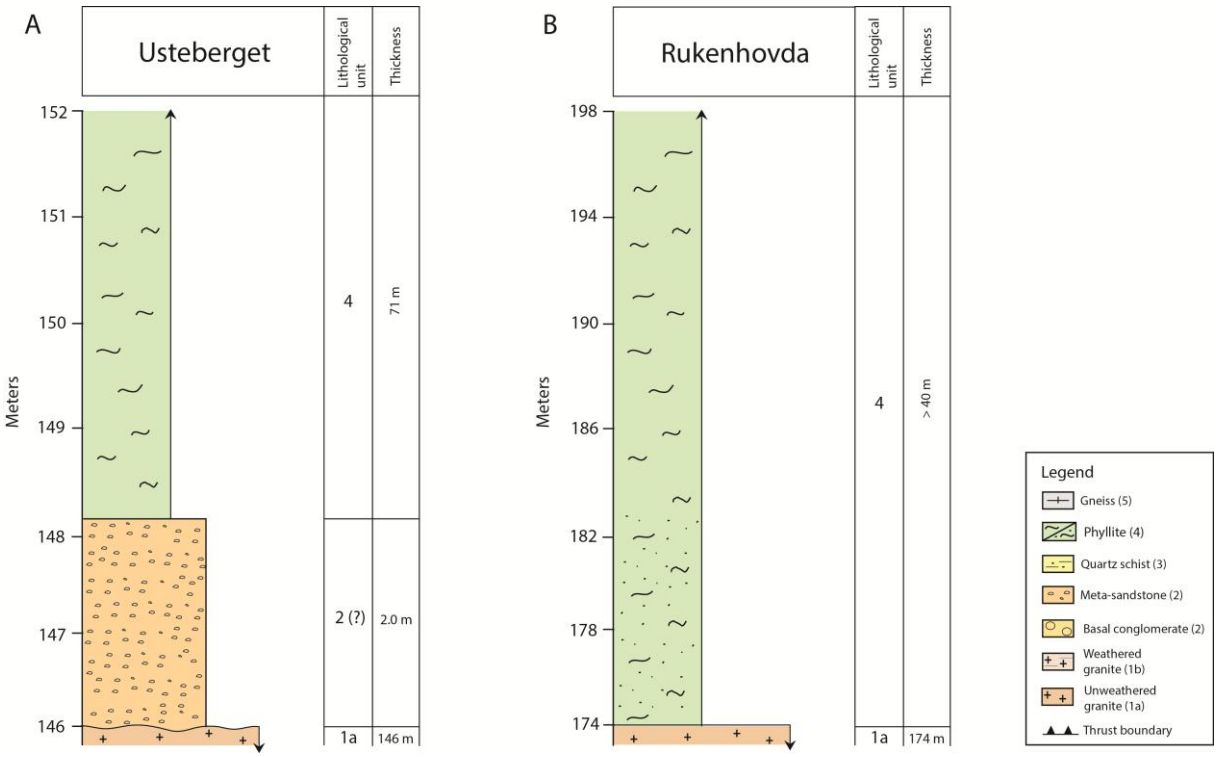

Fig. 44. Simplified lithostratigraphy from Usteberget (A) and Rukenhovda (B) at Ustaoset.

Unit 2: Basal conglomerate and meta-sediments

The outcrop view of Usteberget indicates an approximately 2 meter thick layer which rest on the basement (unit 2 in lithostratigraphy A, Fig. 44) and has a yellowish to orange color. Compared to the underlying basement, the lithology of this layer occurs with a less massive and unconsolidated texture. However, as the study of the layer is only based on outcrop-scale observations makes it difficult to clearly verify its properties and thus lithology.

Unit 4: Phyllite

The phyllites at Usteberget and Rukenhovdat are characterized by the dark grey to black color and straight and well-developed foliation planes. The exposure surfaces are often weathered and occur with a rust brown color. At Rukenhovda the lower ~10 meters of the phyllite is quartz-rich displayed by undulating layers of dark clay (2 mm) and quartz (5 mm). Thin-section studies indicate a minor content of biotite, plagioclase and calcite.

4.2 Deformation structures

The most prominent deformation structures in the basement (generally found in the weathered granite, unit 1b), basal conglomerate, and other meta-sediments are presented at micro-scale. The distinctive microfabrics mainly includes recrystallized quartz, twin geometries in calcites, kinked and bent twins in feldspar and calcite crystals, and (secondary) fluid inclusions in quartz, strain shadows, and impingement microcracks of quartz grains.

Considering the phyllites the sense of shear is mainly described by the S-C structures at macro- and micro-scale and asymmetric folds. Additional measurements of crenulation lineations and detailed descriptions of fold geometries are presented. The structural features in the Caledonian nappe pile are presented from macro-scale field observations, which include fold geometries, slickenlines and foliations.

4.2.1 Finse

Unit 1: Unweathered and weathered basement

The Precambrian basement mainly lacks deformation structures. However, the upper section with weathered basement (<1.3 meters) indicates foliation dipping to E(SE) (Fig. 45a). Subhorizontal joints, which mainly seem to follow the topographic surface, are located in the uppermost 100 meters of the basement at Jomfrunuten at Finse. Additional steeply-dipping vertical joints are found (Fig. 45b).

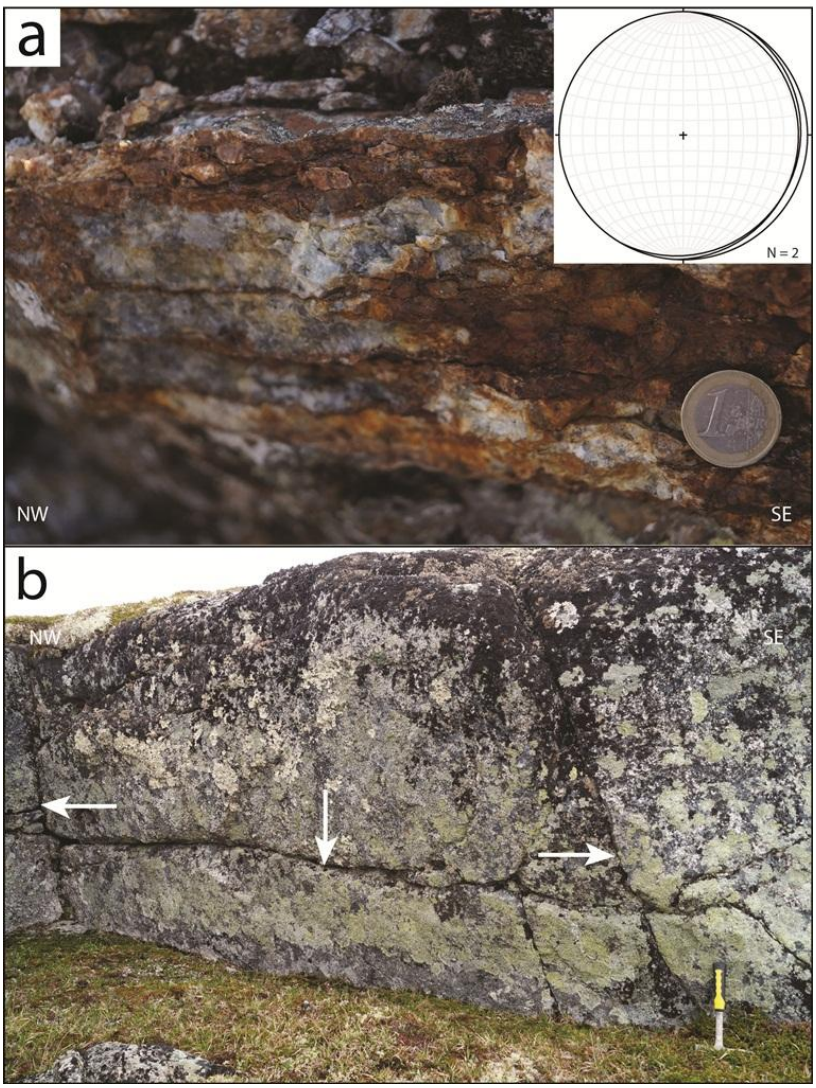

Fig. 45. **a)** E(SE)-dipping foliation in the weathered granite at Jomfrunuten on Finse. **b)** Sub-horizontal and vertical joints in the uppermost part of the basement at Finse.

The samples of weathered granite from Jomfrunuten and the Hardangerjøkulen area vary in their content of deformation structures. The fractures and weathered zones in the weathered grantite from Jomfrunuten, described in section 4.1.1, contain mantle porphyroclasts of plagioclase and clasts of quartz aggregates, enclosed by finer-grained muscovite (Fig. 46a). Some of the rigid crystals and clasts display a right lateral shearing (Fig. 46a, b). The weathered zones have generally a high content of clay minerals, which commonly provides local C-type shear band cleavages (Fig. 46b). Larger grains of quartz are sometimes located in the altered zone of the weathered basement, and smaller porphyroclasts and micas are found in the region between (Fig. 46c). This zone is also characterized by the lacks of foliation, which is marked with the arrow.

The overall deformation structures in the weathered granite in the Hardangerjøkulen area are displayed by larger quartz grains with undulatory extinction that are surrounded by moat of dislocation-free subgrains of quartz, separated by straight to bulging boundaries (Fig. 46d). Note that recrystallized quartz is not presented in the unweathered granite (KOE-8).

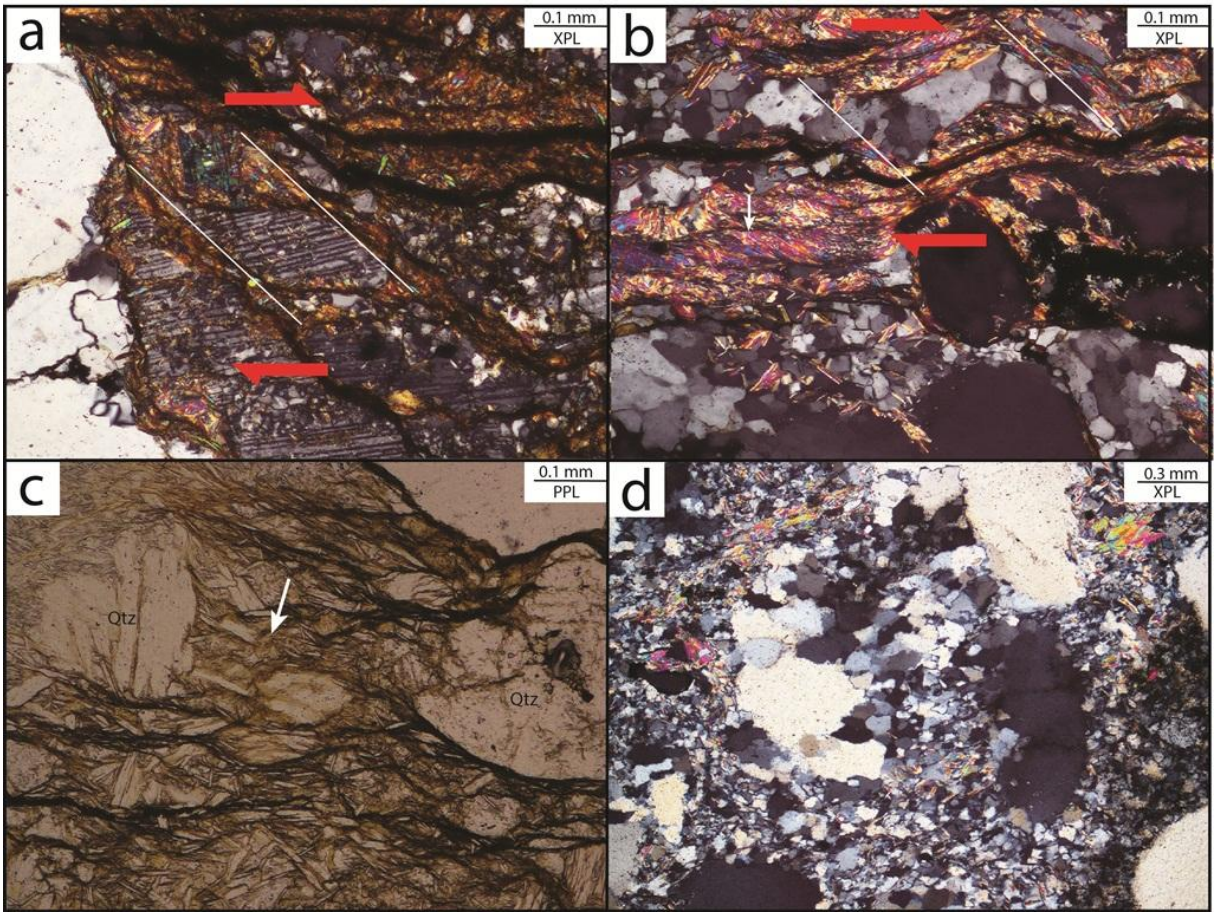

Fig. 46. Deformation structures presented in weathered granites at Jomfrunuten (a-c, sample KOE-6) and in the Hardangerjøkulen area (d, sample KOE-10) at Finse. **a)** Right lateral sense of shear determined from the mantle porphyroclast of plagioclase and clast of quartz situated in the weathered zone. **b)** C-type shear band cleavage defined by orientation of micas. The sigmoidal clast of quartz indicates right lateral shearing. **c)** Lack of foliation between the larger grains of quartz. **d)** Recrystallized quartz from two larger quartz grains.

Unit 2: Basal conglomerate and meta-sediments

Thin-section analyses of the conglomerate at Jomfrunuten (KOE-5) displays a slightly preferred orientation of the clasts (Fig. 47a). Some of the quartz grains contain impingement microcracks that are filled with the material that constitute the matrix of the conglomerate (Fig. 47b). Parallel oriented secondary fluid inclusions are commonly observed in the larger quartz grains in the conglomerate (Fig. 47c). By comparing the traces of fluid inclusions for several quartz grains, these seem to be oriented parallel with respect to each other. A few crystals of calcite have developed narrow and straight twins (Fig. 47d).

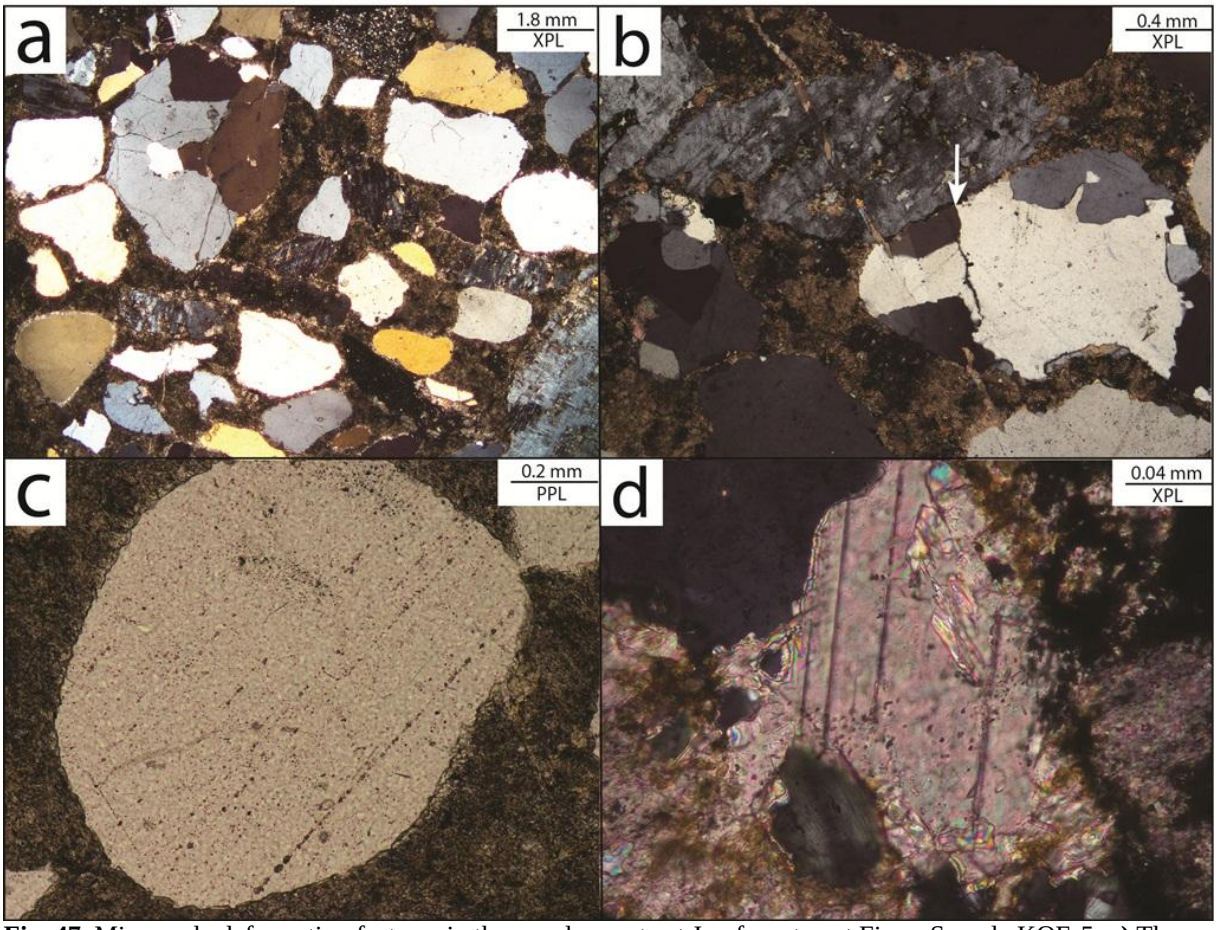

Fig. 47. Microscale deformation features in the conglomerate at Jomfrunuten at Finse. Sample KOE-5. **a)** The clasts in the conglomerate show a slightly preferred orientation, in which the longest axis trends top left to bottom right. **b)** Impingement microcracks in the quartz grains. **c)** Linear trails of secondary fluid inclusions in a quartz grain. **d)** E-twins in calcite crystal.

The two distinguished meta-sandstones in the Hardangerjøkulen area (unit 2 in lithostratigraphy B, Fig. 10) show restricted deformation structures. Micro-scale analyses of the medium-grained meta-sandstone, which rest directly on the basement, display a remarkable calcite-filled crack (<0.86 mm) that cuts the sample (Fig. 48a). The calcites occur as almost well-developed crystals with twin geometries that vary from being thin and straight to even more curved and thick (Fig. 48b). An irregular thin crack (0.2 mm), that is oriented normal to the calcite-filled crack, truncates the sample (Fig. 48a). Thin-section analyses of the meta-sandstone sampled closer the phyllite at Hardangerjøkulen, display strain shadows adjacent to the larger grains of feldspar, which are composed of calcite and quartz (Fig. 48c).

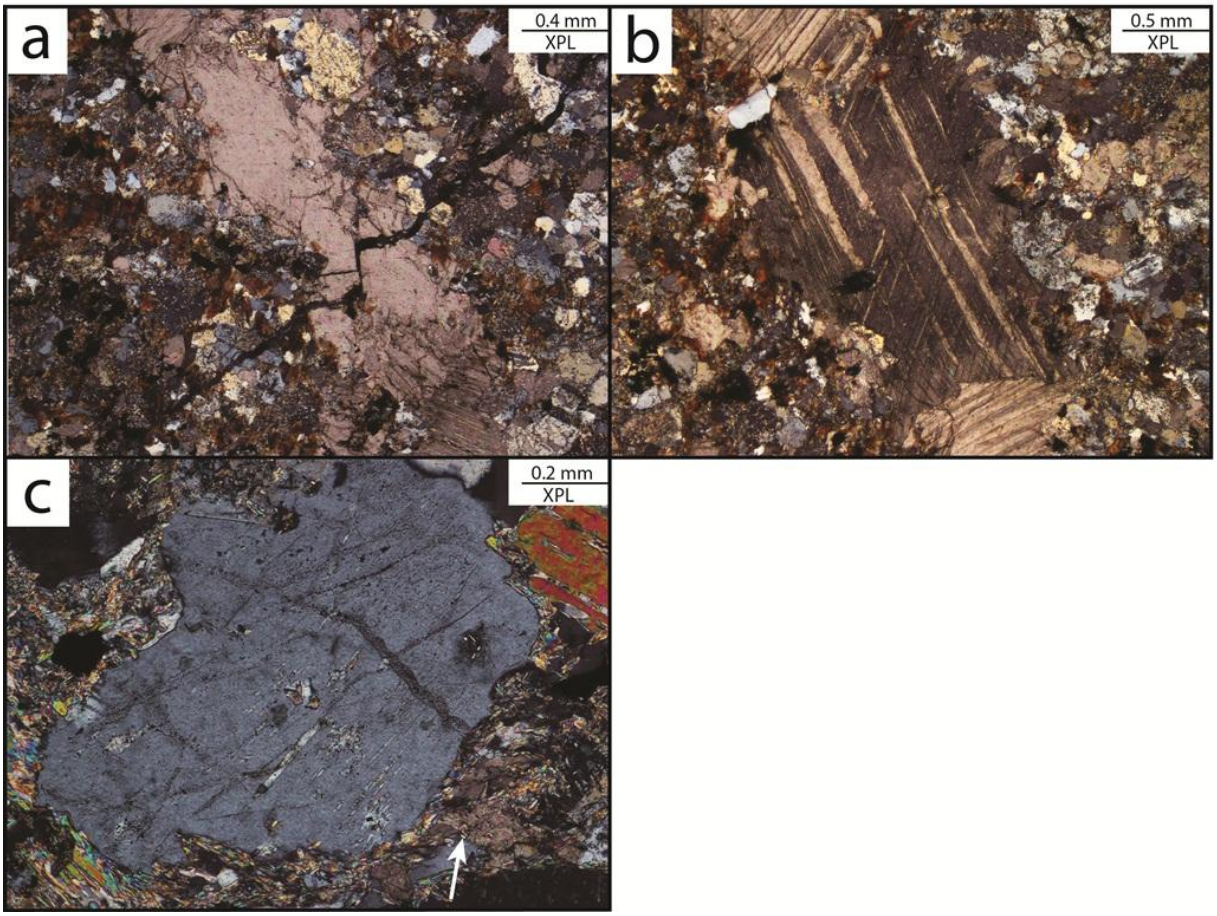

Fig. 48. Microscale deformation structures in the meta-sandstones in the Hardangerjøkulen area. **a)** Calcite-filled tension crack truncated by later fracture with a respectively normal orientation. Sample KOE-13. **b)** Calcite twin geometries vary from narrow and straight, to thick and sometimes curved. The photo is taken from the calcite-filled crack. Sample KOE-13. **c)** Feldspar surrounded by crystals of calcite and quartz, and fine-grained mica. Sample KOE-14.

Unit 3: Quartz schist

Petrographic analyses of the quartz schist at Jomfrunuten (unit 3 in lithostratigraphy A, Fig. 10) is characterized by the parallel arrangement of fine-grained muscovite and subgrains of quarts which make up the foliation of the sample. Larger grains of quartz and feldspar are surrounded by a fine-grained mass of muscovite and quartz. Some of the quartz grains suggest to have been recrystallized in the same stress field as the developed foliation (Fig. 49a). Fringe structures composed of elongated and dislocation-free quartz grains are locally found in the quartz schist (Fig. 49b). The asymmetrical shape of the fibers shows sinistral sense of shear.

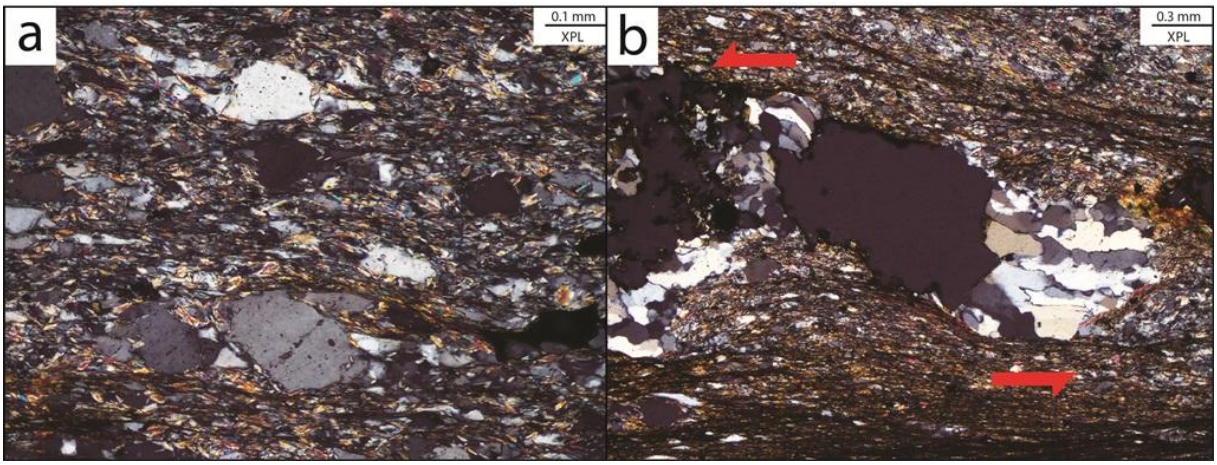

Fig. 49. Deformation structures in the quartz schist at Jomfrunuten. Sample KOE-7. **a)** Recrystallization of larger grains of quartz displayed by the stretched and crystallized edges of the opposite sides of the grains. **b)** Asymmetric fringe structure displays left lateral sense of shear. The rigid fibers are composed of subgrains of quartz.

Unit 4: Phyllite

The phyllites found in the areas near the railway station at Finse (unit 4 in lithostratigraphy A, Fig. 10) are characterized by the overall high content of asymmetric mesofolded quartz veins (~3 cm) indicated by the tight to isoclinal opening angle (~15^0) and W-vergence with axial surfaces dipping about 30^0 and 60-75^0 to SE (e.g. Fig. 50a). Structural data indicate two sets of folds (Fig. 50b); a dominating one with fold axes plunging to the NE and another plunging to the SE. The calculated S-C crenulation axes generally plunging to SW and NE, however some of them represent an opposite orientation. The C-surface generally dips with 10^0-30^0 to NW and NE and the angle relation between the shear bands and the foliation constitute about 35^0-40^0. Lineations, which evidently plunging to the SE, are mainly found on the S-planes and locally also on the C-planes. Micro-scale S-C structures in the phyllite reflect high degree of shearing, as the shear band (C-surface) dipping ~32^o to the NW (Fig. 50c) and intersects the foliation with an angle of 34^0.

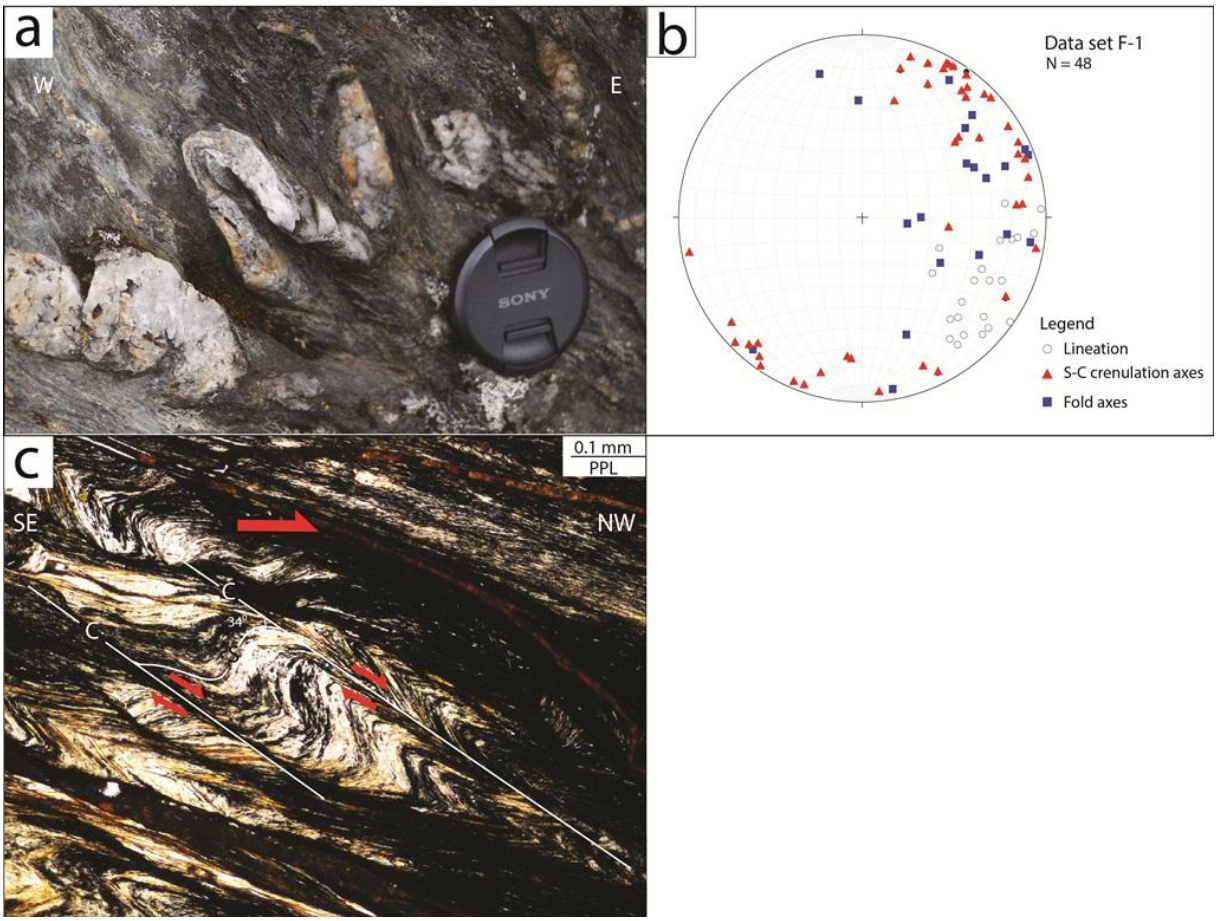

Fig. 50. Deformation features in the phyllite in the area north of Finse railway station. **a)** W-verging folded quartz veins are commonly observed in the phyllite. **b)** Stereographic projection (equal area, lower hemisphere) of structural data for the phyllites. Data set F-1 in appendix B. **c)** The orientation of the well-developed shear bands and foliation reflect shearing towards NW. Sample KOE-9, Store Finsenuten.

The phyllite in the Hardangerjøkulen area (unit 4 in lithostratigraphy B, Fig. 10) contains very well exposed S-C structures. The crenulation axes are mainly plunging to SW with some plunging to the NE, NW and SE (fig. 51a). The shear bands (C-surface) generally dipping 14^0-38^0 to SW and NW, and the foliation (S-surface) develops with an angle of 25^0 to C (Fig. 51b). Thin-section analyses of the phyllite in the Hardangerjøkulen area display sheared and SE-dipping quartz domains, which reflect to-to-the-NW sense of shear (Fig. 51c). Well-developed crenulation lineations are plunging with an angle of 20-30^0 on the SE-dipping S-surface in the phyllite (Fig. 48c).

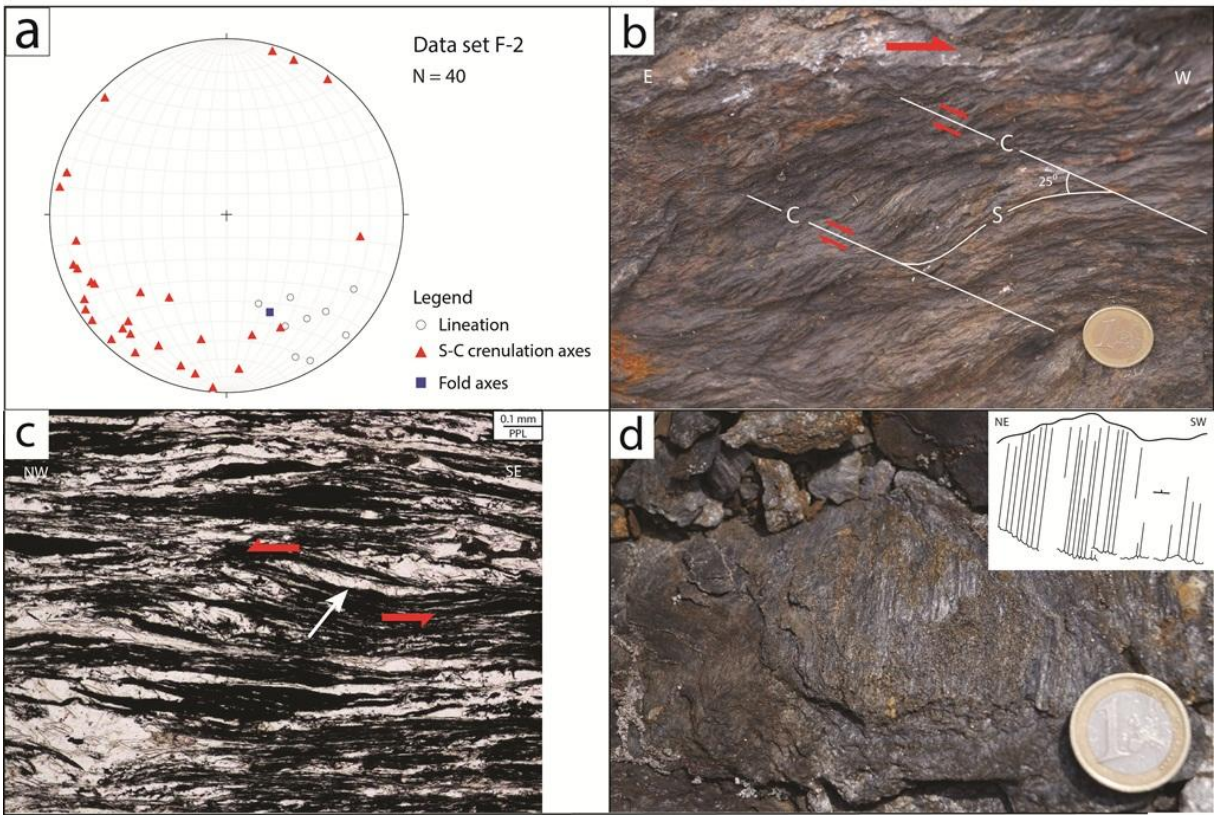

Fig. 51. a) Stereographic projection (equal area, lower hemisphere) of structural data for the phyllites. Data set F-2 in appendix B. **b)** Well-developed S-C structures in the phyllite in the Hardangerjøkulen area. The foliation (S) is affected by gently W-dipping shear bands (C) formed during non-coaxial deformation. **c)** Sheared and SE-dipping quartz domains indicate top-to-the-NW movement. Sample KOE-12. **d)** SE-plunging crenulation lineations are locally displayed at the foliation plane (S-surface).

Unit 5: Gneiss

Significant characteristics of the nappe are the asymmetric SW-verging folds with an opening angle ranging from tight to open. Spherical projections of the structural data reveals fold axis that mainly plunging towards NW (Fig. 52a). At some sites the gneiss is characterized by chaotic fold pattern reflecting intense ductile deformation. Some of the foliation planes, which dipping gentle to the NE and SE, contain slickenlines that generally show top-to-the-SE transport. Sub-vertical fractures filled with quartz occur with an approximate thickness of 0.3 cm in the nappe close to the contact to the underlying phyllite. The fracture sets are oriented parallel to each other, dipping to the NE and the SW (Fig. 52a). Folded and thrusted boudins composed of quartz and feldspar, are locally found in the gneiss at Hardangerjøkulen (Fig. 52b).

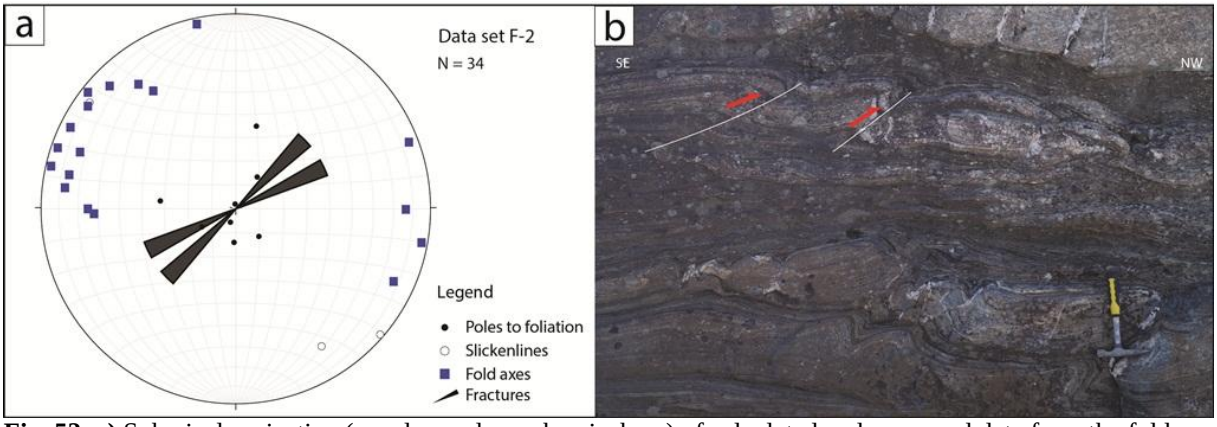

Fig. 52. a) Spherical projection (equal area, lower hemisphere) of calculated and measured data from the folds, foliations and slickenslides sited in the foliation planes in the Hardangerjøkulen area. The rose diagram reflect two sets of subvertical fractures dipping to the NE and the SW. Data set F-2 in appendix B. **b)** Folded and thrusted boudins are locally found in the gneiss.

4.2.2 Sandå

Unit 1: Unweathered and weathered basement

The unweathered basement at Sandå generally lack deformation structures. However, thin-section analyses reveals that some of the biotite crystals appear with a characteristic kink and bent cleavage which reflect brittle-ductile deformation (Fig. 53a). In the weathered granite (KOE-17) the larger quartz crystals are locally enclosed by subgrains of recrystallized quartz. The subgrains appear normally at the grain boundaries and in internal fractures in the crystals (Fig. 53b). Compared to the unweathered granite, recrystallized quartz is not presented. In the altered zones in the weathered granite, muscovites and subgrains of quartz are stretched and sheared in the opposite sides of larger quartz grains (Fig. 53c) and other rigid elements (Fig. 53d).

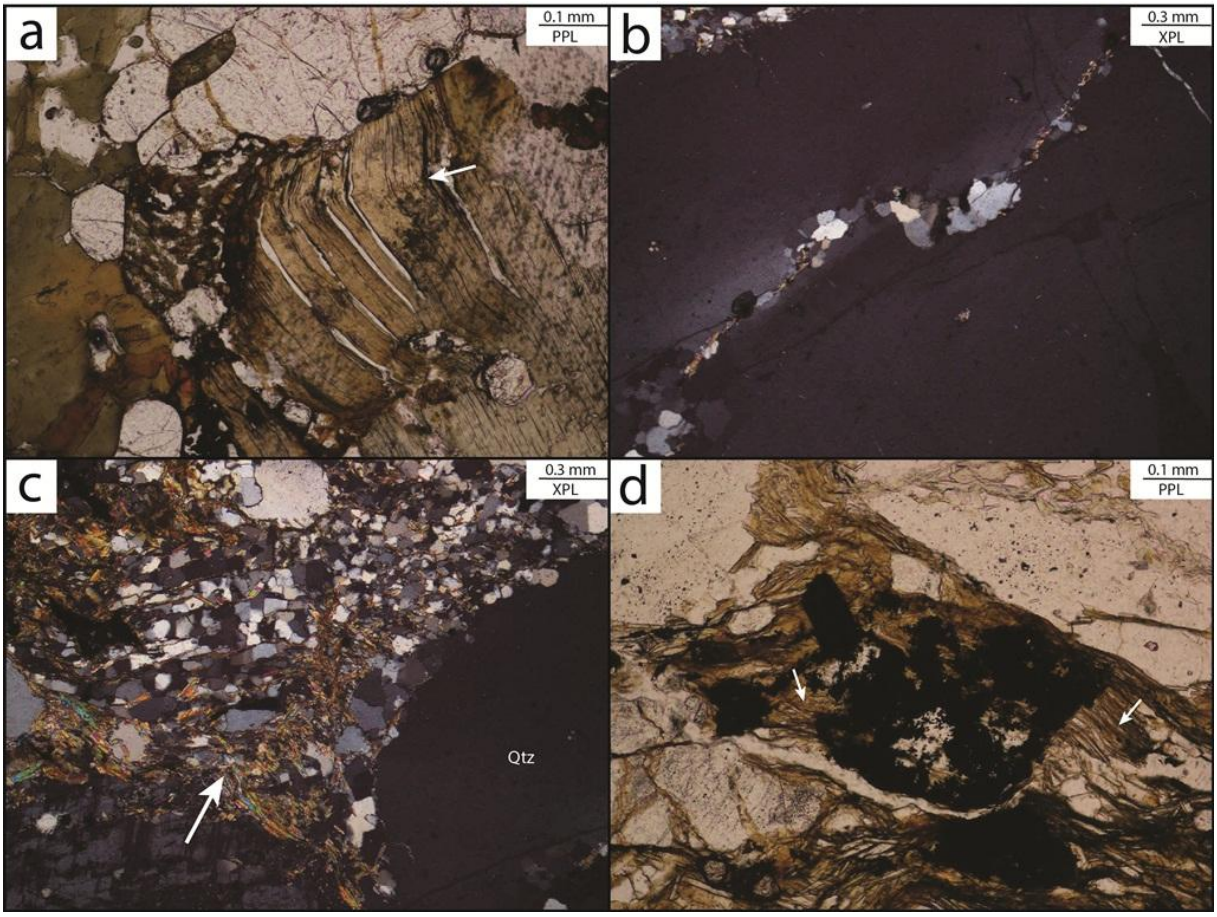

Fig. 53. Deformation structures in the unweathered (a, sample KOE-18) and weathered granite (b-d, sample KOE-17) at Sandå. **a)** Kinked cleavage in biotite crystal in the fresh basement. **b)** Recrystallization of quartz located in internal fractures of the crystal. **c)** Sheared and rotated subgrains of quartz and mica at the edge of a larger quartz grain. **d)** Stretched and bent mica and grains of feldspar around the rigid clast of iron-oxide.

Unit 2: Basal conglomerate and meta-sediments

The clasts in the conglomerate at Sandå are mainly randomly oriented. Deformation structures including fractured quartz grains, recrystallized subgrains of quartz, calcite twins, and secondary fluid inclusions in the quartz grains, characterize the conglomerate (Fig. 54a).

Most of the quartz grains contain parallel traces of fluid inclusion trails (Fig. 54b), which also are arranged parallel with respect to the inclusion paths in the other quartz grains (Fig. 54a). In overall two sets of fractures occur with nearly perpendicular orientation in the larger quartz grains in the conglomerate; one that cuts and almost separates the grains (Fig. 54c-e) and another that joint the crystals internally (Fig. 54c, e). Nearly straight zones concentrated by dislocation-free subgrains of quartz are found in some of the larger quartz grains (Fig. 54d). Some well-developed calcite crystals show narrow and straight mechanical

e-twins, which are normally found at the opposite sides of the quartz grains in the conglomerate.

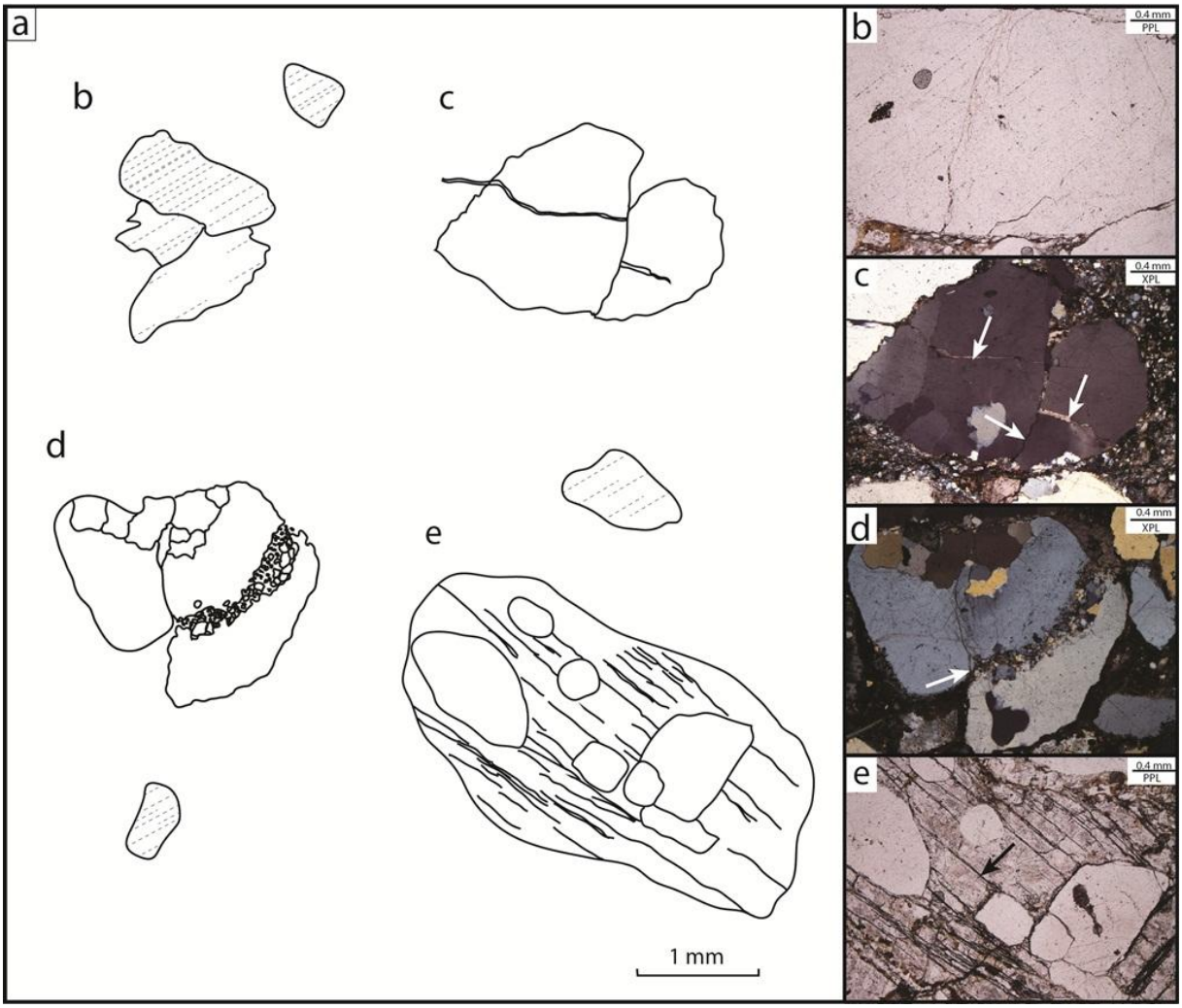

Fig. 54. a) Illustration of the presented microfabrics in the conglomerate at Sandå. Sample KOE-15. **b)** Parallel trails of fluid inclusions in quartz grains. **c)** Microcracks in the quartz grains occur with perpendicular orientation with respect to each other. **d)** Minor subgrains of quartz are located in a fracture that separates the quartz grain. **e)** Fractures crystal of feldspar.

Unit 3: Quartz schist

The quartz schist at Sandå is characterized by well-developed S-C structures found in the concentrated layers of muscovite and quartz (Fig. 55a). The shear bands intersect the S-plane with an angle of about 45^0. Subgrains of quartz, characterized by the poorly defined and bulged grain boundaries, are elongated in the sense that the longest axes of the crystal is parallel to the shear bands (Fig. 55b), and thus suggest to have been formed during the same stage of deformation.

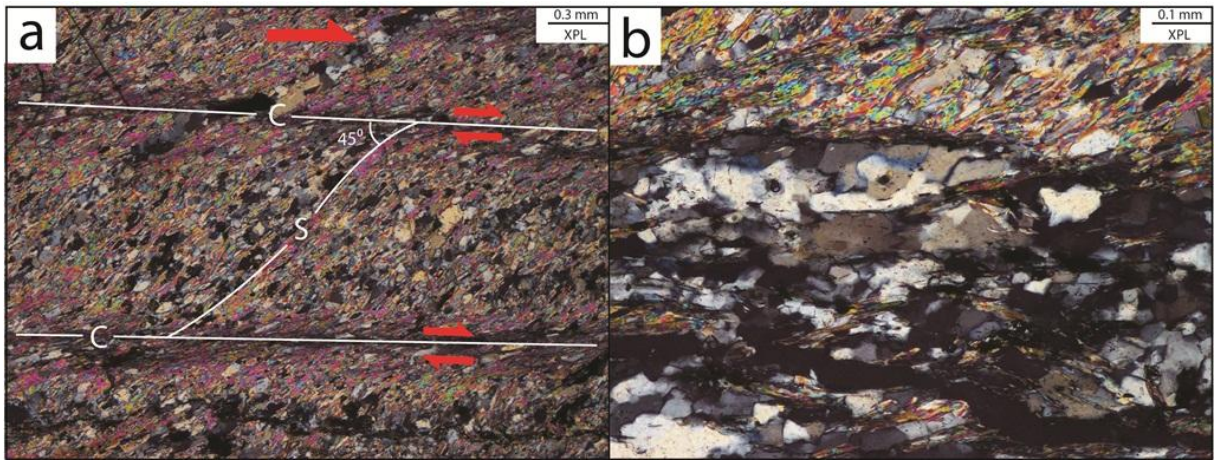

Fig. 55. Deformation structures in the quartz schist at Sandå. Sample KOE-16. **a)** Well-developed S-C structures. The geometry of the S-surface reflects right-lateral shearing. **b)** Recrystallized quartz appears as bands in the quartz schist. The grain boundaries are poorly defined.

Unit 4: Phyllite

The S-C structures are not well-exposed in the outcrops. However, some of them contain a SE-dipping foliation (S-surface) with shear bands dipping to the NW and NNE, which indicates a NNE sense of shear. The S-C crenulation axes are plunging to the NE (Fig. 56).

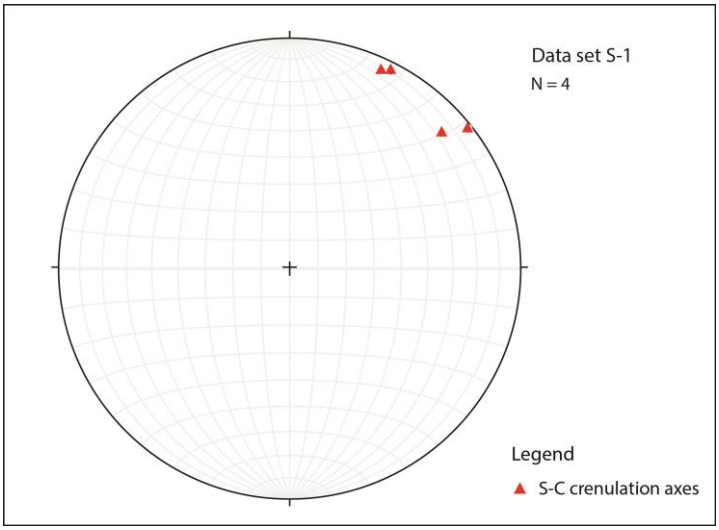

Fig. 56. Stereographic projection (equal area, lower hemisphere) of S-C crenulation axes, based on data set S-1 in appendix B.

4.2.3 Hallingskeid

Unit 1: Unweathered and weathered basement

Subhorizontal joints are found in the uppermost section of the basement at Hallingskeid, just like the ones found at Jomfrunuten at Finse. The most prominent evidence of deformation is, however, found as microfabrics in the weathered granite which includes kinked polysynthetic twinning in plagioclase (Fig. 57a) and dislocation-free subgrains of quartz, with sharp grain boundaries and developed triple junctions (Fig. 57b). Some of the larger clasts of quartz are rotated and, additionally sheared and recrystallized at the edges. Compared to the unweathered granite (sample KOE-19), the subgrains of quartz are not presented.

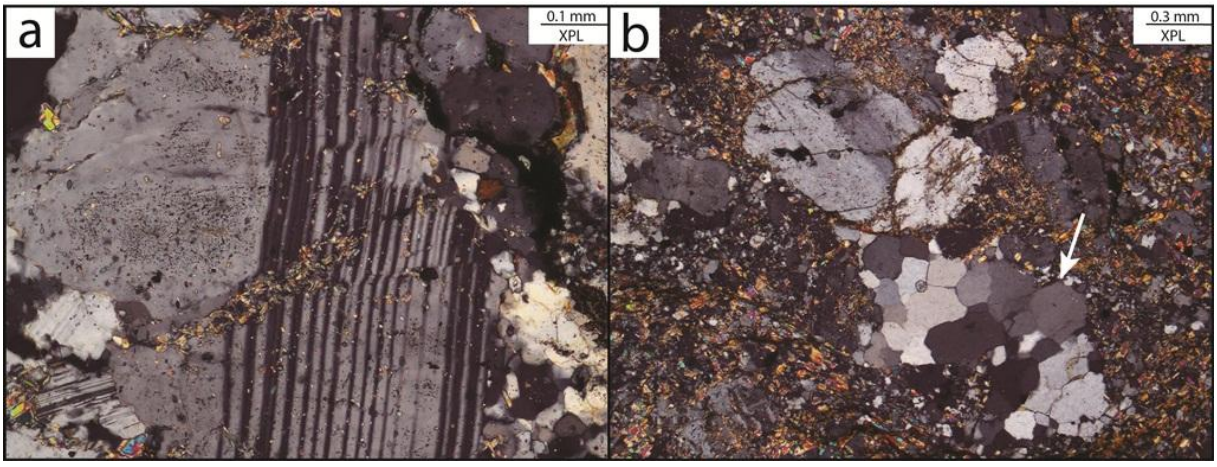

Fig. 57. Deformation structures in the weathered granite at Hallingskeid. Sample KOE-20. **a)** Kinked and bent twins in plagioclase. **b)** Polycrystalline quartz porphyroclast surrounded by a finer-grained mass composed of mica, feldspar, subgrains of quartz, and some epidote.

Unit 4: Phyllite

Most of the S-C crenulation axes plunging to the NE, with some plunging to the SW (Fig. 58a). Lineation are found on both the foliation plane and the C-surface, and plunging to (E)SE and W(NW). Petrographic analyses reveals asymmetric tails of chlorite adjacent to the garnet crystals, which shows shearing towards E (Fig. 58b). In addition, well-developed S-C structures are found in the sample in which shear band (C-surface) tracing the steeply E-dipping foliation with an angle of approximately 20^0-35^0 (Fig. 58c).

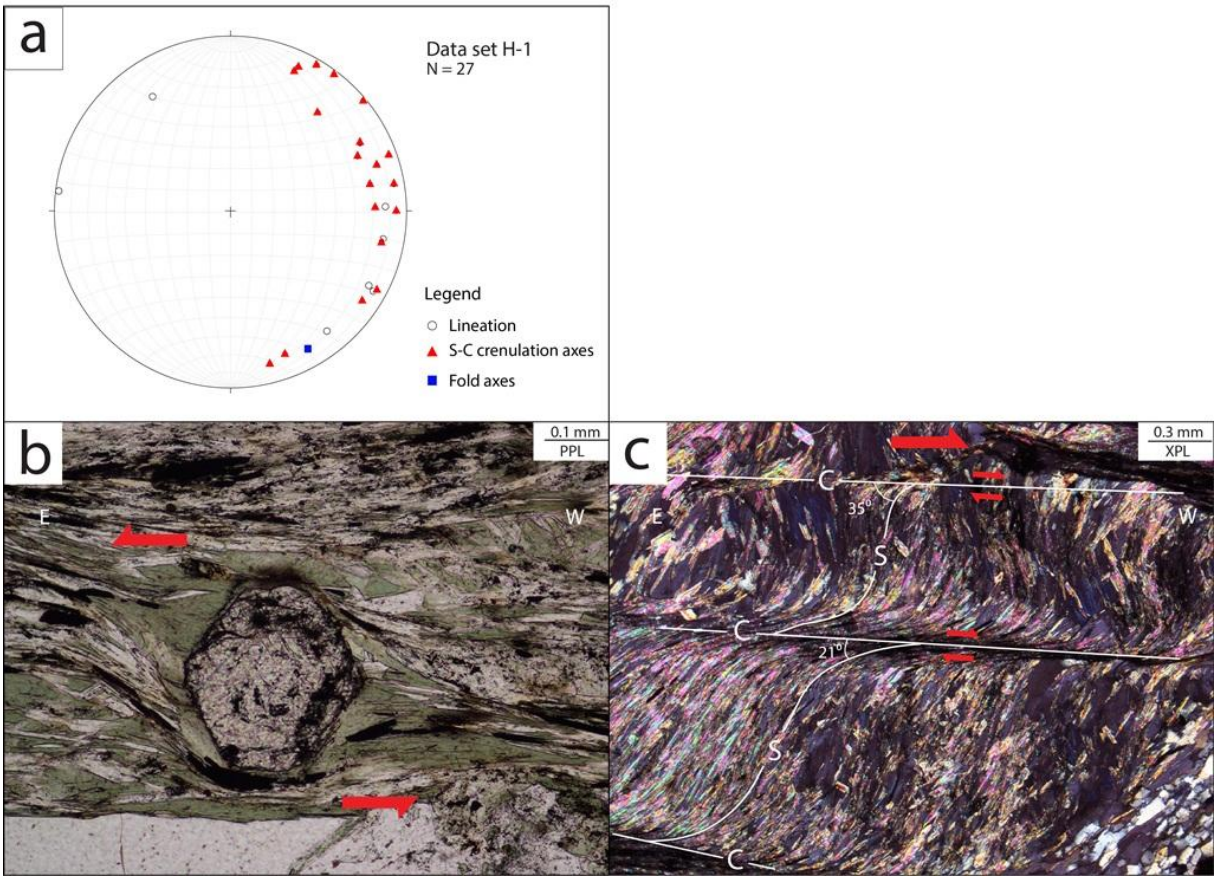

Fig. 58. a) Stereographic projection (equal area, lower hemisphere) of structural data at Hallingskeid. Data set H-1 in appendix B. **b)** Euhedral porphyroblast of garnet with asymmetric tails of chlorite indicating top-to-the-E sense of shear. Sample KOE-21. **c)** Steeply E-dipping foliation (S-surface) is intersected by shear band (C-surface) with and angle of 21^0 and 35^0. Sample KOE-21.

4.2.4 Osa

Unit 2: Basal conglomerate and meta-sediments

The pebbles in the conglomerate at Buadalsbrotet (unit 2 in stratigraphy A, Fig. 37) display a slightly preferred orientation with the longest axis trending to SW-NE. From dividing the long axis by the short axis of the pebbles gives an average aspect ratio of 1.37. Petrographic thin-section analyses of the gneissic clasts display slightly recrystallized quartz that are elongated in a preferred orientation and show undulose extinction (Fig. 59a).

The matrix in the conglomerate, which mainly consists of phyllite, lacks deformation structures. However, micro-scale analyses of the coarser-grained matrix collected from the elongated zone in the conglomerate indicates prominent and well-developed strain shadows composed of calcite and quartz, which are located adjacent to the larger grains of quartz (<0.7 mm) (Fig. 59b). In addition, most of the quartz grains contain secondary fluid inclusions trails

which occur with parallel orientation (Fig. 59c), and compared to the inclusion pattern in the other quartz grains of the sample, these are oriented parallel relative to each other. Larger crystals of calcite are also found in the coarse-grained matrix, in which some of them have developed bent, tapered and thick twins (Fig. 59d).

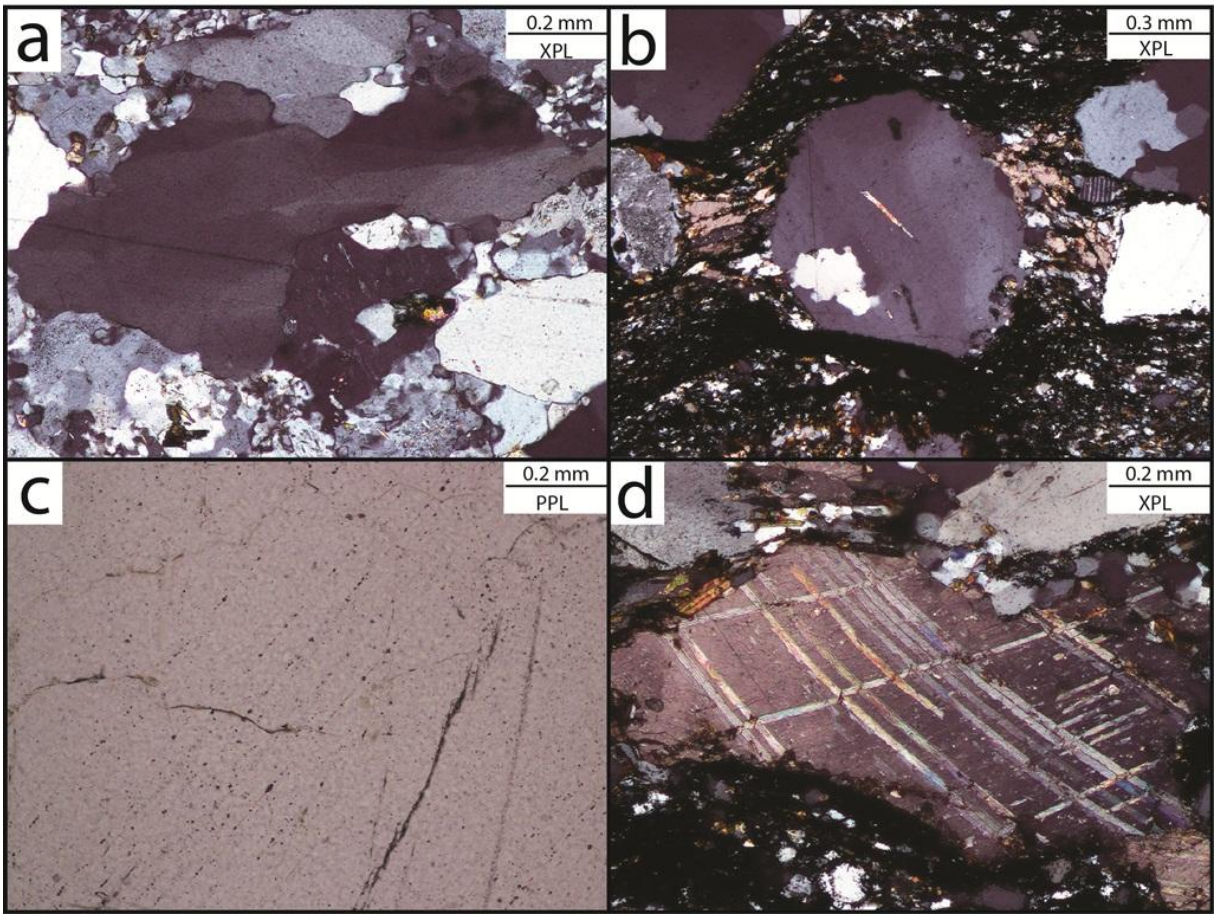

Fig. 59. Deformation structures in the conglomerate at Buadalsbrotet, from the gneissic pebble (a, sample KOE-23) and the coarse-grained matrix (b-d, sample KOE-24). **a)** Elongated quartz grain composed of subgrains. **b)** Strain shadow found adjacent to the quartz grains. **c)** Parallel oriented fluid inclusions in the larger quartz grain. **d)** Thick and bent conjugate sets of deformation twins in calcite.

The pebbles in the conglomerate at Hegrenuten (unit 2 in stratigraphy B, Fig. 37) are displayed with a slightly preferred orientation and the average aspect ratio is calculated to be 1.44. Micro-scale analyses of the clasts in the conglomerate at Osafjellet indicate several quartz grains incorporated in feldspar. Note that the thin-section from the sampled clast cut a larger grain of feldspar, and thus constitutes a certain incorrect preparation in the distribution of minerals (Vol%) in the sample.

Two large fractures truncate the sample with almost oblique orientation with respect to each other (Fig. 60a). The main difference between them is that recrystallized subgrains of quartz are concentrated along the sub-horizontal fracture, whereas the other fracture appear as a joint. In addition, recrystallized quartz occurs as a rim of subgrains along some of the larger quartz grains (Fig. 60a). One characteristic feature for the sample is the parallel oriented perthite flames that seem to have grown around the quartz grains (Fig. 60b-c). Randomly fluid inclusions are also found in quartz grains of the sample.

The matrix of the conglomerate at Hegrenuten (sample KOE-26), that constitutes (meta-) sandstone, gerenally lacks deformation structures. However, some of the larger quartz grains display bulging grain boundaries. Secondary fluid inclusions occur in the larger quartz grains with a parallel alignement.

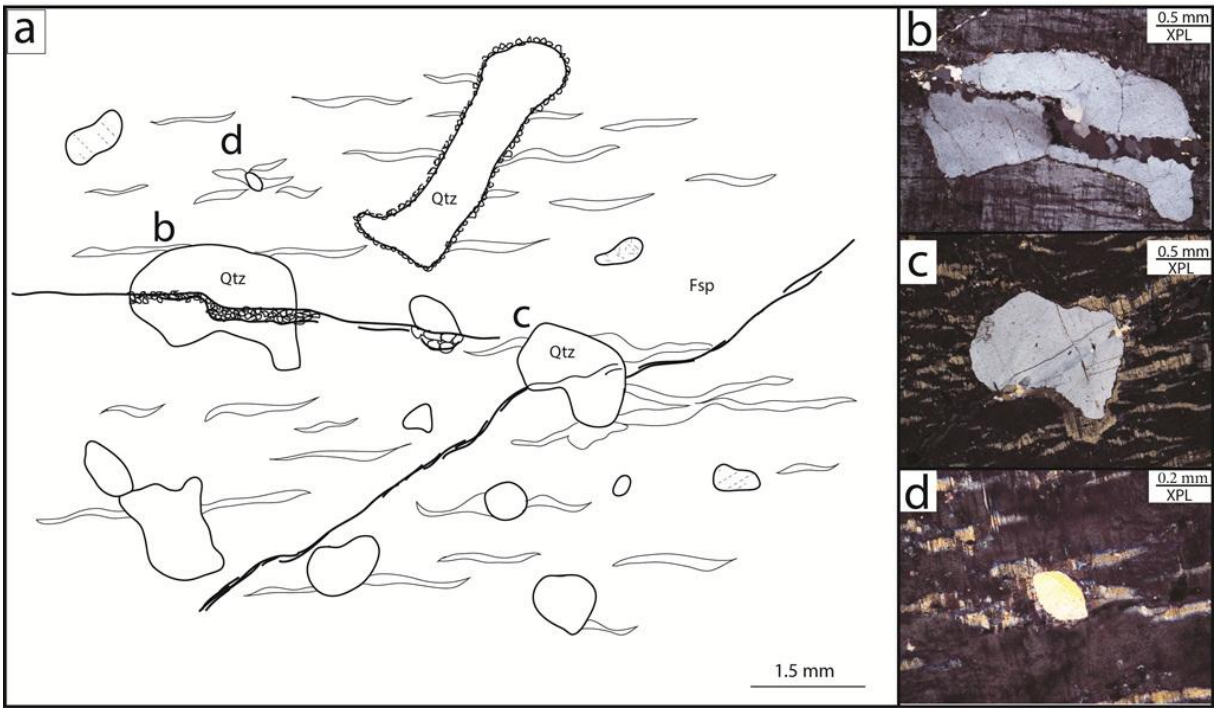

Fig. 60. a) Illustration of the microfabrics found in the pebble and conglomerate from thin-section analyses. Sample KOE-27, at Hegrenuten. **b)** Recrystallized quartz occurs in the larger fracture that cuts the sample. **c-d)** Albite lamellae have grown and bent around quartz grains.

Unit 3: Quartz schist

The quartz schist at Hegrenuten (unit 3 in lithostratigraphy B, Fig. 37) is only slightly strained as it lacks deformation structures. In the quartz bands, the grains show undulose extinction with locally diffuse grain boundaries (Fig. 61), but not to the same extent as in the quartz schist at Sandå and Finse. Some of the quartz crystals occur also as relatively strain-free with polygonal grain boundaries.

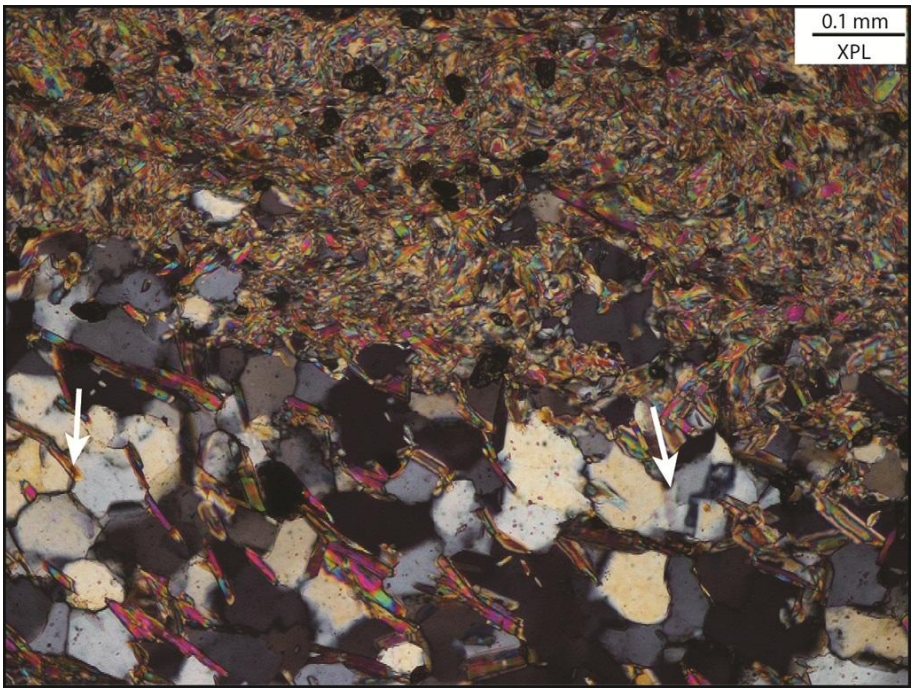

Fig. 61. Deformation structures in the quartz schist at Hegrenuten, sample KOE-28. Most of the quartz grains show undular extinction and bulging grain boundaries (arrow to the right), but also dislocation-free grains with triple junctions occur (arrow to the left).

Unit 4: Phyllite

The few measurements of the S- and C-surfaces indicate crenulation axes plunging to the NE (Fig. 62a). Crenulation lineations are found at the foliation plane (S-surface) plunging to the SE (Fig. 62a). At micro-scale the alternating layers of quartz and muscovite are slightly undulating, reflecting shearing to the SE (Fig. 62b). Thin-section analyses of the carbonate-rich interlayers in the phyllite at Hegrenuten, display E-W oriented and elongated crystals (Fig. 62c). Most of the crystals have developed bent and thick twins.

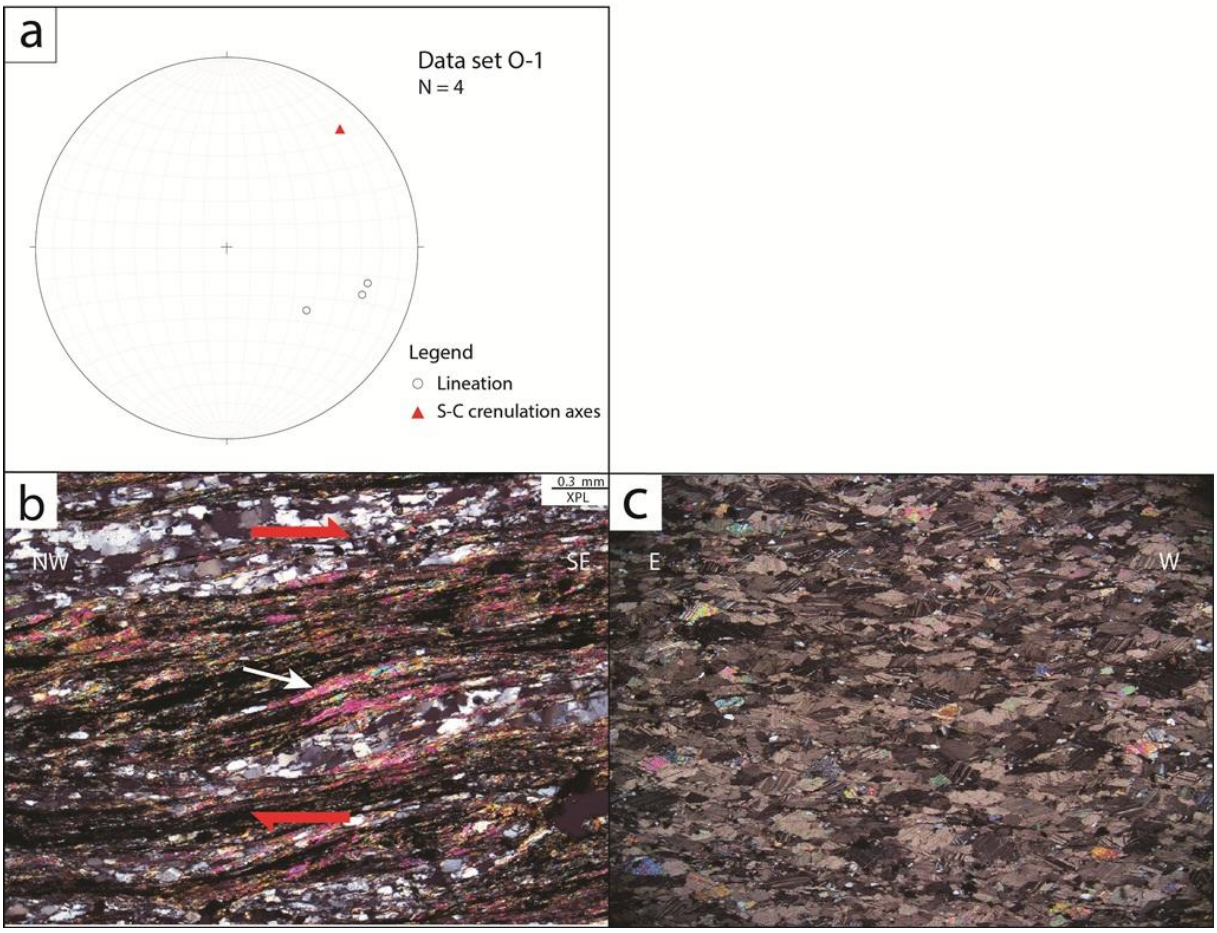

Fig. 62. a) Stereographic projection (equal area, lower hemisphere) of structural data at Osa. Data set O-1 in appendix B. **b)** Undulating interlayers of quartz and muscovite. Sample KOE-29. **c)** E-W elongated calcite crystals found in the carbonate-rich layer in the phyllite at Hegrenuten. Sample KOE-25.

4.2.5 Voss

Unit 4: Phyllite

Deformed quartz veins in the phyllite at Voss occur with two distinct fold geometries. Some is characterized by fold axis which plunge horizontal to SW and an axial surfaces dipping to SE. The angular relation between the limbs indicates the folds to be asymmetric with consistent NW-vergence. The other characteristic folds occur with axis plunging shallow to NE and an axial surface dipping to NW. The angular relation between the two limbs proves the fold to be asymmetric with SE-vergence. Well-developed S-C structures are found in the phyllite on Voss, and the calculated crenulation axes indicate an evident plunging to NE (Fig. 63a). The foliation (S-surface) dips generally to SE, and is intersected by shear bands (C-surface) with an angle of ~25^0 (Fig. 63b). The geometry of the S-C structures, defined both at

macro- and micro-scale, indicates top-to-the-(W)NW sense of shear (Fig. 63b-c). Well-developed crenulation lineations are found both on the C- and S-surface. Some of the foliation planes contain lineations that plunge in different orientations, one to SE which seems to overprint the lineations plunging to NE (Fig. 63d).

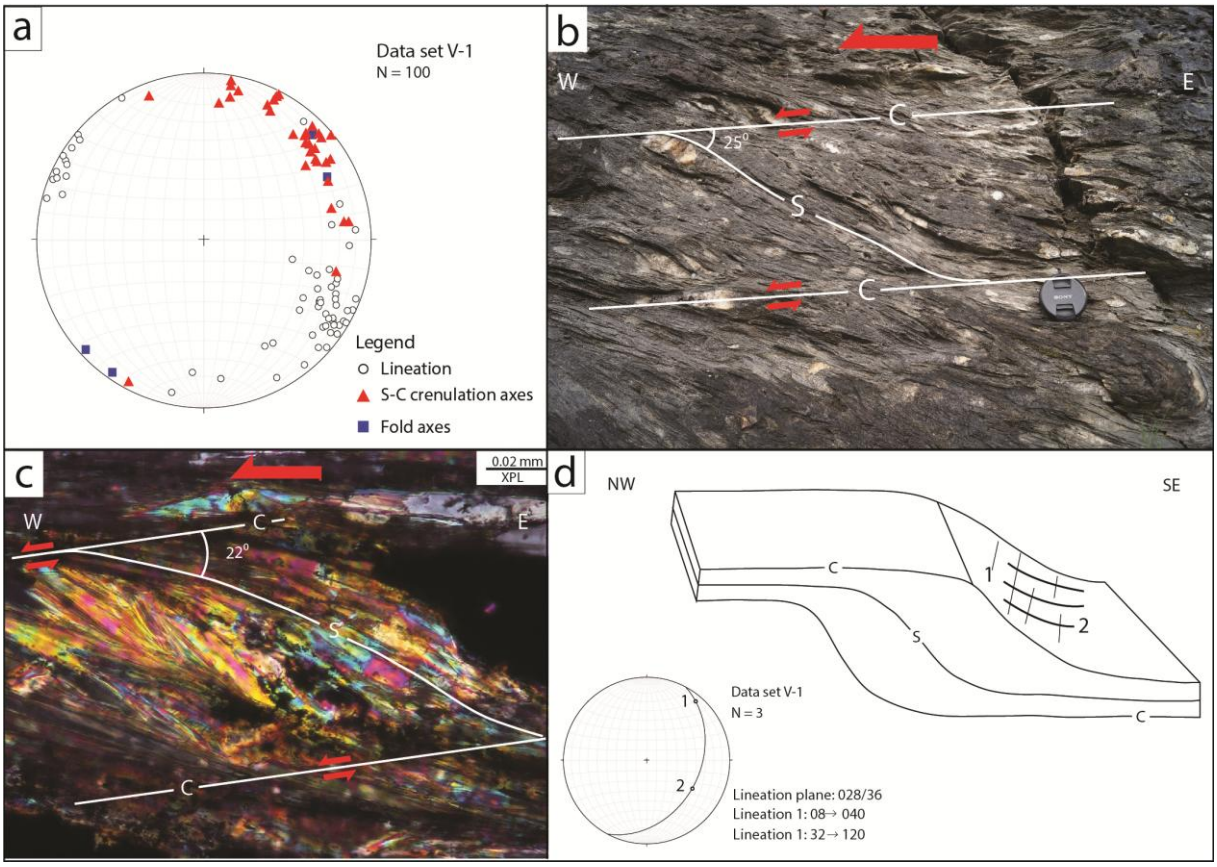

Fig. 63. a) Stereographic projection (equal area, lower hemisphere) of the phyllite at Voss. Data set V-1 in appendix B. **b-c)** S-C structures at macro- and micro-scale indicates top-to-the-W(NW) transport. Sample KOE-30. **d)** Two sets of crenulation lineations which plunge to the NE (1) and SE (2).

4.2.6 Dyranut

Unit 4: Phyllite

The S-C crenulation axes are generally plunging to the NE and some to the SW (Fig. 64), and the shear bands (C-surfaces) are mainly dipping 15^0-20^0 to the N and NW. Well-developed crenulation lineations are frequently found on the SE-dipping foliation plane (S-surface) and plunging with 20^0-40^0 to SE.

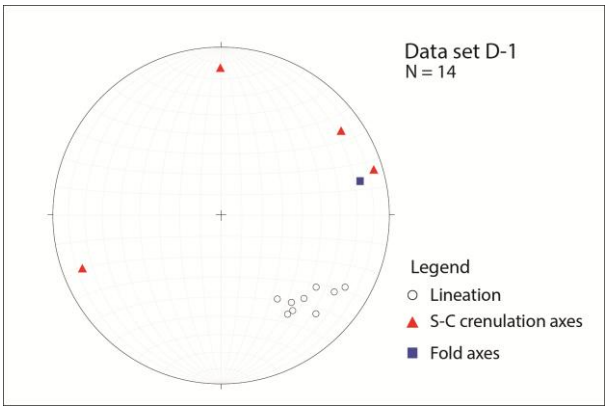

Fig. 64. Stereographic projection (equal area, lower hemisphere) of the phyllite at Duranut. Data set D-1 in appendix B.

Thin-section sample of the phyllite at Dyranut cuts a parallel mesofold (Fig. 65a), where generations of well-developed shear bands are found in the micaceous-rich limbs. The sense of slip is opposite on each limb, as the S-surfaces are dipping specifically to the S (Fig. 65b) and to the N (Fig. 65c). The hinge zone is characterized by S-N-trending cleavage and a higher content of chlorite and calcite compared to the limb areas of the fold (Fig. 65d).

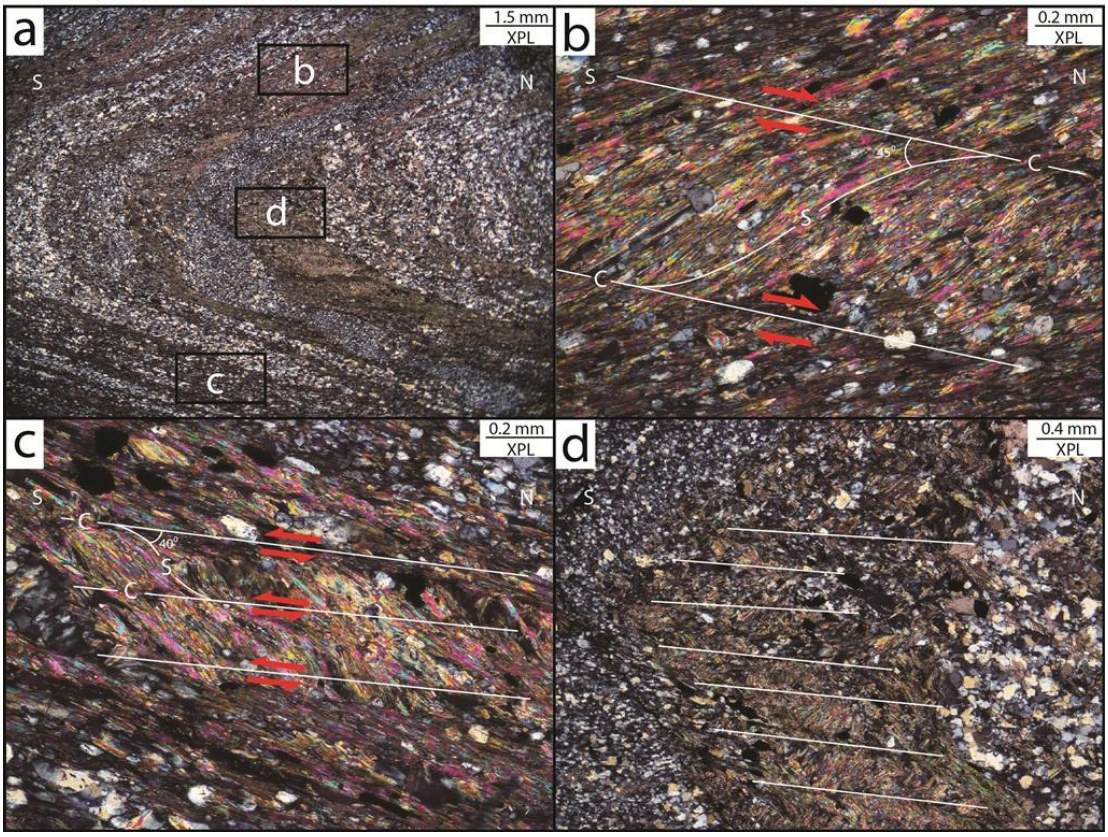

Fig. 65. Cross-section of the S-N trending fold in the phyllite at Dyranut. Sample KOE-4. **a)** Overview thin-section image of the fold. Crenulation cleavage in the limb above the fold hinge indicating right lateral shearing **(b)** whereas opposite sense of shear are found in the limb below the hinge zone **(c)**. S-N axial plane cleavage (white lines) and chlorite are found in the fold hinge **(d)**.

4.2.7 Ustaoset

Unit 4: Phyllite

Most of the study area at Ustaoset is highly covered by vegetation, which restricted field observations and structural measurements. However, at Rukenhovda some meso-scale asymmetric folds are exposed (Fig. 66a). The folds generally occur with a tight opening angle (~40^0) with a consistent (N)W-vergence. The fold axes plunges to the SW and SE (Fig. 66b). A few S-C structures are locally found, in which the shear bands (C-surface) tend to be sub-horizontal, whereas the foliation (S-surface) dips to the N at about 15^0.

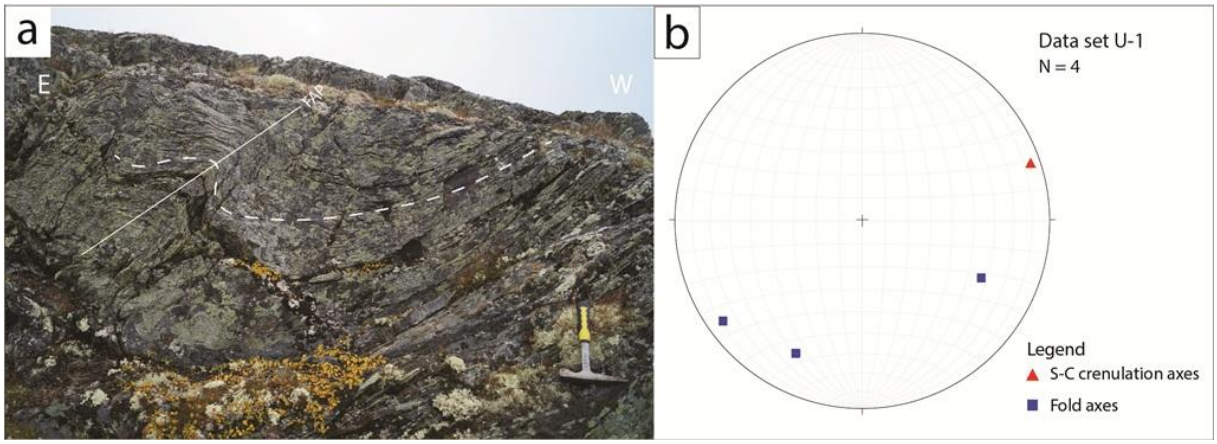

Fig. 66. a) W-verging asymmetric folds at Rukenhovda. **b)** Stereographic projection (equal area, lower hemisphere) of the pyllite at Ustaoset. Data set U-1 in appendix B.

Three samples were collected from Ustaoset, two from Rukenhovda and one from Usteberget. Thin-section analyses of the quartz-rich phyllite at Rukenhovda (described in subsection 4.1.7) indicates alternating layers of quartz and mica which are arranged in a preferred SE-NW orientation (Fig. 67a). Some of the larger grains of quartz are characterized by diffuse and bulged grain boundaries, and strain shadows composed of calcite and quartz are found adjacent to some of the quartz grains (Fig. 67b). Some of feldspar crystals have developed bent polysynthetic twins.

The samples collected stratigraphically higher in the phyllite at Rukenhovda and at Usteberget indicate microstructures which reveal more intense deformation, including chaotic folding and crenulation cleavages in the micaceous layers (e.g. Fig. 67c). Aggregates of recrystallized quartz are sheared and makes up the foliation (S-surface) together with the muscovites (Fig. 67d). Most of the shear bands in the micro-scale S-C structures are dipping to the W, and the C-surface develops at an angle of about 40^0 to S (Fig. 67e). Some of the

foliation planes (S-surface) seem to represent two generations of shearing, in which shearing towards E is strongly overprinted by shearing to the W (Fig. 67f).

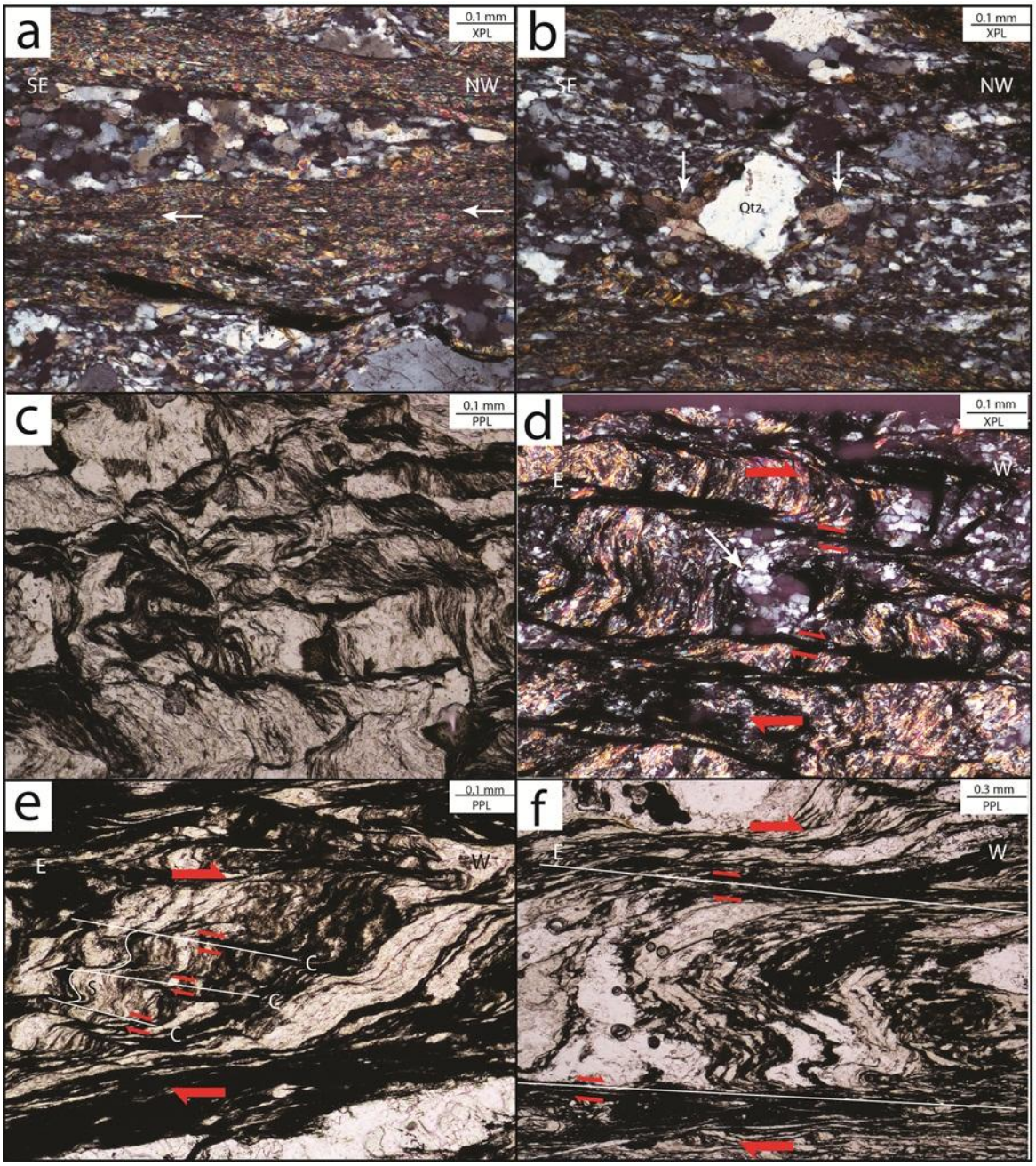

Fig. 67. a) The quartz crystals and muscovites are arranged in a preferred orientation, and crenulation cleavages (arrows) are found in the micaceous layers. Sample KOE-1. **b)** Strain shadows are found on the adjacent to some of the quartz grains. Sample KOE-1. **c)** Chaotic folding and deformed phyllite at Usteberget. Sample KOE-3. **d)** Sheared aggregate of quartz located between developed shear bands. Sample KOE-2. **e)** S-C structures indicates transport to the W. Sample KOE-2. **f)** Re-sheared quartz veins. Sample KOE-2.

4.3 The sub-Cambrian peneplain

4.3.1 Morphological variations

At first sight the sub-Cambrian peneplain seem to represent an almost planar boundary between the basement and the overlying meta-sediments (e.g. Fig. 68a). However, irregularities are also revealed from depressions in the basement, like for instance the 2 meter deep depressions seen at outcrop-scale of Usteberget at Ustaoset (Fig. 68b), which also has been described in earlier literature.

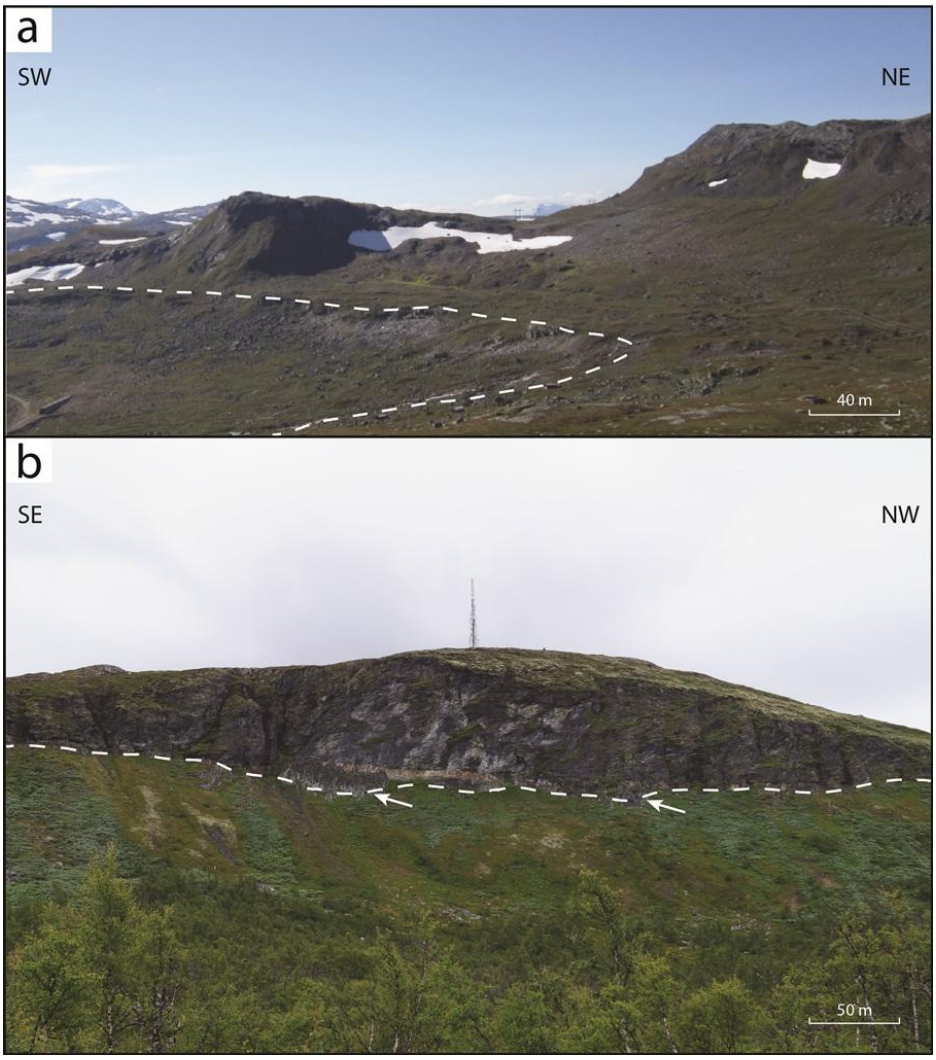

Fig. 68. Exposure of the sub-Cambrian peneplain in the Hardangervidda area. **a)** At mesoscale the peneplain seems to constitute a planar plateau on Finse. **b)** Local irregularities are displayed as depressions in the basement at Ustaoset.

Additionally minor depressions are locally displayed in the Hardangervidda area, like for instance at Jomfrunuten at Finse. Meta-sediments including basal conglomerate and quartz schist, that constitutes a thickness of about 1 meter, rest on the basement. In parts of the location the basement sticks up from the quartz schist displayed as a window (Fig. 69) and representing non-planarity of the peneplain.

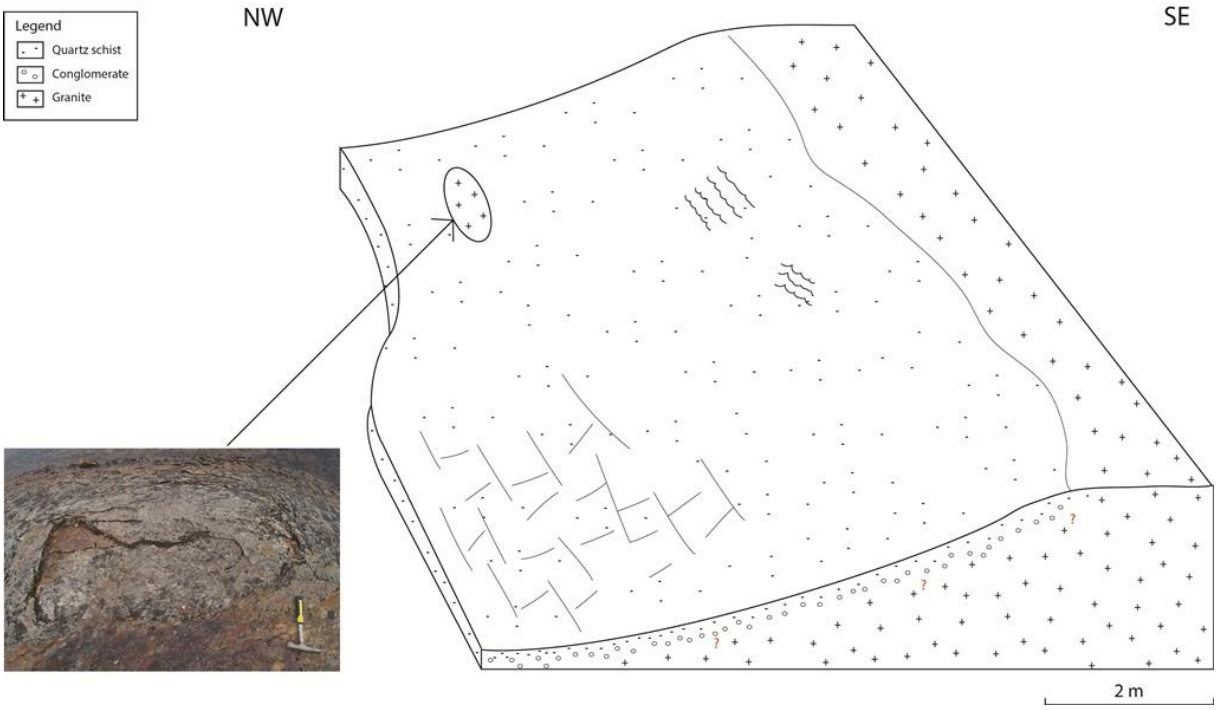

Fig. 69. Location overview at Jomfrunuten, Finse. Irregularities of the sub-Cambrian peneplain are indicated by the window of basement sticking up from the quartz schist.

The contoured map of the contact between the basement and the overlying meta-sediments which represents the study area reveals topographic variations of the sub-Cambrian peneplain by the local depressions up to a few hundred meters (Fig. 70). The NW-SE-trending profiles A-A’ and B-B’, which cross the main localities, indicates a gradual decrease in elevation with about 300 m in the area between Finse and Ustaoset. In the NW part of the profiles the elevation of the peneplain considerably falls. Additionally, irregularities of the peneplain are indicated as depressions up to 250 meters on Finse (profile A-A’) and Hardangerjøkulen (profile B-B’).

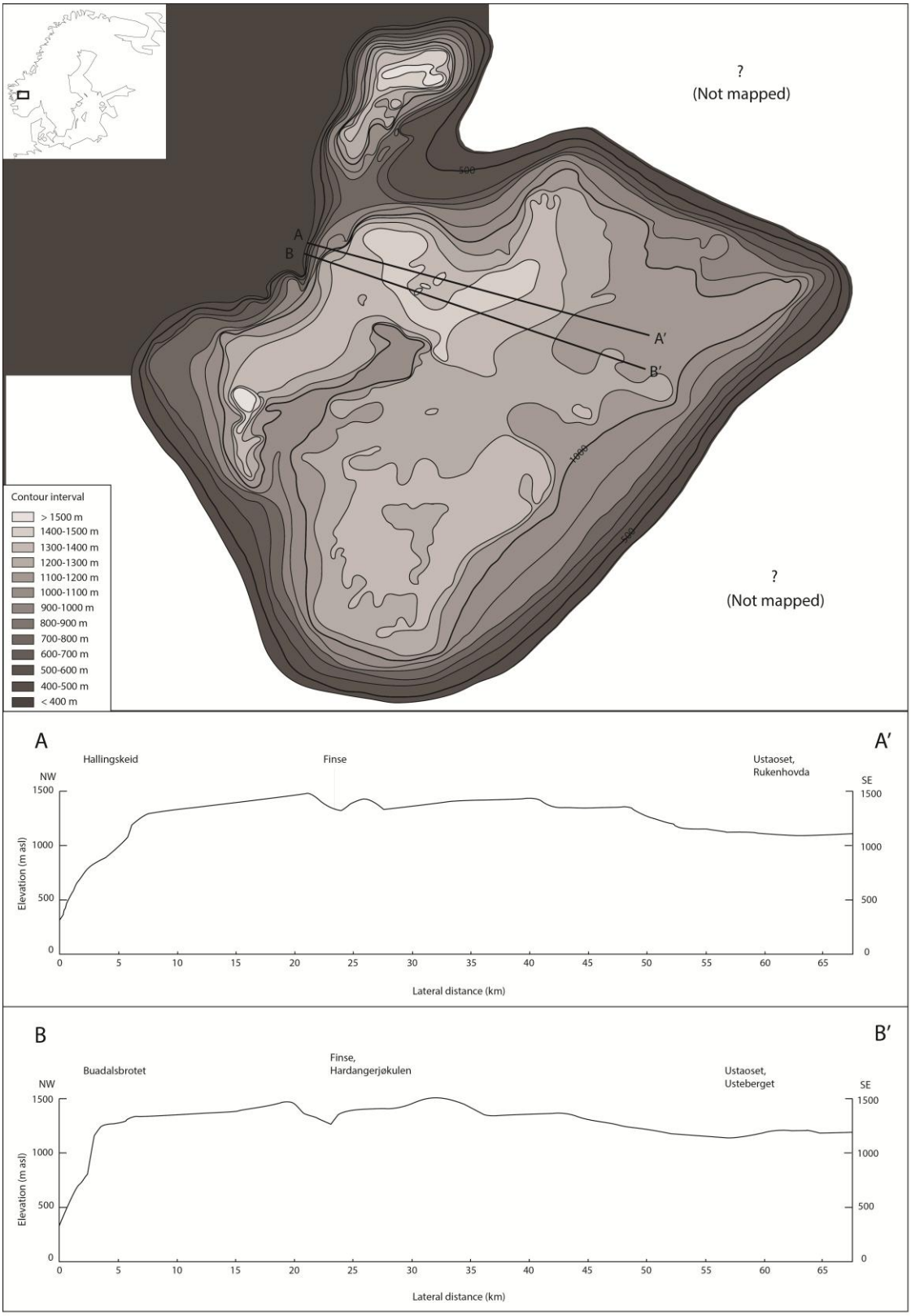

Fig. 70. Contour map of the elevation of the uppermost basement surface in the Hardangervidda area and NW-SE-trending profiles indicates local depressions of up to some hundred meters. Constructed from the geological map Odda 1:250 000 (Sigmond 1998).

4.3.2 Related lithological conditions

The lithologies which rest on the sub-Cambrian peneplain vary locally in the study area (Fig. 71). In general the contact is overlain by phyllite which constitutes the regional Caledonian décollement zone, and represents a tectonic contact between the basement and the overlying Caledonian nappe units. However, basal conglomerate and meta-sediments resting on the basement are locally found in the study area representing a (almost) primary contact. Simple stratigraphic columns of the applicable locations (Fig. 71) show that the conglomerate occurs in the west of the study area (e.g. at Hegrenuten, Buadalsbrotet, Sandå, Finse), whereas meta-sandstones are more prevalent to the east (e.g. at Finse, Usteberget).

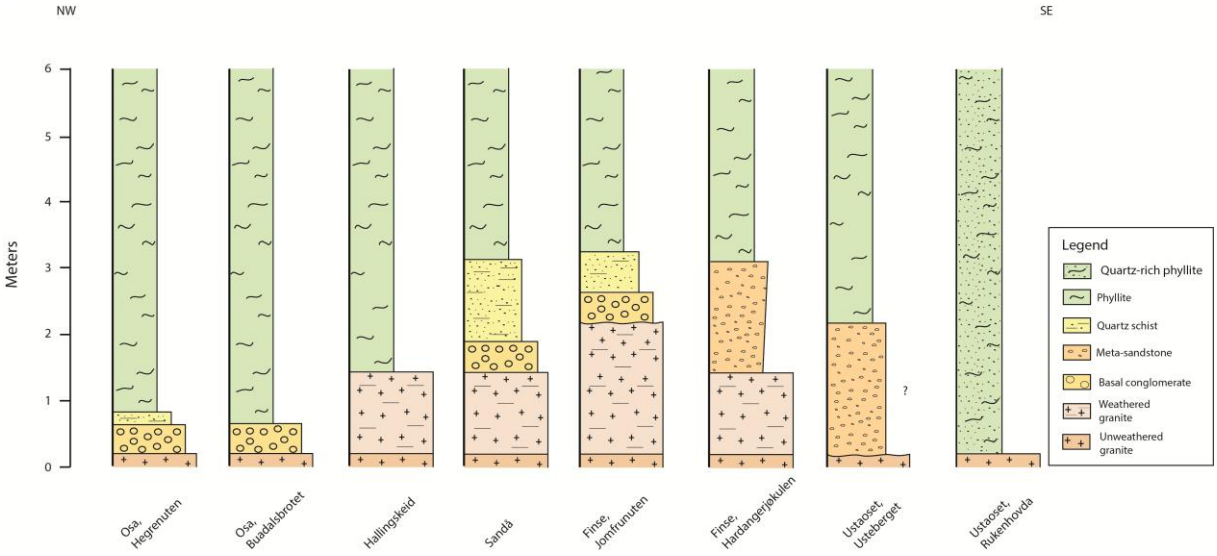

Fig. 71. Simple stratigraphic columns of the meta-sediments including conglomerate, meta-sandstone and quartz schist. Note that the estimated thickness of the meta-sandstone at Ustaoset might be some incorrect, as it is based on outcrop-scale observations.

4.4 Summary of the results

The lithological units found in the Hardangervidda region are represented by granitic basement, basal conglomerate and meta-sandstone, quartz schist, phyllite and locally remnants of the Caledonian nappe unit. The Precambrian basement occurs as a 1.5-2.0 meter thick, weathered zone at Finse, Sandå and Hallingskeid. Basal conglomerate and meta-sandstone rest locally at the basement in most of the main localities, and gravelly conglomerates appear at Finse and Sandå, whereas a poorly sorted conglomerate occurs at the locations at Osa. Microfabrics and crystalloplastic deformation structures, including strain shadows, twin geometries in calcite crystals, kinked and bent twins, microcracks in quartz and

feldspar crystals, parallel trails of fluid inclusions in quartz, in addition to recrystallized quartz, are found in the weathered basement and the overlying basal sediments. Structural features found in the phyllite unit include micro-and macro-scale S-C structures and asymmetric folds which together indicates a dominant top-to-the-NW shear.

The sub-Cambrian peneplain is generally observed as a sub-horizontal transition between the Precambrian basement and the overlying meta-sediment. At Finse and Usteberget the contact occur with pits that reach depths up to ~2 meter. The contour map and the vertical profiles of the uppermost basement surface indicate irregularities of the sub-Cambrian peneplain with depressions up to 250 meters in the Hardangervidda area.

5 Interpretation and discussion

In the present study, the geology of the Hardangervidda area has been mapped representing an evolution from the Neoproterozoic to the Devonian. In the following subsections, the weathering and peneplanization of the Precambrian basement will be discussed, which includes state of weathering, possible factors which accelerated the weathering and a suggested estimate for how long the Baltic craton was decomposed to become the peneplain. The depositional conditions during the Cambrian transgression will be discussed in order to reconstruct the geomorphology, and the irregularities of the peneplain will be explained with respect to whether these are of Neoproterozoic age or could mainly be related to Caledonian and Devonian tectonics. The tectonic evolution with respect to Caledonian thrusting and post-orogenic extension are finally addressed by means of paleotemperature estimates and structural features, in addition to the local variations in strain. Note that the deformation structures recorded in this study are interpreted in terms of Caledonian thrusting (D_1) and post-orogenic extension (D_2).

5.1 Peneplanization and weathering of the Precambrian basement

5.1.1 Erosion of the landscape and weathering of the basement

At the end of the Neoproterozoic, the Sveconorwegian orogeny entered the last tectonic phase (Bingen *et al.*, 2008), and was followed by the global rifting from the breakup of Rodinia (Cocks & Torsvik, 2005). For this reason, the Baltic craton was subjected to intense erosion and peneplanization. A precise number of how long the Precambrian basement was exposed to erosion and weathering lacks in the literature. However, by considering the time period from the uplift and gravitational collapse of the Sveconorwegian orogeny (ca. 970 Ma; Bingen *et al.*, 2006) until the craton was flooded as a result of the transgression in Early Cambrian (ca. 530 Ma; Cocks & Torsvik, 2005), gives a total period with collapse, erosion and weathering of at least 400 Ma.

5.1.2 State of weathering

The degree of weathering of the Precambrian basement is quite important in order to get an idea for how long the Baltic shield was exposed. Based on the differences in textural, mineralogical composition and micro-scale features for the fresh and altered granite, the degree of weathering of the basement at Finse, Sandå and Hallingskeid is determined. Considering the alteration of plagioclases, Gabrielsen *et al.* (2015) suggested that the albitization of the fine-grained muscovite, found in the weathered basement at Hardangervidda, to principally be related to the Caledonian orogeny in the sense of metasomatism sited along the peneplain at the boundary between the basement and the overlying meta-sediments (Franco, 2012). As the data from the present study show well-developed crystals of impure phengite (e.g. Fig. 16b), it is also possible that the plagioclases at first were altered by chemical weathering during the peneplanization in the Neoproterozoic, and later evolved to perfect crystals during Caledonian and Devonian tectonics. Thus, as the white micas were most likely affected by later tectonic events, caution is needed when considering whether the albitization of the plagioclase is a result of alteration generated by weathering and thereby when determining the state of weathering of the granites.

The first impression of the highly unconsolidated and iron-filled fractures in the granite found at Jomfrunuten at Finse (Fig. 12) suggests the basement to be intensively weathered. The higher content of resistant quartz and altered products in the weathered granite (Fig. 14) indicate a high degree of weathering. As the weathered granite at Jomfrunuten has a higher content of resistant microcline (KOE-6) compared to the weathered granite at Hardangerjøkulen (KOE-10), it is suggested to indicate the granite at Hardangerjøkulen to be slightly more weathered. This assumption is strengthened by the lack of biotite in the weathered granite at Hardangerjøkulen. The micaceous inclusions in the plagioclase crystals, found in the unweathered granite at Finse (Fig. 15d), are concentrated in the core of the plagioclases which suggest to represent unmixing from solid solution during crystallization of the granite. On the other hand, in the weathered granites the mica crystals appear larger and scattered throughout the plagioclase crystals (Fig. 15e, f) and are thus suggested to have developed during later weathering and/or metasomatism. Based on all these assumptions, the granite at Finse is determined to be highly weathered, in which the sample at Hardangerjøkulen seems to be particularly strongly weathered. The texture and appearance of the weathered granite at Sandå (Fig. 23) is quite similar as the ones at Jomfrunuten at Finse. The micro-fractures filled with weathering products including mica and iron-oxides (Fig. 26b)

probably indicate hydrological alteration in these permeable zones from the weathering. The high sericitized plagioclases (Fig. 26) in the weathered granite might explain the higher content of muscovite and lower portion of plagioclase compared to in the unweathered granite (Fig. 25).

The high content of alteration products and resistant microcline in the weathered granite, in addition that the biotite is completely decomposed (Fig. 25), indicate that the granite is highly weathered. Compared to the characteristics of the weathered granite at Finse and Sandå, the weathered basement at Hallingskeid seems to have a smooth weathering surface (Fig. 31b). The restricted sericitization of plagioclase (Fig. 34c, d), in addition to the limited changes in volume percentages of biotite and plagioclase (Fig. 33), and the generally limited bleaching and thus oxidation of biotite (Fig. 34e, f) for the unweathered and weathered granites, suggest the basement at Hallingskeid to only be slightly weathered.

Recronstructions of the palaeogeography of Baltica suggest that southern Norway was located almost at equator, i.e. in a tropical climate, during the mid-Neoproterozoic ~750 Ma (Torsvik & Cocks, 2005). As the plants were not evolved in the Precambrian and lower Palaeozoic times, the weathering rate must have been lower during the peneplanization at this time as vegetation modifies pH, generated organic acids and CO_2, in addition that roots from plants perform physical weathering (Ollier & Clayton, 1984; Egli *et al.*, 2008). Considering the tropical climate, the precipitation was most likely characterized by heavy rainfall, and since there was no vegetation to catch the precipitation on the craton, we can expect that the erosion and runoff was quite large. In addition, faults and smaller scale fractures of possible Neoproterozoic age might have allowed fluid circulation and accelerated the chemical weathering locally, as observed from the micaceous and iron-rich cm- to mm-scale fractures in the basement at Jomfrunuten (Fig. 12b and 13b). Additionally, freeze-thaw weathering generated by the possible ice caps (Ollier & Clayton, 1984) might have accelerated the weathering rate, but no evidences of glaciations were observed in the field.

5.1.4 Local variations in degree of weathering

The variations between the highly weathered basement at Finse and Sandå compared to the slightly weathered basement at Hallingskeid can be explained by several factors. First of all, the texture of the granite can influence the weathering rate (Ollier & Clayton, 1984). The smaller-sized crystals comprising the granite at Hallingskeid (Fig. 32a) might be harder to weather, as they constitute a greater surface compared to the larger phenocrystals which

constitute the granites at Finse and Sandå (Fig. 11a, 13a, 24a). The local variations in state of weathering can possibly also be explained by primary irregularities of the basement. At Finse, the weathered basement was found in a pit of the peneplain (e.g. Fig. 69) which might have protected the weathered basement from abrasion during later tectonic events. In this case, the degree of protection depends on the depth of the possible depressions. This will be discussed further in subsection 5.2.2.

5.2 The sub-Cambrian peneplain and sedimentation during the Cambrian transgression

5.2.1 Depositional conditions during the Cambrian-Ordovician

The stratigraphy and the lithological properties of the meta-sediments found at the main locations clearly represent the flooding of the Precambrian craton at the dawn of Cambrian. Compared to the lithostratigraphy of the Hardangervidda group, presented in Fig. 8, the meta-sediments described in the present study are interpreted to represent the lowermost Låven formation (Andresen, 1978). Nielsen & Schovsbo (2011) suggest the deposition conditions during the transgression of the Baltic shield to initiate by a shallow shelf environment characterized by high clastic supply during Early Cambrian times, which followed by a reduced clastic supply during the mid-Cambrian to Ordovician.

Basal conglomerate and meta-sandstone

The basal conglomerate, described as unit 2 in subchapter 4.1, occurs with significantly different character at the locations, for instance as the poorly sorted conglomerate at Osa in west and the more well-sorted gravel found at Sandå, and at Jomfrunuten and Hardangerjøkulen at Finse. The sub-rounded to rounded quartz grains enclosed by calcite-cemented matrix of the gravel at Sandå and Finse can suggest a high energy and marine depositional environment. However, it is also important to consider that calcite-cementation can occur in a fluvial environment. As the conglomerates show a certain degree of sorting and occur with alternating layers of sand, this can indicate changes in the water energy level in both a marine environment and in rivers. Previous studies of the conglomerates at Sandå and Finse (Goldschmidt, 1912a), and at Ustaoset (Goldschmidt, 1925) includes findings of marine fossils (Gastropod; *Torellella Lævigata*, Trilobite; *Strenuella Linnarssoni*) representing upper Early Cambrian, and phosphate concretions which typically precipitates from sea water (Allaby, 2008). This suggests that the gravel was deposited in a foreshore environment.

Whether the fossils were deposited *in situ* in a period with lower energy or were transported from a low energy environment has not been discussed in the literature.

The coarser and poorly sorted conglomerate at Buadalsbrotet and Hegrenuten at Osa (Fig. 38 and 39) raises the question concerning the linkage between depositional environment and erosional irregularities of the sub-Cambrian peneplain. The occurrence of the conglomerate coincides with descriptions in Reusch *et al.* (1902); the conglomerate is composed of granitic and gneissic pebbles, sited in a matrix of black phyllite. However, the depositional environment of the conglomerate was not further discussed.

Two depositional environments, upper shoreface and terrigenous (alluvial), can be suggested on the basis of the textural features of the conglomerate described in this study. As the pebbles in the conglomerate lack grading and evident orientation, a beach environment seems rather unlikely. In addition, the largest pebbles are up to 51 cm in diameter, which is quite large for being deposited in a foreshore environment. Therefore, an alternative interpretation can be that the conglomerate was deposited in a continental environment. The fact that the conglomerate occurs as poorly sorted, and the pebbles shows restricted imbrications and grading, suggest that it represents alluvial fan deposits formed by debris flows. However, this is problematic as we need to consider that the conglomerate was deposited on an assumed flat and erosive surface of the basement at the entrance of the Cambrian (e.g. Artyushkov *et al.* 2000; Cocks & Torsvik 2005; Nielsen & Schovsbo 2011; Gabrielsen et al. 2015), especially in the Hardangervidda area. This raises the question of what triggered the potential gravitational flow. Considering the conglomerate being deposited by rivers would bring to the same issue: how could a river transport such large cobbles in what appears to be an area of regionally low topography? In this case, the peneplain must have constituted a greater relief in the Neoproterozoic than earlier presumed. It is also conceivable that steep faults generated during the rifting events ca. 570-550 Ma (Cocks & Torsvik, 2005) created a local relief that triggered gravitational flow. From the geological bedrock map Odda 1:250 000 by Sigmond (1998), a WSW-ENE trending fault is found in the basement close to the locations at Osa, which might support this theory. As the faults only influenced the basement unit, it is difficult to estimate the offset of the faults and thus how steep the local elevation might have been.

Basal conglomerates found in the Oslo Region are suggested to have been formed in a deltaic or fluvial environment (Kiær, 1916; Vogt, 1924). Most of these conglomerates are

preserved in depressions ranging from 10 cm to 50 m in the basement, which reflects the regional slope and relief of the peneplain in the Neoproterozoic. Further studies of basal conglomerates in eastern Norway (Spjeldnæs 1955) suggested that they were deposited in depressions formed by erosion along joints in the Precambrian basement. Compared to the conglomerate at Osa, this raises a consideration that rivers might have followed Neoproterozoic weakness zones, and thus deposited the conglomerate. Whether the conglomerate was deposited by rivers or debris flows is difficult to determine based on the lack of sedimentary structures. However, it is likely that the conglomerate was deposited in depressions in the Precambrian basement in a terrestrial environment prior to the marine flooding.

Quartz schist

The quartz schist, resting on the basal conglomerate at Osa, Sandå and Finse, displays symmetrical ripple marks (Fig. 20) suggest a shallow shelf depositional environment along a N-trending coastal line. Considering the large content of mica (~45 %) raises the question how the clay-rich sediment could be deposited in that high-energy environment. The lack of slopes of the Baltic shield during the transgression suggest a low degree of sorting of the sediments and thus might explain the high content of clay. The high volume percentages of white mica can also be a result of metasomatism of K-feldspar from an original arkose (e.g. Vernon & Clarke, 2008). As the quartz schist displays structural features including ptygmatically folded quartz veins (Fig. 29c) and microscale S-C shear structures (Fig. 55a), micro-scale fringe structures (Fig. 49b) and recrystallization of the quartz (Fig. 49 and 55b), the deformation and metamorphism is likely to have been generated by the Caledonian and Devonian tectonics.

Phyllite

The phyllite, which stratigraphically rests on top of the basal conglomerates and quartz schist, indicates deposition at higher water depths in which the energy must have been sufficiently low to allow settling of suspended fine sediments including silt and clay. Artyushkov *et al.* (2000) suggested that the sea-level fluctuated only a few tens of meters (~10 to 20 m) during the Cambrian-Ordovician, which may reflect the very low relief of the sub-Cambrian peneplain and the sensitivity of flooding from an only slightly increasing sea-level. For this reason, it is conceivable that the phyllite was deposited at water depths of 20-30 m. The calcareous interlayers found in the phyllite at Hegrenuten at Osa (Fig. 41) is assumed to

originate from calcite-rich materials, like shell fragments, which might have been transported by storms from the shallow shelf to more distal areas, or might reflect periods with lower sedimentation rate. The quartz-rich phyllite found in the lowermost section of the phyllite unit at Rukenhovda on Ustaoset (e.g. see lithostratigraphy B in Fig. 44) may indicate a locally higher clastic supply during the flooding, or might be related to storm events.

5.2.2 Primary depressions in the Precambrian basement

Present literature suggest that the depressions in the sub-Cambrian peneplain in southern Norway and Sweden, and in which basal conglomerate and meta-sediments are found, are likely to have been formed by denudation (e.g. Elvhage & Lidmar-Bergström 1987; Gabrielsen *et al.* 2015). In order to determine whether the basal sediments described in the present study were deposited in primary depressions of the basement surface or if the depressions were developed as a result of later tectonic events, the macro- and micro-structures of the meta-sediments can be compared with the texture of the sediments and the morphological variations of the peneplain.

The microfabrics in the basal conglomerates and in the quartz schist at Finse and Sandå indicate deformation at temperatures of 200-400 °C (e.g. Burkhard, 1993; Passchier & Trouw, 2005). The asymmetrical fringe structures in the quartz schist at Jomfrunuten at Finse (Fig. 49b) indicates non-coaxial deformation, and additional S-C structures indicates shear bands that intersect the foliation at an angle of 45^0 (Fig. 55a), which suggests the meta-sediment to only be slightly sheared (Barker, 1990). In overall, the deformation of the basal sediments is assumed to be related to later tectonic events.

The basal conglomerate at Osa shows relatively restricted deformation structures. As the only microfabrics found in the gneissic pebbles of the conglomerate at Buadalsbrotet appear as recrystallized quartz that are elongated in a preferred orientation (Fig. 59a), these probably represent the primary gneissic texture of the Precambrian basement. The microfabrics found in the elongated zone of the conglomerate (Fig. 38), including strain shadows (Fig. 59b), fluid inclusions (Fig. 59c) and developed e-twins in the calcites (Fig. 59d), represent deformation at low-temperatures (<300 ^{0}C) and might be related to Silurian and Devonian deformation. Perthite flames found in the granitic pebbles of the conglomerate at Hegrenuten, may have grown by unmixing of alkali feldspar during cooling from high temperatures or from deformation (Debat *et al.*, 1978; Pryer & Robin, 1996). As the flames display a preferred orientation throughout the sample (Fig. 60a) and asymmetric tails bends

around the quartz grains (Fig. 60d), it can indicate the flames to have developed from non-coaxial deformation. However, as most of the quartz grains have clear grain boundaries and no evidence of recrystallization (Fig. 60c, d), it is likely that the albite-rich lamellas are related to magmatic crystallization processes. By comparing the phyllite constituting the matrix of the conglomerate at Buadalsbrotet with the phyllite unit found stratigraphically above, the strain is significantly different as the overlying phyllite is well foliated and display undulating layers of mica and quartz compared to what is found in the only slightly foliated phyllite in the matrix. Therefore, it is likely that the conglomerates have been relatively protected from deformation in the Neoproterozoic depressions.

The microstructures found in the quartz schist differ at Finse, Sandå, and Osa, as recrystallized and elongated quartz with bulged grain boundaries (Fig. 49a, 55b), fringe structures (Fig. 49b) and S-C structures (Fig. 55a) are found at Finse and Sandå, and only slightly recrystallized quartz and triple junctions among the quartz aggregates suggesting a lower-temperature diffusion, probably evolved from pressure solution (Van der Pluijm *et al.*, 2004). In overall, this can indicate that the conglomerate at Osa has been more protected from deformation than at Finse and Sandå, and thus must have been deposited in a deeper depression (Fig. 72). The 350 meter deep meteor crater at Ritland, southern Norway, can be used as an analog for this. Here, the Precambrian basement was excavated in the Early Cambrian (Riis *et al.*, 2011). Structural differences of the Cambro-Silurian meta-sediments deposited in the crater and outside the crater rims indicated an evident difference in the strain gradient, and are most likely to indicate protection of the sediments found in the depression.

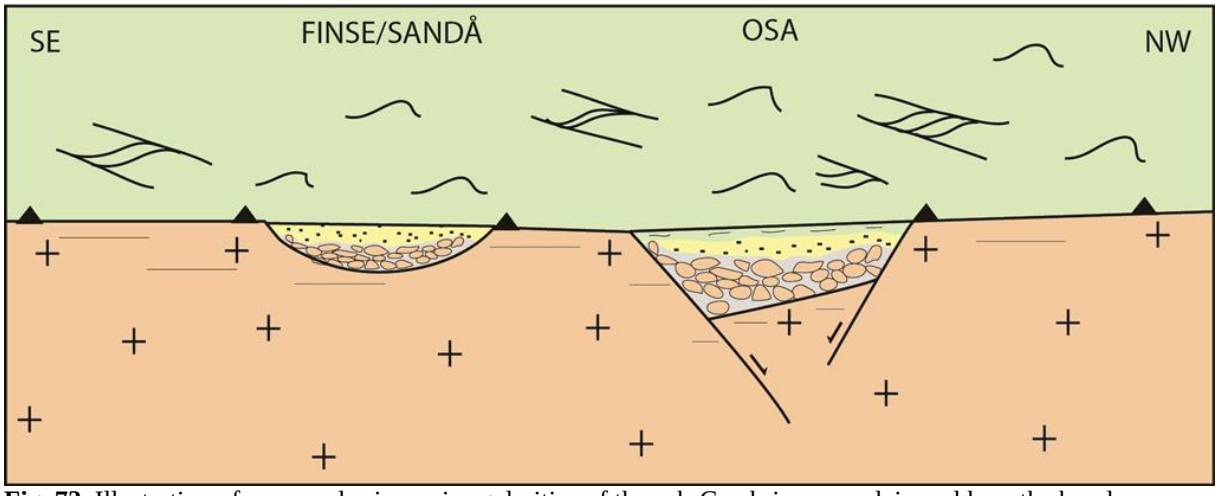

Fig. 72. Illustration of proposed primary irregularities of the sub-Cambrian peneplain and how the basal sediments were protected from Caledonian deformation.

5.3 Caledonian thrusting

The change from divergent to convergent plate motions in the Late Cambrian resulted in subduction of the Baltic margin beneath Laurentia, which eventually resulted in continental collision in early Silurian times (ca. 420 Ma; e.g. Stephens, 1988; Fossen, 1992). In order to reconstruct how the collision and Caledonian thrusting influenced the Hardangervidda area, the paleotemperatures of the autochthonous units are discussed by means of mineral content and microfabric in the following sections.

5.3.1 Paleotemperature

Based on the reconstructed geometry of Baltica during Silurian subduction, prepared by Fossen (2000), the Hardangervidda area seems to have reached a maximum burial depth of ~20 km, corresponding to temperatures of about 500 ^{0}C. An overview map of estimated temperatures in southern Norway during the Caledonian thrusting (Fauconnier *et al.*, 2014) indicates the rock units to have experienced metamorphism at about 450-500 ^{0}C at Voss, Osa and Hallingskeid, temperatures of 400-450 ^{0}C at Sandå, Finse and Dyranut, and about 350-400 ^{0}C at Ustaoset (Fig. 73). In general, the presence of biotite and garnet found in the phyllite unit in the west (e.g. KOE-21, KOE-29, KOE-30) and in the biotite-rich phyllite matrix in the conglomerate at Buadalsbrotet at Osa (KOE-22), indicates upper greenschist facies to lower amphibolite facies, and the chlorite and quartz found in the phyllite in the east (e.g. KOE-2, KOE-3, KOE-4) indicates mid-greenschist facies. This increasing metamorphism from east to west is proposed to reflect the east-southeast tapering of Scandinavia (e.g. Lindquist, 1990; Fossen & Rykkelid, 1992; Fossen 2000).

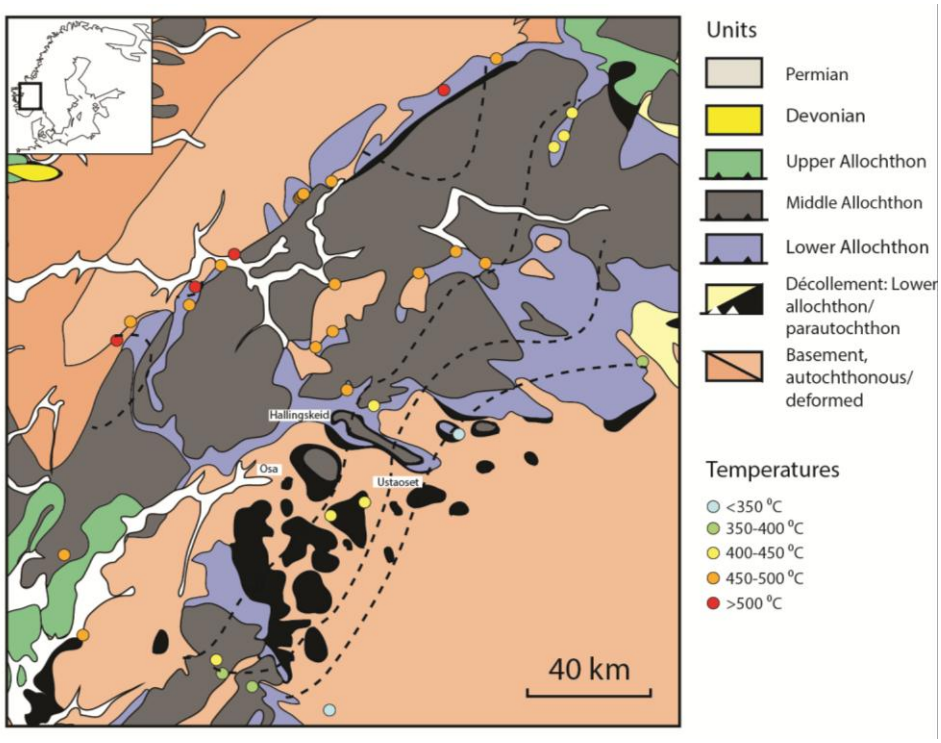

Fig. 73. Estimated temperatures in southern Norway. Modified after Fauconnier *et al.*, 2014.

Garnet, found in the phyllite at Hallingskeid (Fig. 36b), has previously not been recorded that far southeast in southern Norway, as it has only been found approximately 12 km NW of Myrkdalen (Sigmond 1998). The asymmetric tails of chlorite, found adjacent to the garnet crystals, indicates top-to-the-E shear (Fig. 58b) which suggests that the crystallization of garnet is related to the thrusting event (D_1). It might also be suggested that crystallization of garnet occurred further to the west at higher burial depths and were thereafter transported along the basal thrust zone into its present position at Hallingskeid.

The recrystallized quartz with bulged grain boundaries is found in the weathered basement and the basal meta-sediments at Ustaoset, Finse, Sandå and Hallingskeid (e.g. Fig. 46d, 53b, 57b, 67d), and indicates plastic deformation at temperatures of 300-400 °C (Stipp *et al.*, 2002; Passchier & Trouw, 2005). The kinked and fractured feldspar crystals found in the weathered granite at Hallingskeid (Fig. 57a) and in the basal conglomerate at Sandå (Fig. 54e) represent low-medium grade deformation conditions (Pryer, 1993; Passchier & Trouw, 2005) at temperatures ca. 400-500 °C, which correspond to a burial depth of 20 km. Compared to the paleodepth estimates provided by Fossen (2000) and recent temperature estimates mapped by Fauconnier et al. (2014), the microstructures observed in these localities are proposed to represent the event of Caledonian thrusing (D_2).

5.3.2 The importance of the sediments during the Caledonian thrusting

The basal sediments and the phyllite unit at Hardangervidda which constitute low shear strength, acted as a basal décollement zone during the Caledonian thrusting (e.g. Fossen & Rykkelid, 1992, Fossen, 2000). For this reason, the strain was highly localized in this zone. As most of the thrust structures most likely were overprinted by later extensional structures, they are not prominent in the autochthonous unit (Fossen, 1993; Wennberg, 1996). Overprinting relations and kinematic indicators will be discussed further in subsection 5.4.2.

5.4 Post-Caledonian collapse

The exhumation of the Baltic crust was followed by events of orogenic collapse and backsliding of the tectonic wedge (410-400 Ma; Fossen, 1992). Three main extensional stages have been identified (Fossen, 1992; Fossen, 2000; Fossen, 2010). As the crust was uplifted, the temperature decreased and the deformation occurred in a brittle regime.

5.4.1 Paleotemperatures

Most of the microstructures found in the weathered basement and the meta-sediments along the sub-Cambrian peneplain in the Hardangervidda area include strain shadows, asymmetrical fringe structures, impingement microcracks and internal fractures in quartz grains, and parallel trails of fluid inclusions in quartz, which in overall represent deformation at in a low-temperature deformation regime (<300 °C; Roedder, 1984; Passchier & Trouw, 2005). These microstructures are thus proposed to represent deformation in the upper crustal level, estimated to 12 km depths, and might be related to the extension tectonic of the Caledonides (D_2). The narrow and straight to thick and bent e-twins in the calcite crystals, found in the basal conglomerates at Finse and Osa, represent lower temperature deformation regimes (< 250 °C; Ferrill, 1991; Burkhard, 1993), corresponding to a crustal depth of ca. 10 km. The opposite sense of slip in the limbs of the mesofold found in the phyllite at Dyranut (Fig. 65) indicates flexural folding in a layer with mechanical significance in the upper crustal level. Thus, the active folding is proposed to be related to the extensional tectonic of the Caledonian orogeny (D_2).

The subhorizontal joints found in the basement at Finse (Fig. 45b) and at Hallingskeid are proposed to be related to the event of exhumation as they might have developed parallel to the crustal surface. The NE-SW trending fractures found in the nappe unit at

Hardangerjøkulen (Fig. 52a) indicate extension in a NW-SE direction which is consistent to the direction of extensional collapse of the orogenic wedge (e.g. Fossen, 1992; Fossen, 1998; Fossen & Rykkelid, 1992; Fossen, 2000). Thus, it is likely that the fractures, observed in the basement and the nappe unit, represent the exhumation of the crust and Mode III of the post-Caledonian extensional history.

5.4.2 Transport direction during backsliding of the orogenic wedge

Most of the shear sense indicators found in the phyllite unit of the basal décollement zone generally indicates top-to-the-NW movement based on the S-C structures and the NW-verging folds, which are consistent with D_2 shearing. Similar structural features have also been observed in southern Norway (e.g. Fossen, 1993; Fossen & Holst, 1994; Wennberg, 1996), and is interpreted to be a result of back movement of the orogenic wedge (Fossen, 1992). Thus, it is likely that the NW-shearing structures are related to the post-Caledonian extensional event.

For some of the locations, the overprinting relations of the thrust structures are significant. For instance, two stages of deformation are clearly evidenced by the folded boudins found in the nappe unit at Hardangerjøkulen (Fig. 52b). The competent layers seem to have experienced extension in the instantaneous field of stretching to form the boudins (Fig. 74a) during top-to-the-SE movement, which are interpreted to be related to Caledonian thrusting (D_1). As the present boudins are folded and thrusted to the NW, it is conceivable that they were folded in the field of instantaneous shortening (Fig. 74b) during backsliding of the orogenic wedge (D_2).

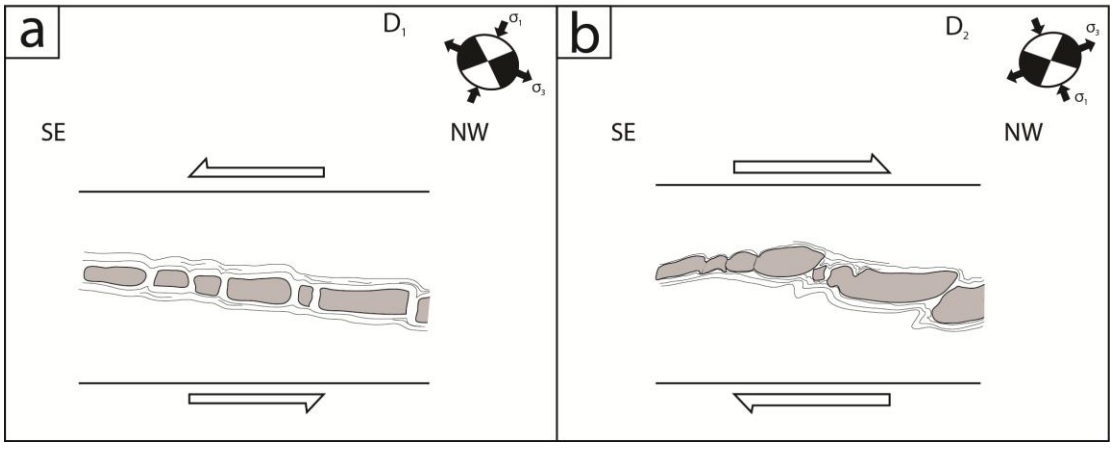

Fig. 74. Schematic illustration of the two tectonic events. **a)** Boudinage of the competent layers in the gneiss accordingly experience compression **(b)** expressed by folding of the boudins, which suggest to represent the event of D1 and D2, respectively.

Overprinting relations are also found among the S-C structures in the phyllite unit at Ustaoset (Fig. 67f). Considering the geometry of the foliation, it is suggested that shear bands were developed from top-to-the-E shearing during Caledonian thrusting (D_1) (Fig. 75a). As a result of the extension tectonic, the sense of shear was basically reversed which resulted in re-shearing of the foliation (Fig. 75b).

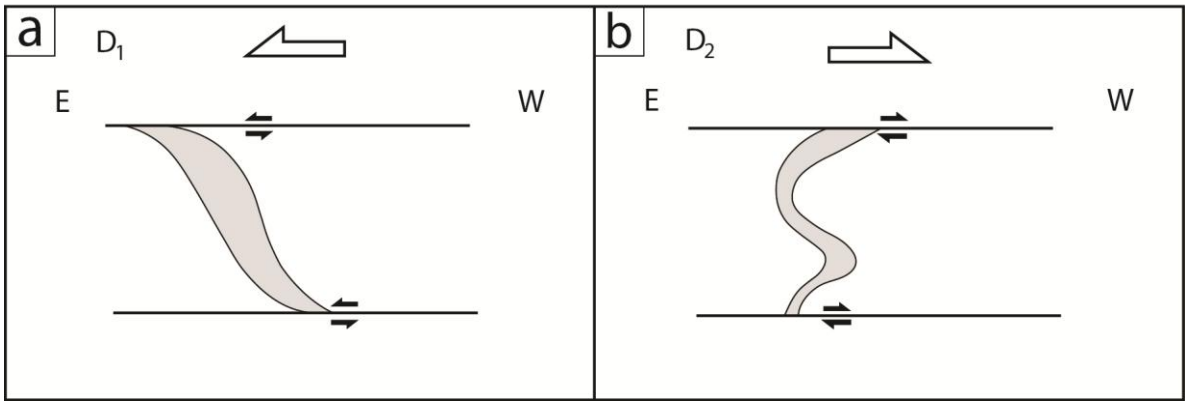

Fig. 75. **a-b)** Schematic illustration of the development of D_2 structures in phyllite by re-shearing the D_1 structure during opposite sense of shear.

Crenulation lineations were commonly found on the foliation plane plunging to the SE, and occasionally also on the C-surfaces. The SE-plunging fold axes, that constitute the lination on the foliation plane (e.g. Fig. 51d), indicate that the mm-scale folds have developed during shortening normal to the folds. For this reason, the shear direction must have been towards the NW, probably as a result of the post-Caledonian extension (D_2). At Voss, the crenulation lineations plunging to NE and SE at the same foliation plane (Fig. 63d), in which the SE-plunging lineations are the most prominent ones. Considering the field of instantaneous stretching and shortening to form the fold axis, it is likely that the crenulation lineations plunging to the NE were developed during Caledonian thrusting (Fig. 76a) and, that the lineation plunging to the SE was eventually developed during top-to-the-hinterland movement (Fig. 76b).

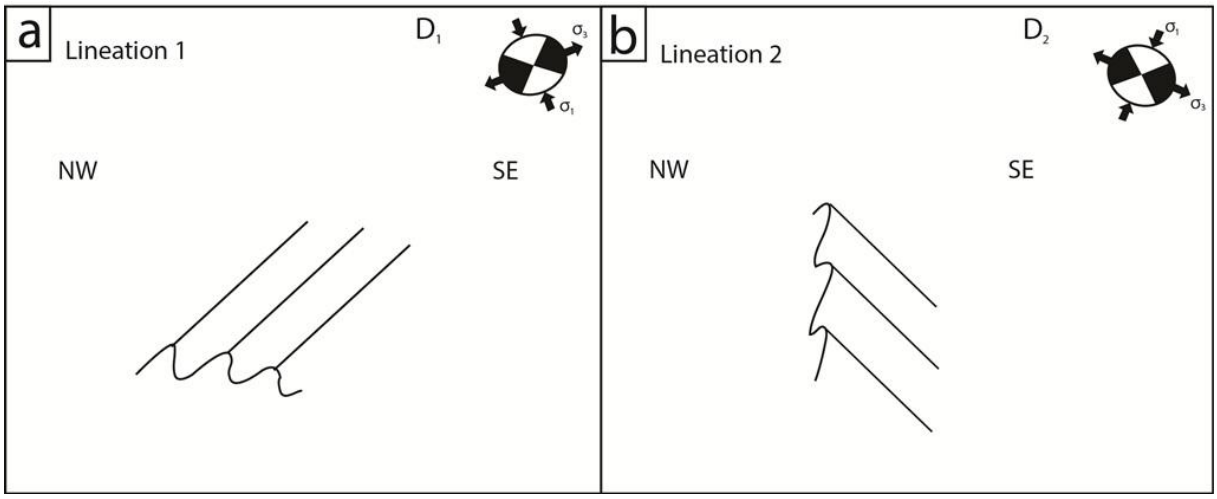

Fig. 76. a-b) The NE- and SE-plunging crenulation lineations suggest the two stages of deformation (D_1 and D_2).

Some of the folds found in the phyllite units occur with axis plunging to the SE and NW (e.g. Fig. 50b, 51a, 58a, 66b) which in general indicate a NE-SW transport direction. However, it is proposed that the fold axis have rotated into these orientations as a result of the non-coaxial flow. In the Caledonian nappe unit at Hardangervidda, the fold axis are mainly plunging to the NW and SE, subparallel to the slickenlines (Fig. 52a), which suggest to reflect rotation of the axis towards the transport direction during deformation. In addition, as most of the structural measurements were recorded from the lowermost section of the nappe unit strengthens this assumption, as the friction and hence the strain is greatest at the basal zone.

5.4.3 Local strain variations

The angles, in which the shear bands intersect the foliation (S-surface), slightly differ for the main locations. The main trend is a higher angle (~35-40^0) in the easternmost locations at Ustaoset and Finse (e.g. Fig. 67e, 50c) compared to the locations closer the west at Hallingskeid, and Voss where the angles are found to be ~20-35^0 (e.g. Fig. 58c, 63b, c). Hence it is suggested that the regions located closer to the hinterland have experienced a slightly higher state of shearing during the extension. However, it is also important to consider the factors that might influence the local variations of shearing, which includes local rheological variations of the rock, the thickness variations of the décollement zone, content of fluids, and primary irregularities of the underlying basement. In the latter case, the phyllite might have been protected from deformation if it was located in the uppermost part of a deeper depression in the basement. Like for instance, as the phyllite at Osa was collected just above the basal conglomerate and quartz schist this might explain the only undulating texture and the lower state of shearing (e.g. Fig. 72).

5.5 Tectonic effect on the sub-Cambrian peneplain

5.5.1 Deformation of the weathered basement

Most of the microfabrics found in the weathered zone of the Precambrian basement at Finse, Sandå and Hallingskeid must be related to Caledonian and Devonian deformation, as the structures including recrystallized quartz and different shear indicators, are not present in the unweathered granite. In general, the weathered granites at Finse and Sandå constitute a higher intensity of microfabrics compared to what is found in the weathered granite at Hallingskeid. This is probably related to the degree of alteration of the granite, as the weathering products including mica and iron-oxides are more susceptible to accumulate strain. The kinked polysynthetic twins in the plagioclase crystals (Fig. 57a) and the dislocation-free and recrystallized quartz (Fig. 57b) at Hallingskeid, indicate crystalloplastic deformation at temperatures at 300-400 °C (Stipp *et al.*, 2002; Passchier & Trouw, 2005). A similar deformation regime is also reflected by the recrystallized quartz (Fig. 46d, 53b) and strain shadows (Fig. 46c, 53c) in the weathered granites at Finse and Sandå.

The lack of deformation structures in the unweathered basement suggest that the 1.5-2.0 meter thick weathered zone of the basement composed of lower shear strength accumulated most of the strain, and is likely to have protected the unweathered basement. The kinked bitotite crystals found in the unweathered granite at Sandå (Fig. 53a) can, however, indicate that the basement was slightly affected by the Caledonian and Devonian deformation, but in overall is it assumed that most of the strain was accumulated in the weathered zone.

5.5.2 Present morphological surface of the Precambrian basement

A comparison of the lithostratigraphies for the main locations (Fig. 71) with the vertical profiles of the basement surface (Fig. 70) do clearly indicates that the conglomerate at Finse and Sandå is located in depressions in the basement (Fig. 73a). As earlier discussed, the depressions are suggested to have evolved from Neoproterozoic faults. The field observations indicates that the conglomerate at Finse was deposited in a depression with an approximately depth of 2 meters (Fig. 69), and depressions of similar size were also observed from the outcrop of Usteberget at Ustaoset (Fig. 68b). Thus, when comparing these observations with the depressions up to 250 meters in the present basement surface (Fig. 77a, b), it is suggested that the deeper depressions were generated from possible Neoproterozoic weakness zones in the basement, and eventually reactivated by post-Caledonian extension (interpreted in Fig.

77), and affected by Mesozoic-Early Cenozoic uplift. As ice caps were covering the Scandes in the Late Cenozoic (Corner, 2005), it is proposed that the weakness zones finally were excavated by glacial erosion.

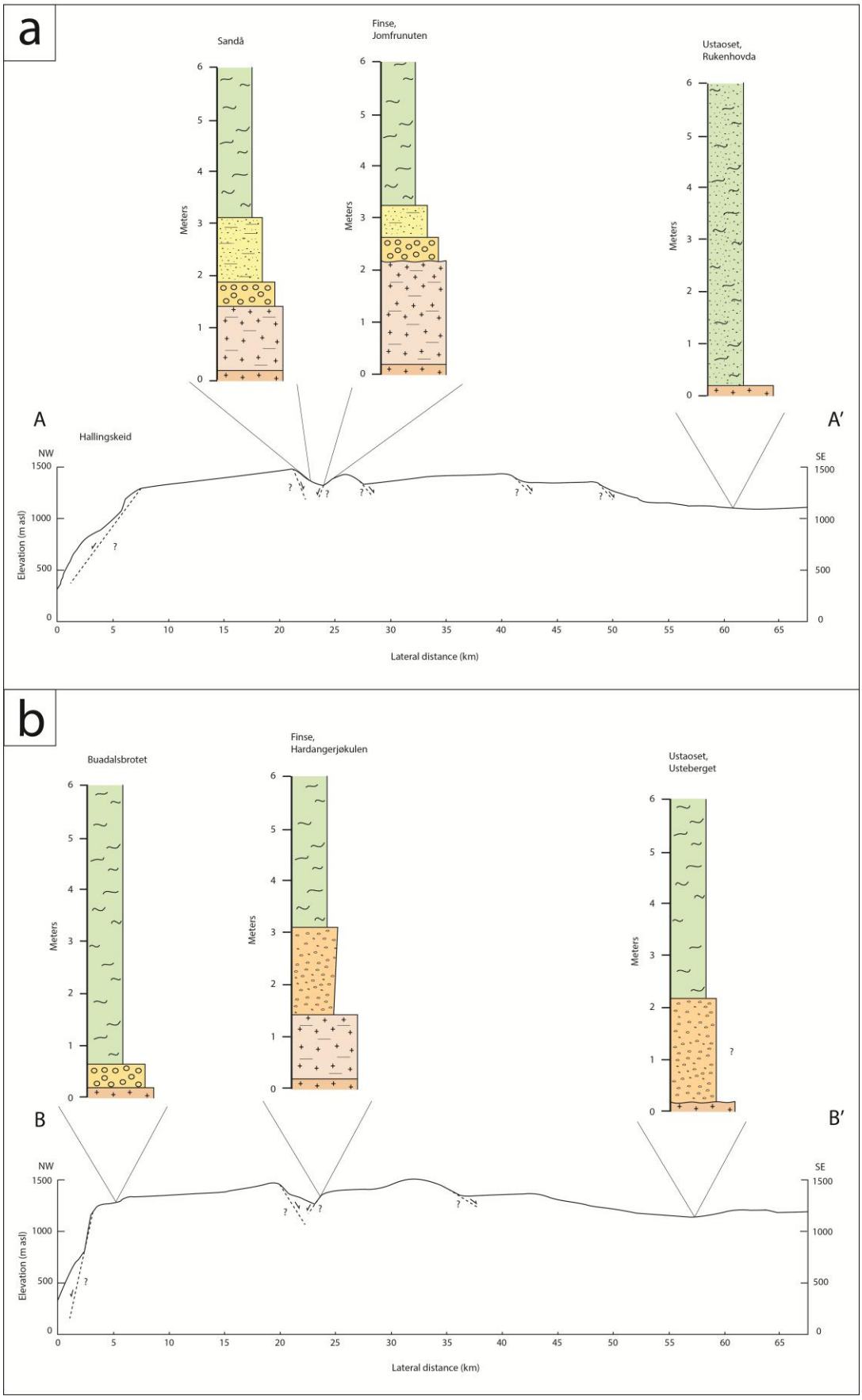

Fig. 77. a-b) Lithostratigraphic logs and the correspond profiles of the present basement surface. The interpreted faults are suggested to be of Devonian age.

5.6 Proposed geological evolution of the Hardangervidda area

From the present study and from the literature, an interpretation of the geological evolution of the Hardangervidda area from Neoproterozoic to late Deconian times is suggested and summarized in Fig. 78. The sub-Cambrian peneplain is proposed to have developed in a period of ca. 400 Ma from the collapse of the Sveconorwegian orogeny to the Cambrian transgression, which included intensively weathering of the basement. When the Baltic craton was flooded in the Early Cambrian (stage 1 in Fig. 78), the peneplain was most likely planar, with exceptions of local depressions with depths of 2 meters and slightly more. When Baltica and Laurentia collided in the early Silurian, the Hardangervidda area was buried at depths of ca. 18 km (stage 2 in Fig. 78). From the structural data in the current study, the structural measurements of the décollement zone clearly indicate top-to-the-NW transport related to the post-Caledonian extension of the orogeny (stage 3 in Fig. 78), and thus confirms with the tectonic model provided by Fossen (1992).

In overall, the tectonic evolution of the Hardangervidda from Neoproterozoic to Devonian times includes successive stages of rifting and seafloor spreading during the breakup of Rodinia in the Neoproterozoic, followed by collision resulted in the Scandinavian Caledonides, and eventually post-orogenic collapse which resulted in rifting, and is therefore stated to represent the Wilson Cycle.

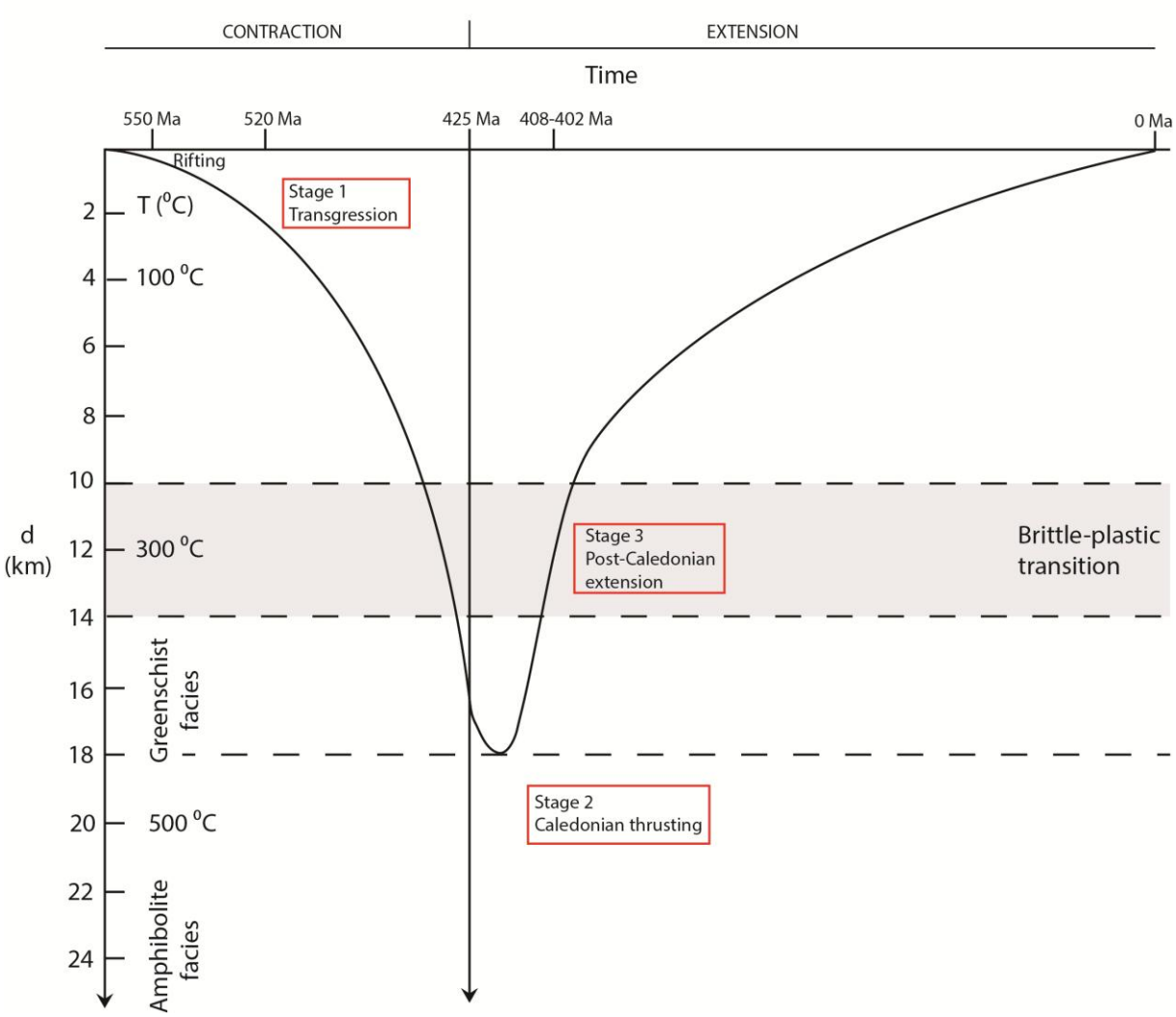

Fig. 78. Proposed geological evolution of the Hardangervidda area focusing in variations of crustal depth from Neoproterozoic to Devonian times. The three main stages include the Cambrian transgression, Caledonian thrusting, and post-Caledonian extension. Data from Goldscmidt, 1912a; Fossen, 1992; Fossen, 1998; Fossen & Dunlap 1998; Van der Pluijm et al., 2004; Cocks & Torsvik, 2005; Nielsen & Schovsbo, 2011.

6 Concluding remarks

On the basis of extensive fieldwork and the study of thin-sections, the following main conclusions are drawn:

- The basement is determined to be weathered in a 1.5-2.0 m thick zone, with accelerated weathering along possible post-Sveconorwegian Proterozoic fractures, and due to heavy rainfall and possible ice caps during the Neoproterozoic. Local variations in degree of weathering are suggested to be caused by textural variations of the granites, topographic variations of the basement or as a result of protection in depressions of the basement for later tectonic deformation.
- Microstructural features in the weathered basement indicate deformation at ca. 300-400 °C and are interpreted to reflect Devonian post-orogenic collapse. The weathered zones with lower strength are interpreted to have accumulated the strain and thus protected the underlying granitic basement as the Caledonian nappes were emplaced.
- The gravelly basal conglomerates, the meta-sandstone and the quartz schist are likely to represent foreshore depositional conditions, whereas the poorly sorted conglomerate at Osa is assumed to represent alluvial fan sediments deposited by rivers or by debris flow generated by faults from the rift event related to the breakup of Rodinia in Neoproterozoic times. The fine-grained phyllite is likely to represent the final flooding of the Baltic craton.
- Depressions in the basement are suggested to represent primary erosional topographic irregularities of the sub-Cambrian peneplain, and some of them may be excavated along Neoproterozoic faults. The suggested depression at Osa is assumed to be deeper compared to the ones found at Finse, Sandå and Ustaoset (ca. 2 m), based on the significantly lower intensity of microfabric found in the basal conglomerate.
- The localities in the west at Voss, Osa and Hallingskeid have experienced middle greenschist-lower amphibolite facies, whereas the locations in the east at Ustaoset and Dyranut have experienced lower degree of metamorphism at greenschist facies. The paleotemperatures are proposed to represent the subduction of the Baltic margin.

- Most of the kinematic indicators, including S-C structures, asymmetric folds, and folded boudins are found in the phyllite unit of the décollement zone indicate a dominant top-to-the-NW transport which is related to post-Caledonian extension. Evidence of overprinting of thrust-related structures is locally found. Hence the structural development in the Hardangervidda area confirms with the general structural-tectonic model presented by Fossen (1992).
- The geological evolution of the Hardangervidda area from the Neoproterozoic to Devonian is determined to represent the Wilson cycle, which started by global rifting in the Neoproterozoic and later changed into convergent plate motion involving the Caledonian orogeny and eventually exhumation, extension and backsliding of the orogenic wedge.

In order to enhance the validity of the study, the possible poorly conglomerate at Hardangerjøkulen should be studied and structural data should be collected from the Caledonian nappe in the area NE of Finse. The peneplain relations at the western Hardangerjøkulen area could be mapped, in addition to other main localities like for instance at Skykkjedalen in Eidfjord and in areas west of Vargebretjørni in NW Hardangervidda. Paleotemperatures of the biotite crystals in the matrix at Osa should be estimated for clearly state the degree of metamorphism during Caledonian thrusting.

References

Ahlmann, H. W. s. (1919) 'Geomorphological studies in Norway', *Geografiska annaler*, 1, 1-20.

Allaby, M. (2008) *A Dictionary of Earth Sciences*, 3rd edition. ed., Oxford University Press.

Allmendinger, R. W., Cardozo, N. C. and Fisher, D. (2013) *Structural Geology Algorithms: Vecrots & Tensors*, Cambridge, England: Cambridge University Press.

Andersen, T. B. and Jamtveit, B. (1990) 'Uplift of deep crust during orogenic extensional collapse: a model based on field studies in the Sogn-Sunnfjord Region of western Norway', *Tectonics*, 9(5), 1097-1111.

Andresen, A. (1974) 'New fossil finds from the Cambro–Silurian meta-sediments on Hardangervidda', *Norges Geologiske Undersøkelse*, 304, 55-60.

Andresen, A. (1978) 'Lithostratigraphy of the Autochthonous/parautochthonous Lower Palaeozoic Metasediments on Hardangervidda, South Norway', *Norges Geologiske Undersøkelse*, 338, 59-69.

Artyushkov, E. A., Lindström, M. and Popov, L. E. (2000) 'Relative sea-level changes in Baltoscandia in the Cumbrian and early Ordovician: the predominance of tectonic factors and the absence of large scale eustatic fluctuations', *Tectonophysics*, 320(3–4), 375-407.

Askvik, H. (2008) 'Berggrunnskart HARDANGERJØKULEN 1416 2, M 1: 50 000 [Map]', *Norges Geologiske Undersøkelse*.

Banham, P. H., Gibbs, A. D. and Hopper, F. W. M. (1979) 'Geological evidence in favour of a Jotunheimen Caledonian suture', *Nature*, 277, 289-291.

Barker, A. J. (1990) *Introduction to metamorphic textures and microstructures*, Glasgow: Blackie.

Berthé, D., Choukroune, P. and Jegouzo, P. (1979) 'Orthogneiss, mylonite and non coaxial deformation of granites: the example of the South Armorican Shear Zone', *Journal of Structural Geology*, 1(1), 31-42.

Bingen, B., Nordgulen, O. and Viola, G. (2008) 'A four-phase model for the Sveconorwegian orogeny, SW Scandinavia', *Norsk Geologisk Tidsskrift*, 88, 43-72.

Bingen, B., Stein, H. J., Bogaerts, M., Bolle, O. and Mansfeld, J. (2006) 'Molybdenite Re–Os dating constrains gravitational collapse of the Sveconorwegian orogen, SW Scandinavia', *LITHOS*, 87(3), 328-346.

Bjørlykke, K. (1974) 'Depositional history and geochemial composition of lower palaeozoic epicontinental sediments from the Oslo region', *Norges Geologiske Undersøkelse*, 305, 1-81.

Bjørlykke, K. (1983) 'Subsidence and tectonics in late Precambrian and Palaeozoic sedimentary basins of southern Norway', *Norges Geologiske Undersøkelse*, 380, 159-172.

Bruton, D. L., Harper, D. A., Gunby, I. A. and Naterstad, J. (1984) 'Cambrian and Ordovician fossils from the Hardangervidda group, Haukelifjell, southern Norway', *Norsk Geologisk Tidsskrift*, 64, 313-324.

Brøgger, W. C. (1893) 'Lagfølgen på Hardangervidda og den såkalte "Høifjeldskvarts"', *Norges Geologiske Undersøkelse*, 11, 1-128.

Burkhard, M. (1993) 'Calcite twins, their geometry, appearance and significance as stress-strain markers and indicators of tectonic regime: a review', *Journal of Structural Geology*, 15, 351-368.

Cardozo, N. and Allmendinger, R. W. (2013) 'Spherical projections with OSXStereonet', *Computers & Geosciences*, 51, 193-205.

Cocks, L. R. M. and Torsvik, T. H. (2005) 'Baltica from the late Precambrian to mid-Palaeozoic times: the gain and loss of a terrane's identity', *Earth-Science Reviews*, 72, 39-66.

Corner, G. D. (2005) 'Scandes Mountains' in Seppälä, M., ed., *The Physical Geography of Fennoscandia*, New York: Oxford University Press, 239-254.

Dahll, T. (1861) 'Om Tellemarkens geologie', *Nyt Magazin for Naturvidenskaberne*, 11, 137-172.

Debat, P., Soula, J.-C., Kubin, L. and Vidal, J.-L. (1978) 'Optical studies of natural deformation microstructures in feldspars (gneiss and pegmatites from Occitania, southern France)', *LITHOS*, 11(2), 133-145.

Dietler, T. N., Koestler, A. G. and Milnes, A. G. (1985) 'A preliminary structural profile through the western Gneiss Complex, Sognefjord, southwestern Norway', *Norsk Geologisk Tidsskrift*, 65, 233-235.

Dobrzhinetskaya, L. F., Eide, E. A., Larsen, R. B., Sturt, B. A., Trønnes, R. G., Smith, D. C., Taylor, W. R. and Posukhova, T. V. (1995) 'Microdiamond in high-grade metamorphic rocks of the Western Gneiss region, Norway', *Geology*, 23, 597-600.

Egli, M., Mirabella, A. and Sartori, G. (2008) 'The role of climate and vegetation in weathering and clay mineral formation in late Quaternary soils of the Swiss and Italian Alps', *Geomorphology*, 102(3), 307-324.

Elvhage, C. and Lidmar-Bergström, K. (1987) 'Some Working Hypotheses on the Geomorphology of Sweden in the Light of a New Relief Map', *Geografiska Annaler. Series A, Physical Geography*, 69(2), 343-358.

Fauconnier, J., Labrousse, L., Andersen, T. B., Beyssac, O., Duprat-Oualid, S. and Yamato, P. (2014) 'Thermal structure of a major crustal shear zone, the basal thrust in the Scandinavian Caledonides', *Earth and Planetary Science Letters*, 385, 162-171.

Ferrill, D. A. (1991) 'Calcite twin widths and intensities as metamorphic indicators in natural low-temperature deformation of limestone', *Journal of Structural Geology*, 13, 667-675.

Fossen, H. (1992) 'The role of extensional tectonics in the Caledonides of south Norway', *Journal of Structural Geology*, 14(8), 1033-1046.

Fossen, H. (1993) 'Structural evolution of the Bergsdalen Nappes, southwest Norway', *Norges geologiske undersøkelse Bulletin*, 424, 23-50.

Fossen, H. (1998) 'Advances in understanding the post-Caledonian structural evolution of the Bergen area, West Norway', *Norsk Geologisk Tidsskrift*, 78, 33-46.

Fossen, H. (2000) 'Extensional tectonics in the Caledonides: Synorogenic or postorogenic?', *Tectonics*, 19(2), 213-224.

Fossen, H. (2010) 'Extensional tectonics in the North Atlantic Caledonides: a regional view', *Geological Society, London, Special Publications*, 335(1), 767-793.

Fossen, H. and Dunlap, W. J. (1998) 'Timing and kinematics of Caledonian thrusting and extensional collapse, southern Norway: evidence from 40Ar/ 39Ar thermochronology', *Journal of Structural Geology*, 20(6), 765-781.

Fossen, H. and Holst, T. B. (1995) 'Northwest-verging folds and the northwestward movement of the Caledonian Jotun Nappe, Norway', *Journal of Structural Geology*, 17(1), 3-15.

Fossen, H. and Hurich, C. (2005) 'The Hardangerfjord Shear Zone in SW Norway and the North Sea: a large-scale low-angle shear zone in the Caledonian crust', *Journal of the Geological Society*, 162, 675-687.

Fossen, H., Pedersen, R. B., Bergh, S. and Andresen, A. (2013) 'En fjellkjede blir til' in Ramberg, I. B., Bryhni, I. and A, N., eds., *Landet blir til: Norges geologi*, 2. utg. ed., Trondheim: Norsk Geologisk Forening, 178-229.

Fossen, H. and Rykkelid, E. (1992) 'Postcollisional extension of the Caledonide orogen in Scandinavia: structural expressions and tectonic significance', *Geology*, 20(8), 737-740.

Franco, P. (2012) 'Effects of Metasomatism on Mineral Systems and Their Host Rocks: Alkali Metasomatism, Skarns, Greisens, Tourmalinites, Rodingites, Black-Wall Alteration and Listevenites' in Harlov, D. E. and Austrheim, H., eds., *Metasomatism and the Chemical Transformation of Rock: The Role of Fluids in Terrestrial and Extraterrestrial Processes*, Dordrecht: Springer, 1-804.

Gaál, G. and Gorbatschev, R. (1987) 'An outline of the Precambrian evolution of the Baltic Shield', *Precambrian Research*, 35, 15-52.

Gabrielsen, R. H., Nystuen, J. P., Jarsve, E. M. and Lundmark, M. A. (2015) 'The Sub-Cambrian Peneplain in southern Norway: its geological significance and its implications for post-Caledonian faulting, uplift and denudation', *Journal of the Geological Society*, 172, 777-791.

Gee, D. G. (1987) 'The Scandinavian alum shales - Mid Cambrian to Tremadoc deposition in response to early Caledonian subduction', *Norsk Geologisk Tidsskrift*, 65, 233-235.

Gee, D. G., Fossen, H., Henriksen, N. and Higgins, A. K. (2008) 'From the early Paleozoic platforms of Baltica and Laurentia to the Caledonide Orogen of Scandinavia and Greenland', *Episodes*, 31(1), 44-51.

Goldschmidt, V. M. (1912a) 'Ein kambrisches Konglomerat von Finse und dessen Metamorphose', *Videnskapsselskapets Skrifter*, 18, 4-18.

Goldschmidt, V. M. (1912b) 'Die kaledonische deformation der südnorwegischen urgebirgstafel', *Videnskapsselskapets Skrifter*, 19, 3-11.

Goldschmidt, V. M. (1916) 'Konglomeratene inden Høifjeldskvartsen', *Norges Geologiske Undersøkelse*, 77, 1-61.

Goldschmidt, V. M. (1925) 'Ueber fossilführende untercambrische Basallagerungen bei Ustaoset', *Fennia*, 45, 3-11.

Harland, W. (1964) 'Critical evidence for a great infra-Cambrian glaciation', *Geologische Rundschau*, 54(1), 45-61.

Henningsmoen, G. (1952) 'Early middle Cambrian fauna from Rogaland, SW Norway ', *Norsk Geologisk Tidsskrift*, 30, 13-31.

Hossack, J. and Cooper, M. (1986) 'Collision tectonics in the Scandinavian Caledonides', *Geological Society, London, Special Publications*, 19(1), 285-304.

Irfan, T. Y. and Dearman, W. R. (1978) 'The engineering petrography of a weathered granite in Cornwall, England', *Quarterly Journal of Engineering Geology*, 11(3), 233-244.

Jarsve, E. M., Krøgli, S. O., Etzelmuller, B. and Gabrielsen, R. H. (2014) 'Automatic identification of topographic surfaces related to the sub-Cambrian peneplain (SCP) in southern Norway—Surface generation algorithms and implications', *Geomorphology*, 211, 89-99.

Kiær, J. (1916) 'The lower Cambrian Holmia fauna at Tømten in Norway', *Videnskapsselskapets Skrifter*, 10, 1-140.

Kjerulf, T. (1879) *Udsigt over det sydlige Norges geologi : med i texten indtagne tegninger, profiler, planer, en atlas, 39 plancher i træsnit, indeholdende grafiske fremstillinger samt den geologiske undersøgelses oversiktskart i 1: 1000,000*, Christiania: Fabritius.

Knipe, R. J. and White, S. H. (1979) 'Deformation in low grade shear zones in the Old Red Sandstone, S.W. Wales', *Journal of Structural Geology*, 1(1), 53-66.

Kumpulainen, R. and Nystuen, J. (1985) 'Late Proterozoic basin evolution and sedimentation in the westernmost part of Baltoscandia' in Gee, D. G. and Sturt, B. A., eds., *The Caledonide Orogen—Scandinavia and Related Areas: 1*, Chichester: John Wiley and Sons: 213-245.

Kvale, A. (1948) *Petrologic and structural studies in the Bergsdalen quadrangle, Western Norway . Parts 1-2*, Bergen: Bergens museums Årbok 1945-1947.

Kvale, A. and Dons, J. A. (1960) 'The nappe area of the caledonides in western Norway : Guide to excursions no. A 7 and no. C 4', *Norges Geologiske Undersøkelse*, 212.

Liestøl, O. (1960) 'Det subkambriske peneplan i området Haukelifjell-Suldalsheiene', *Norsk Geologisk Tidsskrift*, 40, 69-72.

Lindqvist, J. E. (1990) 'Thrust-related metamorphism in basement windows of the central Scandinavian Caledonides', *Journal of the Geological Society*, 147(1), 69-80.

Mason, R. (1978) *Petrology of the metamorphic rocks*, London: George Allen & Unwin.

Matthews, S. and Cowie, J. (1979) 'Early Cambrian transgression', *Journal of the Geological Society*, 136(2), 133-135.

Meert, J. G. and Torsvik, T. H. (2003) 'The making and unmaking of a supercontinent: Rodinia revisited', *Tectonophysics*, 375(1), 261-288.

Milnes, A. and Koestler, A. (1985) 'Geological structure of Jotunheimen, southern Norway (Sognefjell-Valdres cross-section)' in Gee, D. G. and Sturt, B. A., eds., *The Caledonide Orogen—Scandinavia and Related Areas: 1*, Chichester: John Wiley and Sons: 457-474.

Naterstad, J., Andresen, A. and Jorde, K. (1973) 'Tectonic succession of the Caledonian Nappe Front in the Haukelisæter-Røldal area, Southwest Norway', *Norges Geologiske Undersøkelse*, 292, 1-20.

Nesse, W. D. (2009) *Introduction to mineralogy*, New York: Oxford University Press.

Nielsen, A. T. and Schovsbo, N. H. (2011) 'The Lower Cambrian of Scandinavia: depositional environment, sequence stratigraphy and palaeogeography', *Earth-Science Reviews*, 107(3), 207-310.

Ollier, C. and Clayton, K. M. (1984) *Weathering*, 2nd ed., London: Longman.

Passchier, C. W. and Trouw, R. A. J. (2005) *Microtectonics*, 2nd ed., Berlin: Springer.

Pedersen, R. B., Larsen, Ø. and Langeland, K. (1999) 'U-Pb and Rb-Sr dates of late Caledonian fracturing', *Geonytt, 26*, 81-82.

Ponce de Leon, M. I. and Choukroune, P. (1980) 'Shear zones in the iberian arc', *Journal of Structural Geology*, 2(1), 63-68.

Pryer, L. L. (1993) 'Microstructures in feldspars from a major crustal thrust zone: The Grenville Front, Ontario, Canada', *Journal of Structural Geology*, 15(1), 21-36.

Pryer, L. L. and Robin, P. Y. F. (1996) 'Differential stress control on the growth and orientation of flame perthite: A palaeostress-direction indicator', *Journal of Structural Geology*, 18(9), 1151-1166.

Rekstad, J. (1903) 'Fra høifjeldsstrøget mellem Haukeli og Hemsedalsfjeldene', *Norges Geologiske Undersøkelse*, 36, 3-54.

Reusch, H. (1901) 'Nogle bidrag til forstaaelsen af, hvorledes Norges dale og fjelde er blevne til', *Norges Geologiske Undersøkelse*, 32, 124-217.

Reusch, H., Rekstad, J. and Bjørlykke, K. O. (1902) 'Fra Hardangervidden', *Norges Geologiske Undersøkelse*, 34, 1-80.

Riis, F., Kalleson, E., Dypvik, H., Krogli, S. and Nilsen, O. (2011) 'The Ritland impact structure, southwestern Norway', *Meteorit. Planet. Sci.*, 46(5), 748-761.

Roberts, D. and Gee, D. G. (1985) 'An introduction to the structure of the Scandinavian Caledonides' in Gee, D. G. and Sturt, B. A., eds., *The Caledonide Orogen-Scandinavia and Related Areas: 1*, Chichester: John Wiley and Sons: 55-68.

Roedder, E. (1984) *Fluid inclusions : an introduction to studies of all types of fluid inclusions, gas, liquid, or melt, trapped in materials from earth and space, and their application to the understanding of geologic processes*, Washington, D.C: Mineralogical Society of America.

Sigmond, E. M. O. (1985) 'The Mandal—Ustaoset Line, A Newly Discovered Major Fault Zone in South Norway' in Tobi, A. C. and Touret, J. L. R., eds., *The Deep Proterozoic Crust in the North Atlantic Provinces* Springer, 323-331.

Sigmond, E. M. O. (1998) 'Berggrunnskart ODDA, M 1: 250 000 [Map]', *Norges Geologiske Undersøkelse*.

Sigmond, E. M. O., Birkeland, A. and Bingen, B. (2000) 'A possible basement to the Mesoproterozoic quartzites on Hardangervidda, South-central Norway: zircon U-Pb geochronology of a migmatitic gneiss', *Norges geologiske undersøkelse Bulletin*, 437, 25-32.

Spjeldnæs, N. (1955) 'Middle Cambrian stratigraphy in the Røyken area, Oslo region', *Norsk Geologisk Tidsskrift*, 34, 105-121.

Stanley, S. M. (2009) *Earth system history*, 3rd ed., New York: W.H. Freeman.

Stephens, M. B. (1988) 'The Scandinavian Caledonides: a complexity of collisions', *Geology Today*, 4(1), 20-26.

Stipp, M., Stünitz, H., Heilbronner, R. and Schmid, S. M. (2002) 'The eastern Tonale fault zone: a 'natural laboratory' for crystal plastic deformation of quartz over a temperature range from 250 to 700 °C', *Journal of Structural Geology*, 24(12), 1861-1884.

Strand, T. (1960) 'The pre-Devonian rocks and structures in the region of Caledonian deformation', *Norges Geologiske Undersøkelse*, 208, 170-284.

Strøm, K. M. (1948) 'The Geomorphology of Norway', *The Geographical Journal*, 112(1/3), 19-23.

Størmer, L. (1925) 'On a Lower Cambrian Fauna at Ustaoset in Norway', *Fennia*, 45, 12-22.

Størmer, L. (1941) 'Dictyonema shales outside the Oslo region', *Norsk Geologisk Tidsskrift*, 20(3), 161-170.

Torsvik, T. H. and Cocks, L. R. M. (2005) 'Norway in space and time; a centennial cavalcade', *Norsk Geologisk Tidsskrift*, 85(1), 73-86.

Torsvik, T. H. and Rehnström, E. F. (2001) 'Cambrian palaeomagnetic data from Baltica: implications for true polar wander and Cambrian palaeogeography', *Journal of the Geological Society*, 158(2), 321-329.

Törnebohm, A. (1888) 'Om fjällproblemet', *Geologiska Föreningens i Stockholm Förhandlingar, v. 10*, 117, 328-336.

Van der Pluijm, B. A., Marshak, S. and Allmendinger, R. W. (2004) *Earth structure : an introduction to structural geology and tectonics*, 2nd ed., New York: W.W. Norton & Co.

Vernon, R. H. and Clarke, G. L. (2008) *Principles of metamorphic petrology*, Cambridge: Cambridge University Press.

Vogt, T. (1924) 'Forholdet mellem sparagmit-systemet og det marine underkambrium ved Mjøsen', *Norsk Geologisk Tidsskrift*, 7, 281-383.

Wennberg, O. P. (1996) 'Superimposed fabrics due to reversal of shear sense: an example from the Bergen Arc shear zone, western Norway', *Journal of Structural Geology*, 18(7), 871-889.

White, S. H., Burrows, S. E., Carreras, J., Shaw, N. D., Humphreys, F. J., Carreras, J., Cobbold, P. R., Ramsay, J. G. and White, S. H. (1980) 'On mylonites in ductile shear zones', *Journal of Structural Geology*, (1), 175-187.

Worsley, D., Aarhus, N., Bassett, M. G., Howe, M. P. A. M., A and Olaussen, S. (1983) 'The Silurian succession of the Oslo Region', *Norges Geologiske Undersøkelse*, Bulletin 384, 1-57.

Wyllie, D. C., Mah, C. W. and Hoek, E. (2004) *Rock slope engineering : civil and mining*, 4th ed., London: Spon Press.

Appendix A: Sample locations

Sample number	Location	Elevation (m asl)	UTM N UTM E	Outcrop type and description	Sample description
KOE-1	Ustaoset, Rukenhovda	1158	447438 6709575	Beneath cliffs slightly northwest of the marked track.	Bight grey colored and quartz-rich phyllite.
KOE-2	Ustaoset, Rukenhovda	1198	445464 6709954	Mountain outcrop at Rukenhovda. Slightly covered by vegetation.	Dark grey phyllite containing sheared quartz veins. Wavy foliation planes.
KOE-3	Ustaoset, Usteberget	1121	447751 6704886	Mountain outcrop on top of Usteberget.	Dark grey to black colored phyllite. Foliation occurs in nearly straight planes. Rusty brown weathering surface.
KOE-4	Dyranut	1256	419597 6693788	Freshly exposed, 3 m high road outcrop.	Bright grey colored phyllite. Intensively deformed. Foliation occurs in straight planes. Contains folded quartz veins.
KOE-5	Finse, Jomfrunuten	1379	419531 6719763	River outcrop, on the track to Kyrkjedøri.	Moderately sorted conglomerate composed of coarse-grained sand, gravel and pebbles of qtz.
KOE-6	Finse, Jomfrunuten	1373	419673 6719768	Flat mountain outcrop on the plateu northeast of Finse railway station.	Intensively weathered basement, appear as gravel composed of qtz and fsp in a fine-grained alteration product of white mica and iron-oxides.
KOE-7	Finse, Jomfrunuten	1381	419531 6719763	River outcrop, on the track to Kyrkjedøri.	Rusty colored fine-grained quartz schist.
KOE-8	Finse	1257	418189 6719781	Mountain outcrop, north of Finse railway station.	Holocrystalline and inequigranular granite, phenocrysts of qtz, fsp and Ep.
KOE-9	Finse, Store Finsenuten	1391	415897 6720496	Weathered mountain outcrop northwest of Finse railway station.	Greyish black colored phyllite. Foliation occurs in straight planes and shows a metallic luster.
KOE-10	Finse, Hardangerjøkulen	1454	418542 6714446	Flat mountain outcrop southeast of the Blåisen.	Slightly weathered basement. Occur with a smooth and red colored exposure surface.

Sample number	Location	Elevation (m asl)	UTM N UTM E	Outcrop type and description	Sample description
KOE-11	Finse, Hardangerjøkulen	1449	418531 6714651	Well exposed mountain outcrop southeast of the Blåisen.	Grey colored, medium-grained gneiss rich in deformed qtz and fsp. Weakly foliated.
KOE-12	Finse, Hardangerjøkulen	1387	417938 6715475	Flat mountain outcrop on the plateau, next to the river northeast of the Blåisen.	Greyish black colored phyllite. Foliation occurs in straight planes.
KOE-13	Finse, Hardangerjøkulen	1409	418179 6715354	Flat plateau outcrop, northeast of the Blåisen.	Grey to dark blue colored, medium-grained sandstone.
KOE-14	Finse, Hardangerjøkulen (Same location as KOE-13)	1409	418179 6715354	Flat plateau outcrop, northeast of the Blåisen.	Bright grey colored, coarse-grained sandstone. Brownish-red weathering surface.
KOE-15	Sandå	1465	415049 6721600	Flat mountain outcrop, southeast of Florsvegghallene.	Conglomerate mainly composed qtz and fsp grains with size ranging from very coarse sand to gravel.
KOE-16	Sandå (Same location as KOE-15)	1465	415049 6721600	Flat mountain outcrop, southeast of Florsvegghallene.	Yellow-brown fine grained quartz schist, greasy lustre surface. Well-developed foliation in straight planes.
KOE-17	Sandå	1455	414946 6721529	Flat mountain outcrop south of Florsvegghallene. Weathered.	Intensively weathered basement. Appear with a brownish-red surface with remnant crystals of qtz and fsp.
KOE-18	Sandå	1282	415143 6720557	Relatively fresh mountain outcrop along Rallarvegen, next to the river Sandåi.	Fresh holocrystalline and inequigranular granite, with phenocrysts of qtz and fsp.
KOE-19	Hallingskeid	1063	403852 6727156	Flat mountain outcrop along Rallarvegen west of Hallingskeid.	Fresh holocrystalline and equigranular granite.
KOE-20	Hallingskeid	983	402879 6728990	Flat mountain outcrop along Rallarvegen, along Nedre Grøndalsvatnet and southeast	Weathered basement, appear with a smooth rusty-brown colored weathering surface.

Sample number	Location	Elevation (m asl)	UTM N UTM E	Outcrop type and description	Sample description
				of Grøndal.	
KOE-21	Hallingskeid	998	402712 6729308	Flat mountain outcrop along Rallarvegen, along Nedre Grøndalsvatnet and south of Grøndal.	Greyish black colored phyllit, composed of segregated qtz veins. Wavy foliation planes. Rusty-brown colored weathering surface.
KOE-22	Osa, Buadalsbrotet	1279	400348 6725695	Flat mountain outcrop northwest of Buadalsbrotet and on the track to Osa.	Grey colored phyllite as matrix in the poorly sorted conglomerate.
KOE-23	Osa, Buadalsbrotet (Same location as KOE-22)	1279	400348 6725695	Flat mountain outcrop northwest of Buadalsbrotet and on the track to Osa.	Bright colored gneiss as a pebble in the conglomerate.
KOE-24	Osa, Buadalsbrotet (Same location as KOE-22)	1279	400348 6725695	Flat mountain outcrop northwest of Buadalsbrotet and on the track to Osa.	Coarse-grained matrix composed of blue colored qtz grains. Appear in an elongated zone that crops out in the conglomerate.
KOE-25	Osa, Hegrenuten	1354	399463 6723927	Mountain outcrop north of Hegrenuten.	Coarse-grained carbonate that interlayer (c. 0.5 m thick) the phyllite unit.
KOE-26	Osa, Hegrenuten	1253	399966 6724508	Flat mountain outcrop northwest of Søre Grøndalsvatnet.	Fine-grained (meta-) sandstone as matrix in the poorly sorted conglomerate.
KOE-27	Osa, Hegrenuten (Same location as KOE-26)	1253	399966 6724508	Flat mountain outcrop northwest of Søre Grøndalsvatnet.	Bright colored granite as a pebble in the conglomerate composed of qtz and fps.
KOE-28	Osa, Hegrenuten (Same location as KOE-26)	1253	399966 6724508	Flat mountain outcrop northwest of Søre Grøndalsvatnet.	Yellow-brown fine grained quartz schist, greasy lustre surface.

Sample number	Location	Elevation (m asl)	UTM N UTM E	Outcrop type and description	Sample description
KOE-29	Osa, Hegrenuten (Same location as KOE-26)	1253	399966 6724508	Weathered mountain outcrop northwest of Søre Grøndalsvatnet.	Dark grey colored phyllite. Straight to slightly wavy foliation planes with metallic luster.
KOE-30	Voss, Bulken	70	354037 6723515	Freshly exposed 3.4 m high road outcrop along Vangsvatnet.	Grey colored phyllite mingled with sheared qtz veins. Wavy foliation planes.

Appendix B: Structural measurements

Data set	Location	Lithology	Elevation (m asl)	UTM N UTM E	Foliation	S-C structures C-plane	 S-plane	S-C crenulation axes	Fold limbs Limb 1	 Limb 2	Fold axis	Fold axial plane	Fractures	Lineation	Lineation plane
U-1	Usteberget	Phyllite	1134	448254 6704644	030/12 033/08 001/32										
U-1	Usteberget	Phyllite	1195	448575 6704422	065/25 078/22 092/27										
U-1	Usteberget	Phyllite	1144	447807 6704856	321/40 311/50 304/53										
U-1	Usteberget	Phyllite	1103	447679 6704947	128/80 133/72 115/71										
U-1	Storhovda	Phyllite	1281	449261 6703486	060/66 038/52 047/62										
U-1	Ustetind	Phyllite	1210	449228 6704019	032/25 046/42 051/27										
U-1	Rukenhovda	Phyllite	1175	445411 6709473	058/07 070/08										
U-1	Rukenhovda	Phyllite	1216	445440 6709643	024/37 027/39 026/36										
U-1	Rukenhovda	Phyllite	1206	445249 6709609	335/54 350/51 366/58										
U-1	Rukenhovda	Phyllite	1218	445386 6709665	038/28										
U-1	Rukenhovda	Phyllite	1205	445464 6709954					059/35 233/82 206/89	039/31 067/37 080/27	**30→116** **09→234** **22→206**	**302/79** **213/25** **179/42**			
U-1	Bismi	Phyllite	1145	447449 6709545	338/16 326/15 309/20 306/23	020/08	274/16	**06→072**							
D-1	Dyranut	Phyllite	1247	417508 6693341		290/15	336/32	**14→360**						20→124 16→120	031/21 358/18

Data set	Location	Lithology	Elevation (m asl)	UTM N UTM E	Foliation	S-C structures C-plane	 S-plane	S-C crenulation axes	Fold limbs Limb 1	 Limb 2	Fold axis	Fold axial plane	Fractures	Lineation	Lineation plane
														40→146 20→136	027/42 002/28
D-1	Dyranut	Phyllite	1240	419094 6693766		104/21	081/40	**13→249**	294/25	060/46	**16→76**	**259/78**		30→127 30→143 30→146	066/27 056/35 062/32
D-1	Dyranut	Phyllite	1255	419597 6693788	070/26	248/12 004/18	063/30 040/44	**06→074** **14→055**						34→141 31→135	052/32 067/36
F-1	Finse	Phyllite	1355	420451 6718888	353/62 044/52				076/42	022/39	**19→047** 70→098 50→120 12→032 64→089	**034/57** 018/68 050/60 014/69 040/72			
F-1	Finse	Phyllite	1395	420330 6719178	000/54 000/38						30→072	014/36		23→084 24→116	
F-1	Finse	Phyllite	1374	420148 6719400	366/39 005/50 326/36 314/44 342/09				158/28 283/08	000/32 060/35	**06→170** **05→067** 18→070	**170/88** **248/76** 014/36			
F-1	Finse	Phyllite	1356	419285 6719672	055/20 268/06						04→069	032/33		15→143	
F-1	Finse	Phyllite	1383	419104 6719693	028/44 346/14 019/31 345/26 021/44									03→087 31→119 26→136 53→111	
F-1	Finse	Phyllite	1366	418990 6719651	358/54				260/19	178/54	**19→344**	**335/67**			
F-1	Finse	Phyllite	1369	418835 6719902	332/02 336/30 020/32						36→062 34→065	064/62 052/70		02→120	
F-1	Finse	Phyllite	1382	419825 6719766					298/28	001/34	**27→049**	**231/84**			
F-1	Finse	Granite	1366	419700 6719701	298/10 267/05								253/24 347/05 240/22 001/03		
F-1	Finse	Phyllite	1362	419604 6719712	040/41 017/08									17→139 30→113 18→114	

Data set	Location	Lithology	Elevation (m asl)	UTM N UTM E	Foliation	S-C structures C-plane	 S-plane	S-C crenulation axes	Fold limbs Limb 1	 Limb 2	Fold axis	Fold axial plane	Fractures	Lineation	Lineation plane
														16→097	
F-1	Finse	Weathered granite	1381	419580 6719767									030/07 003/08		
F-1	Finse	Phyllite	1318	418730 6719760					165/10	049/42	**08→220**	**217/72**		19→098 07→095	
F-1	Finse	Phyllite	1291	418626 6719866										10→134	
F-1	Finse	Phyllite	1298	420372 6718518	006/44 346/57 002/32 326/38 342/32									10→131	
F-1	Finse	Phyllite	1427	418972 6720077		342/14 330/22 090/24	290/30 314/39 052/06	**14→085** **12→119** **05→100**							
F-1	Finse	Phyllite	1431	419063 6720192	042/18 047/32	176/10 052/33 329/24 359/07 212/14	047/32 031/48 351/33 025/10 058/15	**07→217** **25→186** **21→026** **06→064** **03→226**			22→096			14→212 15→058	
F-1	Finse	Phyllite	1422	418930 6720224		226/16	025/35	**04→031**							
F-1	Finse	Phyllite	1423	418846 6720232	296/52	301/26 243/17	296/39 037/26	**24→056** **05→047**							
F-1	Finse	Phyllite	1420	418763 6720091		220/26 190/23	030/23 056/37	**02→035** **12→220**							
F-1	Kyrkjedøri	Phyllite	1501	422648 6721705					125/49 348/38	018/46 038/36	**33→159** **34→108**	**341/88** **106/88**			
F-1	Kyrkjedøri	Phyllite	1503	422332 6721525	110/29 097/37				330/11	092/55	**09→098**	**282/66**			
F-1	Kyrkjedøri	Phyllite	1507	421408 6721105	350/29 020/33	008/21 345/35	000/43 018/50	**05→175** **33→50**							
F-1	Kyrkjedøri	Phyllite	1445	421251 6720595		094/10 117/14	205/26 170/30	**08→222** **14→195**							
F-1	Kyrkjedøri	Phyllite	1422	420560 6720229	063/18 067/24	062/07 041/11	350/24 027/28	**07→154** **04→199**							
F-1	Store Finsenuten	Phyllite	1337	416663 6719124	330/15 012/31	331/10 085/17	010/25 063/40	**09→029** **10→231**							

Data set	Location	Lithology	Elevation (m asl)	UTM N UTM E	Foliation	S-C structures C-plane	 S-plane	S-C crenulation axes	Fold limbs Limb 1	 Limb 2	Fold axis	Fold axial plane	Fractures	Lineation	Lineation plane
						291/18	348/36	**18→014**							
F-1	Store Finsenuten	Phyllite	1389	416421 6719269	353/60 007/53 023/47 026/40 025/50	315/38 032/44 008/25	354/62 022/56 020/37	**34→015** **24→185** **13→038**	031/50	005/28	**20→049**	**242/59**		50→128	025/50
F-1	Store Finsenuten	Phyllite	1368	416278 6719343		086/16 052/18 015/15	082/35 068/43 021/25	**02→259** **08→076** **04→029**							
F-1	Store Finsenuten	Phyllite	1366	416153 6719524	040/33 050/24	021/28 020/20 347/19	027/62 356/38 002/34	**04→029** **14→158** **10→017**							
F-1	Store Finsenuten	Phyllite	1374	416027 6719809	037/20	018/12 000/42 027/09	050/28 015/50 056/24	**09→068** **35→051** **06→070**						20→144	037/20
F-1	Store Finsenuten	Phyllite	1390	415897 6720496	032/36 036/43 038/24									28→139	038/24
F-1	Store Finsenut	Phyllite	1395	415761 6720642	344/38 355/25	001/09 033/20 022/12 011/20	036/36 025/58 053/55 033/59	**06→045** **04→203** **07→058** **10→039**						25→099	355/25
F-1	Store Finsenuten	Phyllite	1410	415716 6720805	006/40 006/25 028/30 026/23 356/39	348/17 054/07 356/20	055/31 037/43 029/52	**17→085** **02→215** **14→041**						30→130	028/30
F-2	Hardanger-jøkulen	Phyllite	1382	418710 6714622		230/21	094/16	**07→285**							
F-2	Hardanger-jøkulen	Phyllite	1466	418501 6714556		180/26	011/19	**02→185**							
F-2	Hardanger-jøkulen	Phyllite	1477	417509 6715285		205/14 048/20 084/50 230/21 107/38 084/30 219/04 094/44 156/16	022/53 038/51 069/58 031/41 040/32 030/60 015/43 066/66 083/43	**01→023** **05→214** **42→215** **05→037** **30→154** **29→192** **02→017** **35→228** **16→243**						41→142 30→152 27→142 06→150 46→160	 052/15 066/66 156/16 082/42

Data set	Location	Lithology	Elevation (m asl)	UTM N UTM E	Foliation	S-C structures		S-C crenulation axes	Fold limbs		Fold axis	Fold axial plane	Fractures	Lineation	Lineation plane
						C-plane	S-plane		Limb 1	Limb 2					
						157/16	082/42	**17→242**							
F-2	Hardanger-jøkulen	Phyllite	1416	417867 6715384	077/52										
F-2	Hardanger-jøkulen	Phyllite	1389	417194 6715681	112/34	055/13	020/46	**09→191**							
F-2	Hardanger-jøkulen	Phyllite	1388	417938 6715475	050/37 052/41 037/43 053/45										
F-2	Hardanger-jøkulen	Phyllite	1517	417669 6715107		053/32 092/12 100/33 211/10 131/19	041/28 030/42 044/36 054/60 053/62	**24→100** **12→197** **31→168** **04→232** **19→223**							
F-2	Hardanger-jøkulen	Phyllite	1421	418254 6715283	027/17 035/24	192/19 233/18 156/16	050/24 057/35 065/30	**07→214** **01→236** **14→219**						18→120 23→134	027/17 035/24
F-2	Hardanger-jøkulen	Phyllite	1415	418179 6715354		212/13 177/19	051/20 082/21	**03→224** **14→222**							
F-2	Hardanger-jøkulen	Gneiss	1431	418573 6714431	006/32 332/16									18→148	006/32
F-2	Hardanger-jøkulen	Gneiss	1448	418531 6714651	294/06 273/14 124/16									08→306	292/06
F-2	Hardanger-jøkulen	Gneiss	1478	418452 6714633					339/17 284/22 274/14 124/32 277/64 100/71 258/06	176/18 140/29 066/63 063/21 052/22 096/08 112/44	**03→348** **08→305** **06→069** **13→282** **14→091** **01→100** **03→289** 12→277 25→270 16→290 10→314 28→268	**345/90** **304/86** **252/65** **280/84** **084/68** **281/51** **288/71** 041/18 078/30 091/50 110/17 099/23			
F-2	Hardanger-jøkulen	Gneiss	1493	418328 6714634					118/74	016/06	**06→296** 27→325 20→322 04→308	**292/53** 118/34 116/16 134/30			

Data set	**Location**	**Lithology**	**Elevation (m asl)**	**UTM N UTM E**	**Foliation**	**S-C structures**		**S-C crenulation axes**	**Fold limbs**		**Fold axis**	**Fold axial plane**	**Fractures**	**Lineation**	**Lineation plane**
						C-plane	S-plane		Limb 1	Limb 2					
											03→283 14→294	096/36 108/27			
F-2	Hardanger-jøkulen	Gneiss	1462	418322 6715014									064/68		
F-2	Hardanger-jøkulen	Gneiss	1439	418293 6715169	104/36										
F-2	Hardanger-jøkulen	Gneiss	1455	418200 6715124	230/15				106/54	036/12	**12→115**	**301/63**	240/73 041/52 220/80		
F-2	Hardanger-jøkulen	Gneiss	1429	418357 6715080	131/02									02→131	082/02
F-2	Hardanger-jøkulen	Phyllite	1416	418370 6715226	070/30 065/44 032/47	090/20 096/12	368/44 068/40	**18→208** **07→239**			40→156	060/60		12→154	096/12
F-2	Hardanger-jøkulen	Phyllite	1415	418672 6714704		269/14 180/15 163/10 129/13	108/16 100/38 080/51 101/21	**03→279** **15→260** **10→252** **11→250**							
S-1	Sandå	Phyllite	1466	415135 6721657		220/18 236/29	017/23 047/26	**04→027** **02→052**							
S-1	Sandå	Phyllite	1460	414870 6721534		356/16 008/20	030/36 017/38	**13→048** **06→025**							
H-1	Hallingskeid	Granite	1037	403664 6727345									036/38 051/20		
H-1	Hallingskeid	Phyllite	1117	403083 6729019		014/03 350/05 327/04	046/24 050/14 023/26	**02→050** **05→070** **04→030**							
H-1	Hallingskeid	Phyllite	984	402810 6729051		352/19 028/15 233/18 290/10 318/15	018/20 031/22 025/28 008/31 030/20	**19→088** **02→037** **18→062** **10→025** **14→072**						12→118 13→088 13→100 02→277	067/23 027/15 068/21 284/03
H-1	Hallingskeid	Phyllite	959	402134 6730798		311/26	339/16	**14→101**							
H-1	Hallingskeid	Phyllite	974	402332 6730927		038/17 066/12	001/35 023/19	**15→159** **12→166**							
H-1	Hallingskeid	Phyllite	973	402444 6731228		315/24	032/27	**20→079**	337/60	101/15	**12→150**	**145/60**			
H-1	Hallingskeid	Phyllite	960	402537		351/23	032/36	**22→066**							

Data set	**Location**	**Lithology**	**Elevation (m asl)**	**UTM N UTM E**	**Foliation**	**S-C structures**		**S-C crenulation axes**	**Fold limbs**		**Fold axis**	**Fold axial plane**	**Fractures**	**Lineation**	**Lineation plane**
						C-plane	S-plane		Limb 1	Limb 2					
				6731571		330/16 318/26	013/50 006/40	**13→024** **26→041**							
H-1	Hallingskeid	Phyllite	957	402454 6731863										22→326	230/26
H-1	Hallingskeid	Phyllite	956	402567 6732555		324/08 353/14	080/34 109/36	**07→090** **11→124**						14→141	102/21
H-1	Hallingskeid	Phyllite	1007	402807 6732898		330/12 314/08	102/22 060/18	**06→118** **07→080**							
O-1	Osa	Phyllite	1295	400689 6725651	052/22	283/18	023/38	**16→044**						25→104 26→109 46→128	030/26 050/26 094/66
O-1	Osa	Carbonate layer in phyllite	1333	399463 6723927	310/30 314/33										
V-1	Voss	Phyllite	104	350180 6724976		294/16 341/14 342/15 330/19 316/26 333/15 359/22 324/15 318/20 332/16 308/28 310/19 290/15 340/18 011/13 288/20	015/29 355/25 029/18 015/28 349/28 019/23 022/35 023/36 033/33 027/35 007/24 007/26 006/36 360/38 029/26 350/21	**15→044** **07→010** **15→083** **19→055** **26→054** **15→058** **17→048** **15→044** **19→065** **16→051** **23→076** **19→051** **15→027** **10→013** **07→044** **18→047**	308/10 298/22	030/34 038/38	**10→045** **19→063**	**228/75** **247/80**		18→108 23→118 35→106 05→141 02→115 03→292 16→112 10→122	028/18 030/23 019/32 357/07 306/15 284/25 343/16 010/18
V-1	Voss	Phyllite	64	349466 6725098		250/17	336/25	**15→010**						03→111 17→075 18→106 27→113 11→121 05→116 20→110 05→122 20→111 13→116	070/08 046/12 026/24 010/19 034/33 033/07 035/28 041/08 036/23 033/12

Data set	Location	Lithology	Elevation (m asl)	UTM N UTM E	Foliation	S-C structures C-plane	 S-plane	S-C crenulation axes	Fold limbs Limb 1	 Limb 2	Fold axis	Fold axial plane	Fractures	Lineation	Lineation plane
														15→131 18→173 28→150 12→288	058/20 060/16 350/14 176/08
V-1	Voss	Phyllite	71	351027 6724800		245/19 241/12 277/18 320/03 331/18 025/18 310/20 288/09 293/20 267/05	014/48 045/21 026/21 023/38 061/39 026/36 030/40 036/35 348/48 003/36	**12→025** **02→051** **12→058** **03→027** **17→083** **01→027** **19→055** **08→047** **19→006** **05→010**	290/49	051/42	**03→228**	**082/86**		32→120 08→040 22→185 30→126 45→102 08→152 16→121 23→117 22→120 27→146	028/36 028/36 055/30 055/30 020/21 31/09 012/17 026/22 342/25 036/35
V-1	Voss	Phyllite	107	350236 6724573		355/14	015/33	**07→027**						12→125 08→192 22→118 07→133 24→083 14→092	009/13 011/25 034/22 067/10 322/24 316/08
V-1	Voss	Phyllite	94	353528 6724410										10→295 04→120 03→285 05→300	226/09 303/08 292/12 232/07
V-1	Voss	Phyllite	64	356587 6723463		226/10 042/08	314/21 025/41	**09→339** **02→207**	209/36	024/21	**04→215**	**035/62**		02→330 02→120 05→293 07→126 02→310 30→107 10→86 24→103 03→131 13→122 03→295	211/04 016/10 177/04 017/11 107/02 026/28 047/18 009/25 058/02 090/20 130/13
V-1	Voss	Phyllite	70	354037 6723515		314/08 316/19 322/13 321/31	020/16 010/34 359/18 56/26	**08→049** **19→041** **13→044** **20→104**						15→114 04→305 02→301 08→123 03→125	041/18 271/03 055/02 033/06 356/04

Data set	Location	Lithology	Elevation (m asl)	UTM N UTM E	Foliation	S-C structures		S-C crenulation axes	Fold limbs		Fold axis	Fold axial plane	Fractures	Lineation	Lineation plane
						C-plane	S-plane		Limb 1	Limb 2					
														13→126 12→125 05→309 07→299	041/12 45/15 158/05 194/04

Appendix C: Mineral content in the samples

Sample	Lithology	Mineral content (Vol%)															
		Qtz	**Mc**	**Pl**	**Ms**	**Ep**	**Bt**	**Ap**	**Rt**	**Zrn**	**Or**	**Ttn**	**Fe-oxide**	**St**	**Chl**	**Cal**	**Opaque (sheared mat.)**	**Grt**
KOE-1	Phyllite	37		4	23		17						11			8		
KOE-2	Phyllite	29			34												37	
KOE-3	Phyllite	36			42								9				13	
KOE-4	Phyllite	39			30								5		8	18		
KOE-5	Conglomerate	36	11	5	4			3					6		7	28		
KOE-6	Weathered granite	24	25	18	18		6						9					
KOE-7	Quartz schist	32		8	48								12					
KOE-8	Unweathered granite	16	13	18	7	13	11	5			7	3	3	4				
KOE-9	Phyllite	38			27								10				25	
KOE-10	Unweathered granite	53	4	4	20			4					15					
KOE-11	Gneiss	42			12		21						10			15		
KOE-12	Phyllite	24			33												43	
KOE-13	Meta-sandstone	25	12				27						6			30		
KOE-14	Meta-sandstone	20	6	5	17	5	21	10					8			8		
KOE-15	Conglomerate	37	12		10		20	4								17		
KOE-16	Quartz schist	42			47								11					
KOE-17	Weathered granite	18	19	7	25			8	6	5			12					
KOE-18	Unweathered granite	19	15	9	9	6	19	6	5	3			9					
KOE-19	Unweathered	17	20	24		8	15	7			2	3	4					

Sample	Lithology	Mineral content (Vol%)																
		Qtz	**Mc**	**Pl**	**Ms**	**Ep**	**Bt**	**Ap**	**Rt**	**Zrn**	**Or**	**Ttn**	**Fe-oxide**	**St**	**Chl**	**Cal**	**Opaque (sheared mat.)**	**Grt**
	granite																	
KOE-20	Weathered granite	10	27	22	15	2	13	3					8					
KOE-21	Phyllite	23			45										19			13
KOE-22	Phyllite	45					43						12					
KOE-23	Gneiss	60	9	8	4		6						8		2	3		
KOE-24	Meta-sandstone	25	10	7			10						9			11	28	
KOE-25	Carbonate	5											9			86		
KOE-26	(meta-) Sandstone	48	12		24								13			3		
KOE-27	Granite	21	72		2								5					
KOE-28	Quartz schist	33			38					15			14					
KOE-29	Phyllite	40			16		23						5				16	
KOE-30	Phyllite	29			22		15						6			16	12	

Appendix D: Scanning Electron Microscope (SEM) analyses

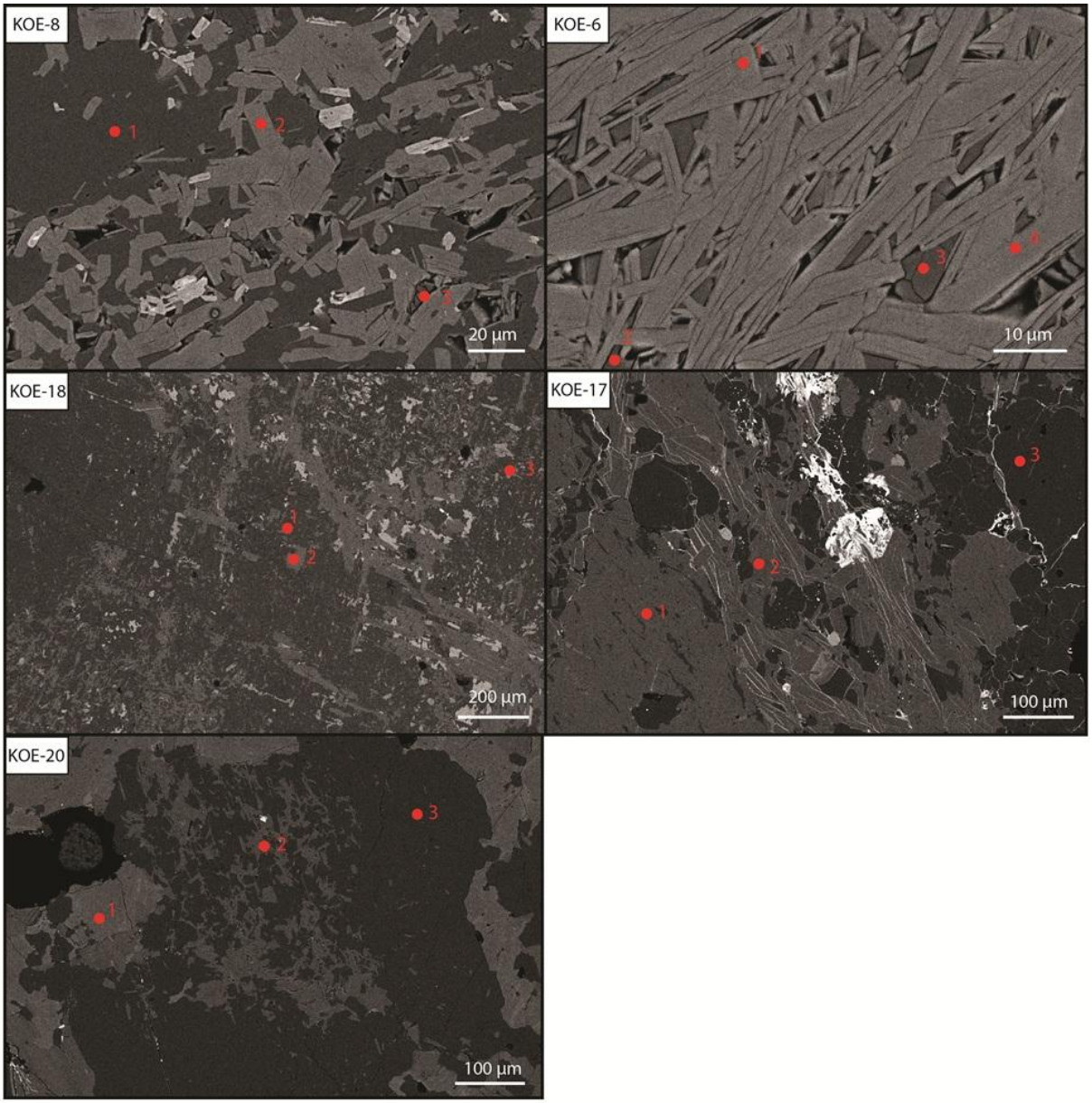

Selected points	Weight percentages of elements											
	C	O	Na	Mg	Al	Si	K	Ca	Ti	Mn	Fe	Ba
KOE-8 (pt_1)	3.04	46.48	8.24		10.30	31.94						
KOE-8 (pt_2)	3.21	43.97		1.47	13.93	23.22	9.13				4.34	0.73
KOE-8 (pt_3)	4.10	46.71	7.45		10.21	29.44	1.41				0.70	
KOE-6 (pt_1)	3.54	44.08		2.44	14.78	23.78	8.55				0.84	1.99
KOE-6 (pt_2)	3.00	46.88	7.94		10.34	31.01	0.83					
KOE-6 (pt_3)	3.04	46.41	8.35		10.29	31.90						
KOE-6 (pt_4)	3.05	44.30	0.27	2.63	14.84	23.94	8.59				0.57	1.81
KOE-18 (pt_1)	3.34	46.02	7.32		10.66	30.52	0.98	0.51			0.64	
KOE-18 (pt_2)	3.45	44.76	0.38	0.59	16.75	21.83	8.59				3.04	0.62
KOE-18 (pt_3)	2.69	44.80	2.12		12.65	20.25		12.44		0.45	4.49	
KOE-17 (pt_1)	3.62	43.25	0.31		9.63	30.29	12.91					
KOE-17 (pt_2)	3.23	43.93		1.62	15.12	22.46	8.72		0.34	3.01		1.59
KOE-17 (pt_3)	3.55	45.64	8.08		10.16	32.38	0.19					
KOE-20 (pt_1)	3.50	43.10	0.52		9.77	29.75	11.74					1.62
KOE-20 (pt_2)	3.11	45.70	2.07	0.95	13.29	23.43	6.47		0.31		3.03	1.64
KOE-20 (pt_3)	2.97	46.25	8.39		10.25	32.14						